Università degli Studi di Trieste

Dipartimento di Fisica
Corso di Laurea Magistrale in Fisica

ANALYSIS OF THE ATMOSPHERIC BOUNDARY LAYER FIELDS

Comparison between models and measurements

Laureando
Francesco Cocetta

Relatore
Dott. Dario B. Giaiotti
Correlatore
Dott. Giovanni Bonafè

Anno Accademico 2016–2017

Riassunto

I flussi computazionali che modellano la qualità dell'aria su scala regionale richiedono una costante verifica e validazione dei parametri implementati al fine di migliorare l'accuratezza delle previsioni nel breve termine. Tali valutazioni devono essere effettuate indipendentemente sui singoli modelli e processori della catena modellistica, con lo scopo di rilevare i pregi e i difetti di ognuno ed investigare le possibili relazioni con le previsioni degli inquinanti atmosferici a valle della catena (i.e. precursori dell'azoto, PM10 e PM2.5). In particolare, questo lavoro ha lo scopo di valutare i parametri di inizializzazione del processore SurfPro, utilizzato nella catena modellistica per descrivere la turbolenza nello strato limite atmosferico; tali parametri (spesso coincidenti con grandezze dello strato limite atmosferico) sono stati definiti in modo univoco per ogni applicazione del modello, in funzione dell'utilizzo del suolo e del periodo dell'anno. Confrontando i parametri di inizializzazione con le rispettive misure messe a disposizione per l'anno 2015 in un sito agricolo del Friuli Venezia Giulia, si evince che essi generalmente necessitano di una revisione sia nei valori che nella struttura della parametrizzazione; da un lato perchè i valori tabulati non riescono a descrivere con sufficiente rigore le grandezze fisiche legate all'utilizzo del suolo nella regione considerata, dall'altro la modulazione stagionale viene messa in discussione perchè non sempre è rappresentativa della variabilità delle grandezze fisiche in gioco. Quindi, al fine di migliorare la performance di SurfPro all'interno della catena modellistica, si è valutata la possibilità di ricavare i parametri di inizializzazione dal modello meteorologico WRF (alla base del flusso computazionale); come prevedibile, si sono ottenute serie temporali più accurate rispetto alle parameterizzazioni statiche, questo però non rende comunque conveniente aggirare le parameterizzazioni tabulate da SurfPro fornendo le grandezze richieste tramite WRF.

Contents

Introduction

The purpose of the thesis is to evaluate the performance of a meteorological pre-processor which is part of the air quality computational chain implemented by the Friuli Venezia Giulia Regional Centre of Environmental Modeling (CRMA - ARPA - FVG); this pre-processor is the widely used SurfPro model which computes the turbulent scaling parameters from meteorological fields and statically fields depending on the land use. In particular, this thesis is focused on the second item, that means the parameterization of micrometeorological quantities of the Atmospheric Boundary Layer (or related to it), by comparing the parameters with actual values collected by surveys.

To face the question, measurements of these physical quantities are obtained from both an eddy covariance experiment and remote sensing acquisitions. The first kind of measures were recorded by the micrometeorological tower sited in Beano (a rural village in Friuli Venezia Giulia region) during the year 2015, they are made available by the Department of Agriculture and Environmental Sciences of the University of Udine. The second ones are provided by the NASA Earth Science Data and Information System (with a further elaboration of Copernicus project for albedo measures) and essentially are used when parameters do not involve turbulent fluxes.

Measurements are compared to SurfPro statically parameterization defining a set of statistical indices in order to assess quantitatively the pros and cons of parameterization. In addition, the same statistical skill scores are calculated comparing measurements with the output fields of WRF model (the meteorological model which feeds SurfPro), in order to check whether SurfPro performances within the computational chain could be improved acquiring initially parameters from WRF outputs instead from lookup tables.

In fact, the optimization of CRMA air quality chain represents the main motivation for this study, which involves the operational tools of the center. The second focus of the thesis is related to its interdisciplinary approach to air quality modeling, by using micrometeorological and environmental data collected for other purposes. This is also an innovative aspect, in fact the method of analysis is applied for the first time in the context of modeling evaluation; defining analysis tools which can be exported for further evaluation.

Acknowledgments: I thank the Agenzia Regionale per la Protezione dell'Ambiente del Friuli Venezia Giulia for the support given, in particular for the computational resources and the tutorial assistance throughout my presence at the Centro Regionale di Modellistica Ambientale. Furthermore I thank the Department of Agriculture and Environmental Sciences of the Univerisity of Udine, namely prof. Giorgio Alberti and prof. Alessandro Peressotti, for the availability of measurements used in this work.

The physical system considered in this thesis, the Atmospheric Boundary Layer, is introduced in the first chapter, in which a general description of it is provided taking into account the structure, the evolution and the characterizing elements, such as the turbulent fluxes. Turbulent fluxes are represented using a statistical notation which allows to describe the governing equations within the Atmospheric Boundary Layer, these equations are bounded from the below by the flux exchanges at the Earth's surface. Furthermore, considering the different types of exchanges that can occur throughout it (i.e. heat, momentum and water), a first contact with SurfPro parameterizations takes place.

In the second chapter an overview of the meteorological part of CRMA air quality computational chain is given, also introducing some general aspects of environmental modeling. Clearly, the focus is on the SurfPro processor, in particular how it works and how it uses the initialization parameters. However, in order to evaluate also the performances of WRF micrometeorological fields in comparison to SurfPro parameterization, an explanation of WRF model is provided focusing on the module which concerns the exchanges at the Earth's surface.

The third chapter deals with the eddy covariance measurements. Firstly, the site description is reported by the points of view both climatological and pedological. In addition, the eddy covariance method is described taking into account the general features, the experimental equipment and the quality controls performed on the measurements. Whilst, the spatial and temporal representativeness of measurements are reported in the fourth chapter by means of a statistical analysis based on the OSMER meteorological network. This network is used for the calculation of correlation coefficients related to quantities measured by Beano station and by OSMER stations, that will be used for the definition of a representativeness radius. Instead, the fifth chapter explores the other source of measurements used for the evaluation of SurfPro statically parameterizations, the remote sensing data; these are obtained by MODIS radiometer which operates aboard the NASA satellites. Rough remote sensing data require different elaborations to obtain the quantities of interest, these developments are also reported in this chapter.

The basis for the implementation of the central analysis are given in chapter 6, where the definition of extraction points for SurfPro and WRF fields are reported. Clearly, they are chosen accounting for proximity criteria to Beano eddy covariance tower. Moreover, this chapter contains another feature which is a common point for the entire study, the availability of eddy covariance measures. In particular, a study is performed to investigate the causes which makes the measures unavailable.

The core of the work is contained in chapters 7 and 8. The first one contains the analysis performed on measurements and on WRF outputs to make them comparable with the SurfPro statically parameterizations; this step is determinant in order to obtain a truthful result of work because two factors must be taken into account: the physical meaning of the quantities and the design of SurfPro parameterization. The results, for each parameter, are annual time series for which statistical skill scores can be evaluated. The formulation and the application of these indeces are reported in the eighth chapter, in which one can compare the statistical qualities of SurfPro parameters and WRF outputs in relation to the measurements.

Finally, the summary of the results is reported in chapter 9 together with the analysis of the performance of SurfPro in two simulation products, i.e. friction

velocity and stability parameter, in which the statically parameterization play a relevant role.

Chapter 1

The Atmospheric Boundary Layer

1.1 Introduction of ABL

Almost all quantities, variables and phenomena which are analyzed in this thesis in order to perform the evaluation of the statically parameterizations of the numerical models implemented within the air quality chain, refers to the micrometeorology, the science that focus on the atmospheric micro-scale. This scale includes meteorological phenomena with horizontal dimension smaller than 3 km and with time scale shorter than 1 hour, that take place in the Atmospheric Boundary Layer(ABL), the region of the Atmosphere directly influenced the Earth's surface and bounded at the top by outer Free Atmosphere.

First chapter of the thesis is meant to provide an overview about this layer, that constitutes the system of the study, with particular emphasis placed on the physical interactions with the Earth's surface. It will be seen that there are three kind of exchanges between Atmosphere and the medium which borders it: mass, momentum and energy exchanges. Nevertheless, before proceeding in a deep investigation of these important aspects of the problem, an operative definition of Atmospheric Boundary Layer is required. Following Stull (1988) and Garratt (1992), it is defined as the part of troposphere directly above the Earth's surface, in which the effects of the surface are felt directly on time scales less than a day.

Along with the definition, two important strictly connected aspects require a further exploration: the surface forcing and the length scales involved in the coupling process. On the one hand surface forcing include frictional drag, heat transfer, evaporation and transpiration, pollutant emissions and terrain induced flow modification; on the other hand, all these coercive factors enter in the balancing of the fluxes of momentum, heat or matter through turbulent motions of size equal to or less than the depth of the boundary layer, ranging from hundred of meters over oceans to a few kilometers over well warmed land surface, as will be seen in the next paragraph.

However, at the moment the attention is focused on the peculiarities of Atmospheric Boundary Layer, that means the features that distinguish it from other fluid dynamic boundary layers. In fact, the general meaning of *boundary layer* indicates the portion of every fluid in close contact with the confining surface or with an obstacle that can deflect or distort it. Firstly, we must consider the gravity force, which is able to compress half of the mass of the atmosphere in the first 5 km from

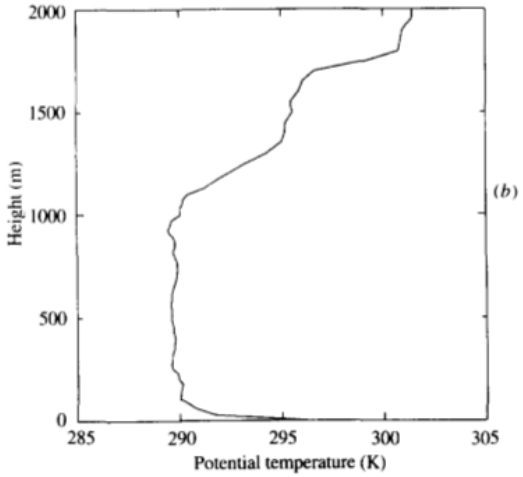

Figure 1.1: Potential temperature observed at 11.00 local time at Tarong, Queensland on 7 September1989. From *The Atmospheric Boundary Layer*, by Garratt J.R, 1992.

the Earth's surface. In addition, the atmosphere is limited from below by a complex system like the Earth, and therefore the surface forcings are different from position to position and evolve with their own characteristic time. Finally, turbulent motions (i.e. flows observed in boundary layers that solves particular conditions) in the ABL are characterized by the coexistence of thermal convection turbulence with mechanical wind shear generated turbulence, and by the interaction with a mean flow associated to the rotation of the Earth (Garratt, 1992). Considering the generating factors of turbulence (i.e. buoyancy and shear terms), a roughly classification can be defined: if the buoyant term prevails the ABL flows are in a state of free convection, while if mechanical term is predominant the turbulent motions are in a state of forced convection.

All these reasons clearly explain that atmospheric boundary layer is not reproducible in the wind tunnel and can only be studied using field measurements or by numerical models that must be carefully implemented according to the specific study.

There are a lot of evidences that show the presence of Atmospheric Boundary Layer (ABL). One of these can be found by the analysis of the vertical air temperature profiles, which exhibits inversion of the lapse rate at the top of the boundary layer, called entrainement zone during the daytime or capping inversion during the nighttime (figure 1.1). The reason why this behavior is detected will be clear later, for the moment the only discontinuity in the physical properties is underlined. Another example is reported in figure 1.2, in which the time evolution of potential temperature during a whole weak at different altitudes is plotted. In opposition to highest layer, included within the Free Atmosphere (i.e. the region of the atmosphere not directly conditioned by the Earth's surface) a daily modulation of temperature is detected in the evolution of lower layers, contained in the ABL. Therefore, the figure shows that Earth's surface influence on the atmosphere decreases according to quote; indeed, diurnal peaks are not caused by direct forcing of solar radiation, but it is the result of its absorption and subsequently emission by the Earth's surface, which is the responsible to air heating.

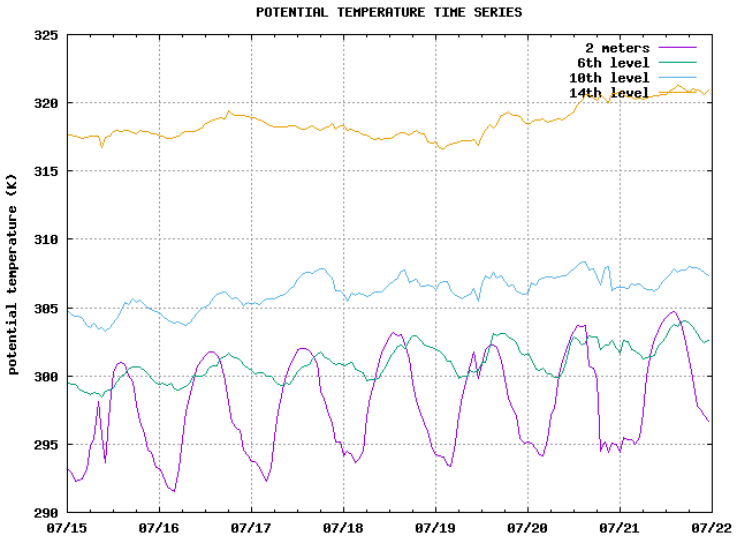

Figure 1.2: Potential temperature simulated by WRF model at Beano, Friuli Venezia Giulia during a whole summer week of 2015, from July 15^{th} to 21^{st}. Potential temperature at 2 meters is extrapolated; instead, other potential temperatures refer to computational layers of the model.

1.2 Boundary Layer Depth and Structure

As shown by figure 1.1, the top of the boundary layer is almost always well delimited, but its height is not uniquely defined in time and space. In a first approximation, its depth changes temporally during the day and during the seasons, and spatially according to the Earth's Surface (land, ocean, ice sheet) and to cloud cover; however, general nature of the boundary layer is to be thinner in synoptic high-pressure region than the low-pressure regions (Stull, 1988), so the shallower depths can be mainly associated with cloud-free regions in statically stable conditions. In this paragraph different micro and mesoscale situations are considered, and a further layering within the Atmospheric Boundary Layer is defined.

First of all, the characteristics of the ABL over open mid-latitude oceans, i.e. far from inter-tropical convergence zone, are studied. In this case, the absence of high obstacles and the distance from convergence zones that can develop cumulus clouds, joined to the large heat capacity of the water, ensure that ABL depth does not overcome a few hundred of meters, with slowly variations in space and time. In fact, induces little variations of ocean surface temperature during the day, and consequently the thermal forcing of the boundary layer does not change considerably. Then, most of the changes in ABL depth over oceans are related to synoptic and mesoscale processes, like the advection of air masses having lower temperatures than the ocean below, or the development of tropical hurricanes.

As far as the boundary layer depth over land surfaces, we consider a situation of total absence of cloud cover, in which the boundary layer has a well defined structure that evolves with the diurnal cycle. This evolution is shown in figure 1.3, where we can find the characterizing regions of the ABL, that are the mixed layer, the residual layer and the stable boundary layer. From the sunrise on, and

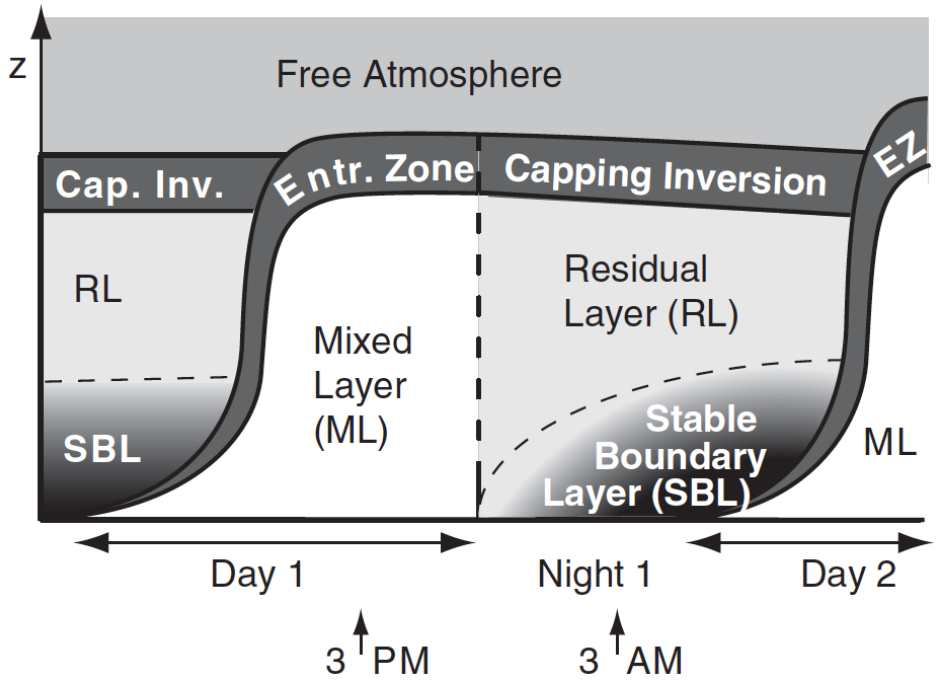

Figure 1.3: Schematic diagram of diurnal variation in the Atmospheric Boundary Layer over land under clear skies. From *Meteorology for Scientist and Engineers*, by R. Stull, 2010, third edition.

throughout the daylight hours, a description of their features is provided.

Starting from the sunrise, sun heating of Earth's surface ensures that turbulence motion in ABL becomes convectively driven, in fact the heat transferred from the warm ground surface to the atmosphere represents the main source of turbulent motion, creating thermals of warm air rising from the ground (Stull, 1988). Moreover, convective motions are promoted by secondary effects having place on the top of the boundary layer, such as the radiative cooling of a cloud layer and synoptic wind shear across it; the first produces thermals of cool air sinking from cloud top, while the second contributes to generate mechanical turbulence, even if it still not remains the dominant mechanism.

So stated, the region of the ABL that grows up during the day thanks to the sun heating of Earth's surface is called mixed layer; which name reflects the intense mixing due to unstable situation of the atmosphere, defined by the presence of heated air layer below cold air layer. Entering in the details, the growth starts about one hour after the sunrise, and reaches the maximum in late afternoon, when it stars to decrease. At the top of the mixing layer is located the entrainement zone, characterized by temperature inversion (i.e. atmospheric stability) that stops the thermal rise. Finally, is remarked the point that convectively driven turbulence tends to mix heat, moisture and momentum, as well as others variables, uniformly in vertical component (Stull, 1988).

As said, the warm Earth's surface stops to act as a forcing for the atmosphere about a half hour before the sunset, and consequently thermals cease to form. During this process, the remaining thermals place in the upper part of the mixed layer, that

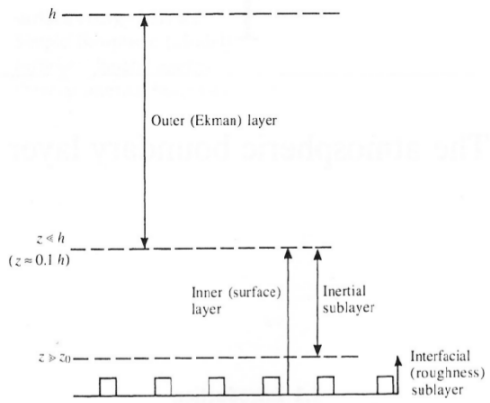

Figure 1.4: Vertical structure of atmospheric boundary layer. From *The Atmospheric Boundary Layer*, by Garratt J.R, 1992.

takes the name residual layer and is delimited from the top by the capping inversion. Meanwhile, as the night progresses the lower region is affected by the progressive cooling of the Earth's surface that cools faster than the air and cools down the lower layers of the atmosphere, starting from those in direct contact. In this situation, the atmosphere is stable, because the warm air stays above cool air and no motion starts, for this reason during nighttime the layer is named nocturnal stable layer; whatever turbulent motion in this region is produced by wind shear (e.g. nocturnal jet).

Diurnal cycle of Atmospheric Boundary Layer was just studied considering particular conditions (i.e. clear sky conditions), however in every situations a more detailed structure is observed. In fact, it could always make a distinction between the ABL region where the flows are mainly dependent on the surface characteristics, called surface (or inner) layer, and another region where the Coriolis force due to the Earth's rotation prevails, the outer layer. As shown in figure 1.4, the last one is a unique region extended from the surface layer to the capping inversion; instead, the inner layer, that correspond to about 10% of boundary layer depth, is divided into the roughness layer and the inertial layer.

Roughness layer, also called inter-facial layer, is important because is strongly affected by the structure of the surface elements (i.e. trees, crops and buildings) able to perform exchanges through molecular diffusion with the air. Moreover, most of the initialization parameters of the numerical models studied in this thesis concern this sublayer; for this reason exchanges having place here will be carefully taken into account.

1.3 Turbulent flows

Turbulence was introduced in the previous paragraphs as a fundamental feature of flows having place in the Atmospheric Boundary Layer; nevertheless, it is a fluid dynamic peculiarity of every boundary layer and it was studied for the first time by engineering experiments, in which boundary layers were created by immersion of a body into a moving fluid, therefore some useful quantitative tools (e.g. Reynolds

number, that permits distinction between turbulent and laminar fluids) come from this field of research. Summarizing the common aspects of every turbulent flows, three features are mainly relevant. Firstly, the flows are rotational and the swirls created are three dimensional, but nothing prevents a preferred direction; additionally, turbulence is dissipative and external forcings are needed to ensure and maintain turbulent flows; finally, turbulent flows transport energy and other quantities (e.g. momentum) for suppress the heterogeneities into a fluid perturbed by external forcing. Considering last aspect, the rates of turbulent transfer and mixing are several order of magnitude greater than the rate of molecular diffusion.

That said, a complete definition of turbulence is provided referring to atmospheric environment and in particular to an air flow, that can be considered as the superimposition of three distinct features: mean wind, turbulent part and waves. In the Atmospheric Boundary Layer mean wind dominates the horizontal component, while turbulence the vertical one. Quoting Stull (1988) turbulence can be visualized as *consisting of irregular swirls of motion called eddies.*

Moreover, every eddy which constitutes the turbulence has got a definite ray, and the overlapping of all the eddy sizes with the associated frequency defines the turbulence spectrum, that constitutes an important tool for the definition of turbulent part of flows. Referring to figure 1.5, an example of wind speed spectrum is reported, in which common features of the Atmospheric Boundary Layer can be found. Starting from low frequencies, the spectral peak at 10^{-2} cycles/hour is referred to synoptic scale movements characterized by a period of about 100 hours corresponding to the passage of weather fronts (i.e. Rossby waves); next smaller peak at 10^{-1} cycles/hour detects the behavior of wind during the day (period of 24 hours); finally, the broad peak closed to the 100 cycles/hour is formed by the microscale eddies having a period ranging from 10 seconds to 10 minutes. In the middle between the peaks related to large eddie size and the peak of microscale movements lies the spectral gap, that delineates the lack of an intermediate eddy size. However, it has to be remarked that the width of spectral gap varies according to the studied flow (i.e. large cumulus clouds acts with time scale of the order of the hour) but in every case can split the motions related to mean flow (low frequencies) and the turbulent part of the flow (high frequencies).

Furthermore, also wind speed can be helpful to perform a further distinction between the motion components of a fluid into the ABL. As said previously, mean flow prevails on the vertical one by approximately 10^2 or 10^3 magnitude orders and takes a value ranging reasonably from 2 to 10 m/s. While, turbulent part of flows prevails in vertical component ranging between 0 and 5 m/s with respect mean wind component.

Having underlined the differences of the two components of the flows in the ABL, a statistical representation consisting in the summation of the mean flow and the turbulent part (with the last one described as the deviation from the mean value) is taking shape. Before explaining that, Taylor's hypothesis is considered in order to facilitate the specific study of Atmospheric Boundary Layer, even if in the time line of scientific conception it came later (statistical representation of turbulent fluid was made by Reynolds in 1895, while Taylor wrote this hypothesis for ABL in 1938). To overcome the difficulties related to the definition of the eddy sizes, Taylor suggested that turbulence can be considered frozen if the turbulent eddies evolve with a time

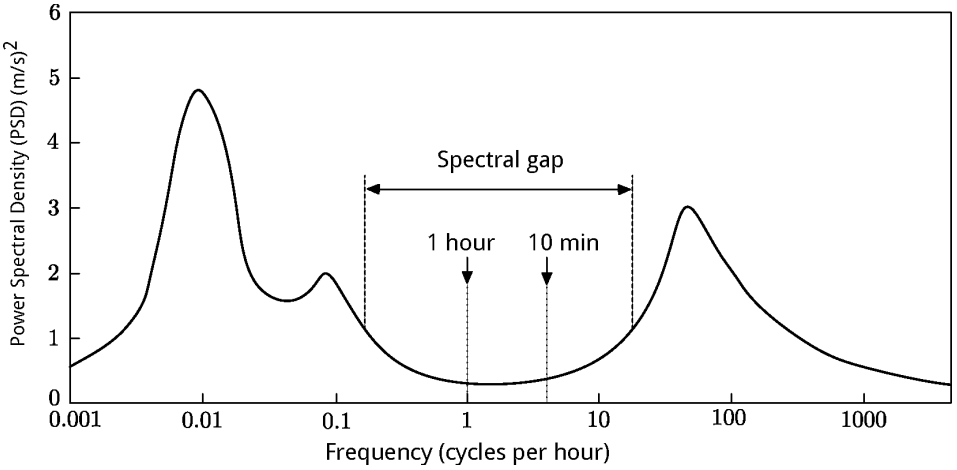

Figure 1.5: Power spectrum of horizontal wind speed based on measurements done at Brookhaven National Laboratory. PSD is related to fluctuating kinetic energy on a certain frequency and is a measure of the portion of kinetic energy associated with a particular size eddy. From *Wind Power Variability and Singular Events, Advances in Wind Power*, by Martin-Martinez et al., 2012.

scale longer that the sampled time (approximately stationary and homogeneous). Consequences of this hypothesis permit to determinate the eddy size starting from measurements made at one point in space, passed by turbulence, instead of scattered measurements in a wide region of space; this is because frozen turbulence hypothesis states that turbulent fields advect with mean wind. Finally, a turbulent flow drags with it a frozen vortex.

For example an eddy of 100 m in diameter is considered[1], with a 5 K temperature difference across it in the direction of wind speed (M = 10 m/s). If it pass upon a tower of measurements, a local change in temperature of $\frac{\partial T}{\partial t} = -0.5$ K/s is measured, assuming that eddy does not change during advection (frozen hypothesis). From this, it is easy to verify that expression of Taylor's hypothesis for temperature in one dimension is

$$\frac{\partial T}{\partial t} = -M \frac{\partial T}{\partial x_d}. \tag{1.1}$$

1.3.1 Statistical description

Rather than a deterministic approach, the study of turbulent flows is managed using statistical tools in order to describe at the same time all the eddies that form the fluxes. As seen by turbulent spectrum, the splitting in mean and turbulent part can be mathematically reproduced as the sum of these components, considering the wind speed in x-direction it means

$$U = \overline{U} + u', \tag{1.2}$$

where $\overline{U}$ is the speed of mean flow and u' is the speed of the turbulent part; following it, an operative definition of turbulence for x-direction wind speed can be derived,

[1] The example is extracted from *An Introduction to Atmospheric Boundary Layer*, by R. Stull, 1988.

i.e. $u' = U - \bar{U}$. Obviously, the representation is still valid for the quantities transported by the flows (i.e. temperature, humidity, pollutant fields) that can be separated into the part transported by turbulence from that transported by mean flux. Finally, a remark is made about the widely used ergodic condition, which is assumed for homogeneous and stationary turbulence flows; the condition permits to equal the averages calculated within the time, space (volume and one-dimensional) and ensemble domains. However, time averages are the most popular and the easier to treat and will be used in this thesis.

Having introduced a statistical description of turbulent flows, any study that involves them must necessarily consider their statistical characteristics, in terms of moments and probability distributions. In order to investigate these features the hypothetically variable $S = \overline{S} + s'$ of turbulent flow is defined and interesting statistical moments are evaluated.

Firstly, the calculation of the first moment, i.e. the mean, leads to an important property of the turbulent part: its mean equals to zero. In fact, applying average properties,

$$\overline{S} = \overline{\overline{S} + s'} = \overline{\overline{S}} + \overline{s'}, \tag{1.3}$$

and considering left and right sides of 1.3 it is obtain that

$$\overline{s'} = 0. \tag{1.4}$$

The turbulent part was defined as the difference with respect to the mean, therefore this result was predictable. However, if a further quantity of the turbulent flow is considered, i.e. $W = \overline{W} + w'$, the result of a mean operation is more interesting because the turbulence non-linearity enters in the equations: it can see averaging the product of the two variables, using previous results the following is obtained

$$\overline{WS} = \overline{(\overline{W} + w')(\overline{S} + s')} = \overline{W}\ \overline{S} + \overline{a's'}. \tag{1.5}$$

Therefore, non-linear term can not be neglected even in a first order approximation, because it is a constitutive part of the turbulent statistical model.

Additionally, second momentum (i.e. variance) is evaluated as estimate of the dispersion with respect the mean value; for $N < \infty$ unbiased variance is preferred to biased because it gives a better evaluation of it. If a sample of N measurements of a turbulent fluid is considered, variance can be written according to the only turbulent part,

$$\sigma_S^2 = \frac{1}{N}\sum_{k=0}^{N-1}(S_k - \overline{S})^2 = \frac{1}{N}\sum_{k=0}^{N-1}(s'_k)^2 = \overline{s'^2} \tag{1.6}$$

where definition of S within turbulent flow is used. The standard deviation, defined as the root square of the variance, has got the same dimensions of the original variable and may be suitable to indicate the magnitude of the turbulence. Moreover, turbulence intensity can be defined as $I = \sigma_S/\overline{S}$ and is a measure of the spreading due to it respect the mean value associated with the mean flow.

Furthermore, the covariance between two variables is defined in order to describes quantitatively the relationship between them. As variance, it can be written using

the only turbulent part of the flow, that in this case is a non-linear term

$$\sigma_{WS} = \frac{1}{N}\sum_{k=0}^{N-1}(S_k - \overline{S})(W_k - \overline{W}) = \overline{w's'}. \tag{1.7}$$

Thus, the correlation between two quantities is equal to the average of the turbulent terms product, this result will be extremely important when turbulent fluxes of ABL quantities will be evaluated.

Finally, consequences of statistical representation of turbulent motion involved also the kinetic energy associated with the flows, that can be split in a portion associated with the mean wind, and a portion associated with the turbulent part. Focusing on the turbulent part and considering an air parcel with mass m, turbulent kinetic energy can be written as

$$TKE = \frac{1}{2}m(u'^2 + v'^2 + w'^2), \tag{1.8}$$

where u', v' and w' are the components of turbulent wind. However, this quantity is of fundamental importance in the description of the Atmospheric Boundary Layer and of his evolution during the day. In a condition of convective boundary layer the warm Earth's surface provides the kinetic energy for air parcels to rise and thick boundary layer can develop, in this case TKE is rather constant throughout the depth of the ABL; during the night, i.e. stable boundary layer, TKE is provided only by mechanical shear and only in the first meters of the ABL, this avoids the development of a deep boundary layer; finally, when neutral conditions occur, the superposition of the two factors allows for a vertical profile of TKE that decreases with the depth.

1.3.2 Eddy flux

Having defined the mathematical context of the study, the focus is now on the quantities that characterized the Atmospheric Boundary Layer and in particular on how they can be transported within it. This topic is faced providing the definition of flux, as the transfer of a quantity per unit time per unit area, and directly introducing the fluxes that have place into the ABL, that are mass, heat, buoyancy momentum, moisture and pollutant fluxes. Because of some of these quantities (like heat and momentum) are difficult to measure, kinematic form of the fluxes is usually introduced[2]. This permits to write the fluxes as easy-measurable quantities (i.e. temperature and humidity) times the velocity of the flow.

However, evaluating the fluxes in the Atmospheric Boundary Layer mean fluid velocity or turbulent velocity can be chosen, and consequently two different fluxes are obtained; even if this passage seems trivial, the physical consequence is that turbulence can transport quantities even if its average motion is zero, e.g. $\overline{w'} = 0$. In addition, the characteristics of the ABL flows cause that particular attention is placed on the vertical components of eddy fluxes; these features are the upward movement of the Earth's surface influence started from below, the predominance of

[2]Kinematic form of the flux is obtained dividing the conventional flux by the density of moist air; for sensible heat flux, it must be divided also by the specific heat of the air.

the vertical turbulent fluxes on the advective ones in terms of speed scale (i.e. $w' >> \overline{W}$), the widely used horizontal homogeneity hypothesis and the more effectively of horizontal advective transport on the horizontal turbulent one.

Before displaying the fluxes involved in the study of the ABL, it must be underlined that a flux is an instantaneously quantity that in the real atmosphere usually consists of many large positive and negative values (Stull, 1988). Therefore, a physical significance can be attributable only if an average is performed, the obtained mean value is called net flux.

After all these specifications, this kinematic form of the mean vertical turbulent fluxes in the Atmospheric Boundary Layer are presented keeping in mind that they vary according with the surface forcing and to atmospheric condition (stability, instability or neutral). Considered fluxes are

- the horizontal components of eddy momentum flux, $\overline{u'w'}$ and $\overline{v'w'}$;
- the eddy sensible heat flux, $\overline{w'\theta'}$, with θ potential temperature;
- the eddy buoyancy flux, $\overline{w'\theta'_v}$, with θ_v virtual potential temperature (see appendix A);
- the eddy moisture flux, $\overline{w'q'}$, with q the relative humidity, it is useful to rewrite it as latent heat flux multiplying by the latent heat of vaporization of water and obtaining $L_v\overline{w'q'}$, with $L_v \cong 2.4510 \times 10^3 kJ/kg$;
- if a pollutant has to be traced, eddy pollutant flux is $\overline{w'c'}$, with c pollutant concentration.

As an example, the behavior of eddy sensible heat flux in unstable and stable atmospheric environments are presented. Firstly the eddy mixing process into an unstable environment is considered (i.e. potential temperature decreases with the height, as shown in the left figure of 1.6) and the journey of an air parcel is described starting from the average temperature profile, point A. The vortex lifts the air parcel providing it a positive turbulent vertical velocity ($w' > 0$) and a positive turbulent potential temperature ($\theta' > 0$) with respect parcels at the final quote, that have got $\theta' = 0$ (point B). Therefore in this upward movement the sensible heat flux is positive. After that, the eddy mixing process sinks the air parcel providing it a negative turbulent vertical velocity ($w' < 0$) and a negative turbulent potential temperature ($\theta' < 0$) with respect parcels at the final quote, point A. Also in this path, sensible heat flux is still upward and moreover average net flux $\overline{w'\theta'}$ in convective environment is positive for this small-eddy mixing process.

On the contrary, if the eddy mixing process takes place into a stable environment (i.e. potential temperature increases with the high, as shown in the right figure of 1.6) the sensible heat flux results downward. In fact, during the rising process starting from point A the air parcel has got positive turbulent vertical velocity ($w' > 0$) but it acquires negative turbulent potential temperature ($\theta' < 0$) with respect parcels at the same quote; while during the sinking ($w' < 0$) air parcel acquires positive turbulent potential temperature ($\theta' > 0$). Therefore, in both the paths eddy sensible heat flux is negative.

Taken together the two environments, common features can be delineated; first of all, in both cases turbulence transports heat from the cold part of atmosphere to

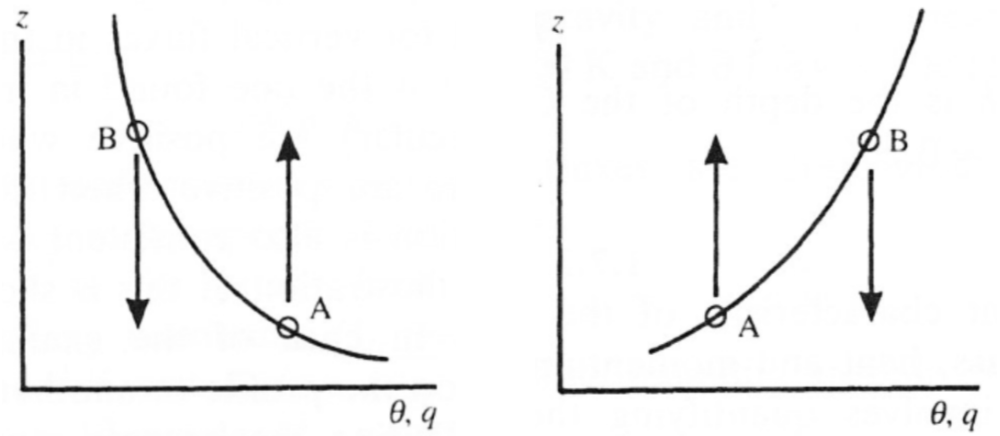

Figure 1.6: Schematic representation of small eddy mixing process into unstable (left) and unstable (right) atmospheric environment. The parcels in unstable environment have got positive eddy sensible heat flux (upward), while in stable environment have got negative eddy sensible heat flux (downward). From *The Atmospheric Boundary Layer*, by Garratt J.R, 1992.

the warmer part (e.g. for the unstable environment, from the bottom to the top) with the consequence of making the atmosphere homogeneous. This feature can be wrote in mathematical language by a parameterization of the flux, that can be written according to the gradient of the mean part of the involved quantity, as

$$\overline{w'\theta'} = -K\frac{\partial\overline{\theta}}{\partial z}, \tag{1.9}$$

where K is the diffusivity coefficient greater then zero, note that mean part of quantities is taken in order to consider the mean vertical profile.

1.3.3 Governing equations

Eddy fluxes are defined using a statistical approach because reflects the intrinsic nature of turbulence, nevertheless a deterministic description can be used for modeling their behavior and provide a total picture of the Atmospheric Boundary Layer. To perform this approach, governing equations of interesting fluxes need to be implemented. In particular, the implementation process must consider the statistical definition of the turbulent flows (i.e. mean part plus turbulent part) that consequently brings[3] to the definition of two different sets of prognostics equations: one set for the mean variables in a turbulent flow, and the other for the turbulent fluxes. They are not independent to each other, in fact the mean parts of variables enter in the set of turbulent flow, as well as the average turbulent fluxes enter in the set of mean flow. In the following, a summary of the implementation is reported.

In order to define a total picture of the Atmospheric Boundary Layer, the needed governing equations are the equations for the conservation of momentum (the Navier-Stokes equations), for the conservation of mass (the continuity equation), for the conservation of heat (the first thermodynamic law), and for the conservation of

[3]The entire mathematical development is not reported in this thesis; a complete dissertation is found into *An Introduction Boundary Layer Meteorology*, by Stull R.B., 1988.

water vapor, plus the gas state equation. Considering time and spatial scales of the ABL and assuming the fluid Newtonian and incompressible (i.e. respectively the viscosity does not depend on velocity and the total derivative of the density is equal to zero), all these equations can undergo simplifications to remove low-order terms. A further simplification is performed thanks to Boussinesq approximation, that states that density changes resulting from pressure changes are negligible, while density changes resulting from temperature changes are important only as they directly affect buoyancy (Businger, 1982).

Once applied the simplifications, next steps are the splitting of the quantities in mean and turbulent part and the evaluation of the Reynolds averaging. After some manipulations the two sets of governing equation can be derived; firstly the governing equations for the mean variables are presented.

The equation of state for mean flow contains the gas constant for dry air, the density of the moist air and the virtual temperature,

$$\overline{p} = R\,\overline{\rho}\,\overline{T_V}. \tag{1.10}$$

The continuity equation is direct correlated with the incompressible fluid approximation and results

$$\frac{\partial \overline{U_j}}{\partial x_j} = 0. \tag{1.11}$$

The equation for the conservation of mean momentum is reported in 1.12 and contains the Lagrangian derivative of the mean velocity at the l.h.s., while at the r.h.s. there are respectively the gravitational acceleration, the Coriolis term due to Earth's rotation, the pressure-gradient forces, the viscous term and the divergence of the Reynolds's stress tensor divided by the mean density. The Reynolds's stress tensor $\tau'_{ij} = \rho\,\overline{u'_i u'_j}$ is a second order symmetric tensor that describes the three-dimensional effects produced by a turbulent flow acting on an air parcel; it also can be viewed as the turbulent momentum flux along the i-direction and it permits the implementation of the no-slip condition at the Earth's surface (i.e. $\tau'_{ij} = 0$). Using Einstein's summation notation the equation results

$$\frac{\partial \overline{U_i}}{\partial t} + \overline{U_j}\frac{\partial \overline{U_i}}{\partial x_j} = -\delta_{i3} g + f_c \epsilon_{ij3} \overline{U_j} - \frac{1}{\overline{\rho}}\frac{\partial \overline{p}}{\partial x_j} + \nu \frac{\partial^2 \overline{U_i}}{\partial x_j^2} - \frac{\partial}{\partial x_j}\overline{u'_i u'_j}. \tag{1.12}$$

The equation for the conservation of mean moisture (1.13) shows the same structure of the previous one: at the l.h.s. there is the Lagrangian derivative of the total specific humidity (i.e. the mass of water at all phases per unit mass of moist air); at the r.h.s. the terms related to molecular diffusion of water vapor (ν_q) and to mean net source of moisture (S_{qt}) are combined with the divergence of the turbulent total moisture flux.

$$\frac{\partial \overline{q_t}}{\partial t} + \overline{U_j}\frac{\partial \overline{q_t}}{\partial x_j} = \nu_q \frac{\partial^2 \overline{q_t}}{\partial x_j^2} + \frac{S_{qt}}{\overline{\rho}_{air}} - \frac{\partial}{\partial x_j}\overline{u'_j q'_t} \tag{1.13}$$

Finally, the equation for the conservation of heat (1.14) contains the Lagrangian derivative of the mean potential temperature at the l.h.s., while at the r.h.s. are found the term of mean molecular conduction of heat (ν_θ), the mean net source of

heat, the source term associated with latent heat release and the divergence of the turbulent total heat flux.

$$\frac{\partial \overline{\theta}}{\partial t} + \overline{U_j}\frac{\partial \overline{\theta}}{\partial x_j} = \nu_\theta \frac{\partial^2 \overline{\theta}}{\partial x_j^2} - \frac{1}{\overline{\rho} c_p}\frac{\partial \overline{Q_j^*}}{\partial x_j} - \frac{L_\nu E}{\overline{q} c_p} - \frac{\partial}{\partial x_j}\overline{u_j' \theta'} \tag{1.14}$$

At least for the last three equations (i.e. conservation of mean momentum, of mean moisture and of mean heat) common features can be observed: the Lagrangian derivative split into the storage and the advection term, the body forces, the viscosity term and the contribution of turbulent flux. Therefore, as said previously the turbulent fluxes enter into the equations for the mean variables, and for all of them this happens by the turbulent fluxes divergence. Furthermore, considering the governing equations for mean quantities the viscosity terms (associated to molecular behaviors) can be neglected compared to other contributions; for example, the kinematic viscosity ν is analyzed in the surface layer starting from the definition of Reynolds number[4],

$$Re \equiv \frac{VL}{\nu}, \tag{1.15}$$

where V and L are the velocity and the length scales of motions. For the ABL $Re \simeq O(10^7)$ and suitable scaling values of V and L in the surface layer are respectively 5 m/s and 100 m; therefore kinematic viscosity coefficient is of the order of 10^{-5} and $\nu\frac{\partial^2 \overline{U_i}}{\partial x_j^2}$ can be neglected in the 1.12.

Referring again to the last three equations and having studied the influence of turbulence flux on mean variables, now the focus is on the governing equations for the turbulent part of the flow. In order to the usability of the dissertation, prognostic equations for the turbulent fluxes are directly presented omitting the equations for the mean variances of the turbulent quantities (i.e. $\overline{u_i'^2}$, $\overline{q'^2}$). In fact, it was previously seen that turbulent fluxes can be easily used for describe the motions having place in the Atmospheric Boundary Layer forced mainly by anisotropic source (i.e. Earth's surface). In addition, the equations for the turbulent fluxes constitute an approximation of higher order compared to that for mean variances, as will see later.

Firstly, the equation for the turbulent momentum flux is considered with particular focus on the vertical component and considering a mean wind along the x-direction, in order to perform a suitable description of the Atmospheric Boundary Layer system; therefore the general turbulent momentum flux $\overline{u_i' u_j'}$ is substituted by $\overline{u'w'}$ and $\overline{U_i}$ by $\overline{U}$. After scale simplifications that bring to neglect Coriolis effect and molecular diffusion in turbulent flux and assuming horizontal homogeneity with no subsidence, the equation for the vertical turbulent momentum flux with mean wind along x-direction results

$$\frac{\partial\left(\overline{u'w'}\right)}{\partial t} = -\overline{w'^2}\frac{\partial \overline{U}}{\partial z} - \frac{\partial\left(\overline{u'w'w'}\right)}{\partial z} + \frac{g}{\overline{\theta}_v}\left(\overline{u'\theta_v'}\right) + \frac{1}{\overline{\rho}}\left[\overline{p'\left(\frac{\partial u'}{\partial z} + \frac{\partial w'}{\partial x}\right)}\right] - 2\epsilon_{uw}. \tag{1.16}$$

[4]Reynolds's number is a non-dimensional quantity defined as the ratio of inertia to viscous forcings, and can be used to discriminate turbulent and laminar motions. Typically, a flow is turbulent when $Re > 2 \times 10^5$.

Analyzing the terms on the r.h.s. the contribution of mean part, the transport of momentum flux by turbulent motion, the buoyancy term, the return-to-isotropy term and the viscous dissipation term are respectively found. All these contributions are present in the other prognostic equations for the turbulent fluxes, i.e. moisture and heat flux, and can be considered at once; equations 1.17 and 1.18 report the time evolution of the vertical part of these fluxes considering the ideal case of horizontal homogeneous setting with no subsidence,

$$\frac{\partial\left(\overline{q'w'}\right)}{\partial t} = -\overline{w'^2}\frac{\partial \overline{q}}{\partial z} - \frac{\partial\left(\overline{q'w'w'}\right)}{\partial z} + \frac{g}{\overline{\theta_v}}\left(\overline{q'\theta'_v}\right) + \frac{1}{\overline{\rho}}\left[\overline{p'\frac{\partial q'}{\partial z}}\right] - 2\epsilon_{qw} \tag{1.17}$$

$$\frac{\partial\left(\overline{\theta'w'}\right)}{\partial t} = -\overline{w'^2}\frac{\partial \overline{\theta}}{\partial z} - \frac{\partial\left(\overline{\theta'w'w'}\right)}{\partial z} + \frac{g}{\overline{\theta_v}}\left(\overline{\theta'\theta'_v}\right) + \frac{1}{\overline{\rho}}\left[\overline{p'\frac{\partial \theta'}{\partial z}}\right] - 2\epsilon_{\theta w}. \tag{1.18}$$

Before proceeding, a remark is made on the fact that horizontal homogeneous conditions and the omission of subsidence have made negligible the advection term in the previous equations.

At this point, terms entering in the computation of vertical eddy fluxes can be investigated starting from those related to mean quantities; these term could suggest a production or a consumption of turbulent flux in accordance with the mean quantity lapse rate. Considering for example the equation 1.18 describing vertical eddy heat flux, in this case the term increases or decreases vertical turbulent flux if the atmosphere is respectively unstable or stable (see figure 1.6), as previously analyzed.

The Second addends of r.h.s. describe the transport of momentum, humidity and heat by the turbulent motion. Each of them contains a statistical third moment of the quantity involved and represent a further variable of the governing equations system; if we want to make them explicit new equations containing a fourth moment variable must be derived, this is an iterative process that does not permit to resolve analytically the system because of fourth momentum constitutes further variables; this is called closure problem and is summarized in the table 1.1 for moment equations. Solution are provided trough the parameterization of the moments entering in the equations, this arrangement can be performed at different stages of the process, i.e. for different statistical moment. The moment that is parameterized determines the number of governing equations used for the motion description and the closure order; furthermore, closure can be divided in local or non-local closure according with the features of parameter used. For example, a first order local closure for vertical heat flux is $\overline{w'\theta'} = -K_H\frac{\partial \theta}{\partial z}$, where K is the turbulent thermal diffusivity; usually, meteorological models use this type of parameterization.

Proceeding with the analysis of the equations from 1.16 to 1.18, the third terms of r.h.s. are related to the buoyancy of the air parcels and therefore are present only considering the vertical turbulent fluxes. In particular, these terms represent the covariance between the involved quantity and the virtual potential temperature (see appendix A); if there is correlation between the two turbulent variables the contribution to vertical eddy fluxes will be positive, otherwise it will be negative. For example, considering the equation 1.17 for vertical eddy moisture flux, if a parcel of warmer air rises (as expected) and at the same time is more moist with respect surrounding air the correlation is positive and this process contributes to the upward moisture flux.

Prognostic equation for	Moment	Equation	Number of equations	Number of unknowns
$\overline{U_i}$	First	$\frac{\partial \overline{U_i}}{\partial t} = ... - \frac{\partial \overline{u_i' u_j'}}{\partial x_j}$	3	6
$\overline{u_i' u_j'}$	Second	$\frac{\partial \overline{u_i' u_j'}}{\partial t} = ... - \frac{\partial \overline{u_i' u_j' u_k'}}{\partial x_k}$	6	10
$\overline{u_i' u_j' u_k'}$	Third	$\frac{\partial \overline{u_i' u_j' u_k'}}{\partial t} = ... - \frac{\partial \overline{u_i' u_j' u_k' u_m'}}{\partial x_m}$	10	15

Table 1.1: Scheme of closure problem for momentum equations in a turbulent flow; m index is referred to the last index of u' that constitute the fourth momentum $\overline{u_i' u_j' u_k' u_m'}$.

Fourth terms are called the return-to-isotropy terms and are present only if single eddy flux-components are considered, these terms disappear if a sum of all components is performed. Each of these terms tends to move energy from more energetic components to less energetic ones making turbulence more isotropic.

Finally, last terms describe the loss of turbulent motion by viscous dissipation. They are strongly dependent to the eddy size and can not be neglected especially considering small eddy sizes for which the vorticity is quickly dumped by viscosity. To be thorough, as example is reported the definition of viscous dissipation ϵ for the equation 1.16,

$$\epsilon_{uw} = \nu \overline{\frac{\partial u' \partial w'}{\partial z^2}}. \tag{1.19}$$

With the set of equations just described and knowing the initial conditions of the Atmosphere one could simulate the fluxes in the Atmospheric Boundary Layer far from the Earth's surface and from the upper boundary; however this description does not take into account the continuous action of the surface forcings on the Atmospheric flows. Therefore, for a suitable representation of the system the boundary conditions have to be defined, in particular the exchanges that occur throughout the atmosphere-Earth's surface interface; however this conditions mutate during the day and in according to the season to their implementation is to fundamental importance in the field of atmospheric models.

1.4 Flux exchanges at the Earth's surface

Atmosphere and Earth's surface are in direct contact and may interact with each other through exchanges of previously defined fluxes, which are momentum, heat and moisture fluxes. Clearly, the exchanges are strongly dependent on the type of surface involved and on the elements on it; however, considering a unique surface kind and making the assumption of horizontal local homogeneity, studying the surface forcings on the atmosphere the only vertical part of turbulent fluxes can be considered. Facing this topic, focus is on land surfaces which are roughly split into urban and rural zones, however further subgroups can be delineated according for example to the building density or to the plant cover.

Moreover, studying the exchanges between atmosphere and land surface we bump into the parameters that constitute the object of study of this thesis. In this part, they will introduced by the theoretical point of view leaving for the further chapters the modeling considerations and the explanation of how these quantities are

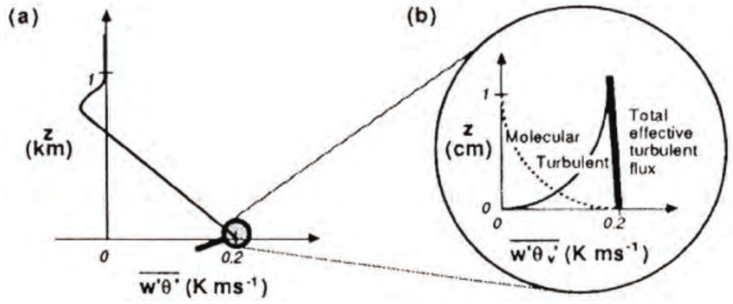

Figure 1.7: The effective turbulent heat flux in daytime convective conditions. From *An Introduction to Boundary Layer Meteorology*, by Stull R.B., 1988.

implemented.

Before proceeding is useful to explain that turbulence by itself can not transfer quantities across the interface, and turbulent transport starts to be effective after few millimeters from the Earth's surface; before this quote molecular process are involved as the molecular conduction of heat, the molecular diffusion of water and the molecular viscous transfer of momentum, all of these cause transport of quantities between the surface and the lowest millimeters of air, and rapidly decrease with the distance from the ground (figure 1.7). To simplify the matter, it is convenient to define and consider the effective turbulent flux, that is the sum of the molecular and turbulent fluxes (Stull, 1988); as seen in figure, the molecular and the turbulent part respectively prevail at the surface and above the lowest few centimeters.

1.4.1 Radiation Budget

The primary forcing of the Atmospheric Boundary Layer over the land is the solar radiation absorption at the ground which results in diurnal variations of the surface temperature and of the turbulent heat fluxes. Therefore, an estimation of net radiation reaching the Earth's surface must be firstly provided in order to assess the amount of radiative flux available for the ground, as will see later a well-defined part of this flux constitutes the thermal forcing for the atmosphere and can be said that it is available for the atmosphere-Earth's surface coupled system.

Net radiation at the surface is considered distinguishing between the shortwave and the longwave component, the first is governed by solar radiation and the second by Earth emission; nevertheless, both of them are constituted by the incoming and the outgoing components with respect the Earth's surface, by convention they are respectively positive and negative in the widely used reference frame. The sum of all these quantities simply constitutes the radiation budget at the surface

$$R_n = K_0^u + K_0^d + I_0^u + I_0^d, \tag{1.20}$$

where K denotes the shortwave components and I the longwave ones. Immediately can be inferred that during the daytime, incoming solar radiation prevails and R_n results positive, while during nighttime shortwave terms go to zero and the net radiation becomes negative due to radiative Earth's emission.

Considering shortwave component, the spectrum of solar radiation must be known: it can be approximated as a black body spectrum with maximum energy

emitted at a wavelength of 480 nm, corresponding to Sun surface temperature close to 6000 K. However, before reaching the Earth's surface, the flux of solar radiation passes through the atmosphere, where physical processes as scattering, absorption and reflection by cloud and atmospheric particles reduce it. In particular, shortest wavelengths radiation disappear in accordance with the quote and the most of solar radiation that reaches the surface is the visible light. Part of the downwelling radiation at the surface (both direct and diffuse) is reflected and returns back to the atmosphere (term K_0^u of 1.20); as will see later the fraction of solar flux involved in this process strictly depends on the kind of affected surface and is described by the albedo of the surface α_s defined as the ratio of reflected shortwave flux over the global incident flux. The surface albedo is one of the parameters studied by this thesis.

Now, the focus is on the longwave radiation that enters into the budget because the Earth emits radiation in the infrared region; in fact considering an Earth's skin temperature closed to 273 K, the radiation is mainly confined to the wavelength range 4 - 100 µm, in accordance with Wien's law that links skin temperature with emitted wavelength. However, the radiation intensity depends to the surface by the emissivity constant ϵ_{ir}, that enters in the Stephan-Boltzmann law for the flux of radiation emitted by a black body $I_0^u = \epsilon_{ir}\sigma_{sb}T^4$, and that can vary in the range from 0.9 to 0.99 for most Earth's surfaces. Once the infrared radiation emitted by the Earth is traveling upward, it can be diffused by particles in the atmosphere (as molecules of water into the clouds or greenhouse gases) and can be forced downward to the Earth's surface; with clear-sky conditions this term can be considered constant during the time.

To summarize the radiation budget, figure 1.8 shows an example of the diurnal cycle of radiative fluxes. As previously anticipate, during the daytime solar incoming radiation dominates the balancing, while during nighttime the infrared radiation emitted by the Earth prevails and the net radiation becomes negative. After the 16:00, cloudy-sky conditions increases the longwave downward radiation at the surface.

1.4.2 Surface energy balance

So far, it was seen that Earth's surface holds an amount of energy derived from the radiation budget represented by net radiation; this available energy is used partly as thermal forcing for the atmosphere (fluxes of latent and sensible heat), partly as heat flux into the soil (previously focus has placed on land surface) and partly as energy stored into canopy (i.e. heat accumulated by everything is in the middle between surface and atmosphere, as threes and buildings). The relationship among them is summarized by the equation of the conservation of energy at the surface, that is

$$R_n = H_0 + L_v E_0 + G_0 + \Delta Q. \tag{1.21}$$

With reference to paragraph 1.3.2 the definition of the turbulent fluxes are recalled: the sensible heat flux at the surface is denoted by $H_0 = \frac{1}{\rho C_p}\overline{w'\theta'}_s$ and the latent heat flux as $L_v E_0 = \frac{L_v}{\rho}\overline{w'q'}_s$; in particular, the last one can be described as a flux that transfers heat from the Earth's surface to the atmosphere, once the condensation takes place the energy stored as heat is released even at great distances. Moreover,

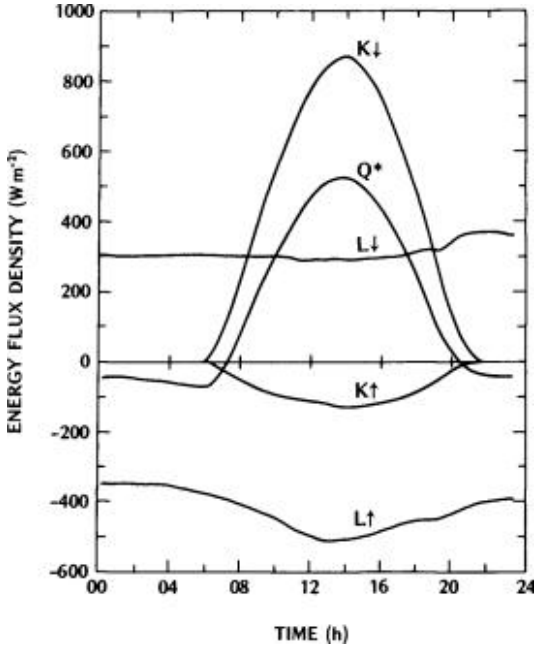

Figure 1.8: Radiation budget components for 30 July 1971, at Matador, Saskatchewan (50°N) over a 0.2 m stand of native grass. Cloudless skies in the morning, increasing cloud in the later afternoon and evening. Q* is referred to net radiation, in the text noted by R_n and longwave radiation is denoted by L instead of I. From *Boundary Layer Climates*, by Oke T.R., 1978, 2nd edition 1987.

at the l.h.s. of the equation another term eventually comes out if urban surfaces are considered, the anthropogenic heat flux that describes the human activity influence and comprehends heating homes, exhaust gas and presence of industries.

Obviously, the values of fluxes reported in the previous equation are highly variable according to the land surface type and to the soil texture, the first is mainly referred to land use and the second to the fraction of soil basic components (i.e. sand, silt and clay). However, by the conceptual point of view a bare soil is easy to consider (i.e. without elements between surface and atmosphere), this leads to neglect the storage. Considering this widely used approximation, all the energy comes from net radiation is addressed downward through the soil by thermal conduction (ground flux, G_0) or upward to the atmosphere (turbulent heat fluxes); the rate between ground flux and total net radiation is called soil parameter (h_c) and it is one of the parameters studied in this thesis.

Related to the surface energy budget, another studied parameter is the Bowen ratio, that is the ratio between sensible and latent heat flux, and therefore describes the distribution of available energy between the atmospheric turbulent fluxes over a specific surface. It is important because of it can be used as proxy for the surface forcings of the atmosphere; for example if a urban land use is compared with a rural one, the sensible heat increases because of the higher surface skin temperature due to building materials, although the latent heat decreases due to the reduced water available for the evaporation; as a consequence Bowen ratio increases considering urban land use compared to rural one.

Finally, a typical example of the diurnal cycle of fluxes at the land surface is

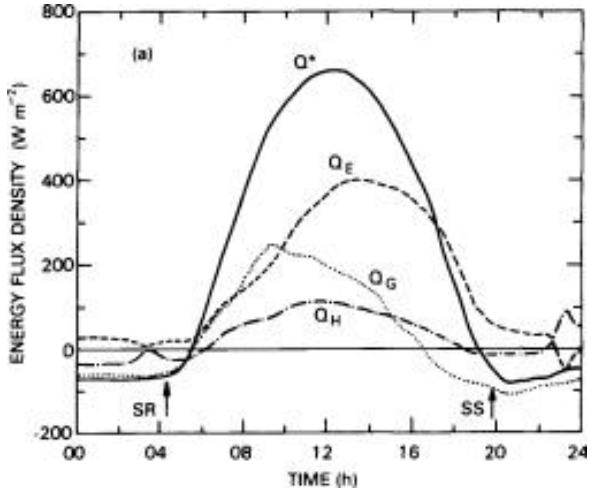

Figure 1.9: Energy balance components for 30 May 1978 with cloudless skies at Agassiz, B.C. (49°N) for a moist, bare soil. Q* is referred to net radiation, in the text noted by R_n, while Q_E, Q_H and Q_G are respectively the flux density of latent, sensible and ground heat at the surface. Remark that absolute values are pictured, therefore the opposite of the net radiation and soil heat fluxes are pictured. From *Boundary Layer Climates*, by Oke T.R., 1978, 2nd edition 1987.

shown in figure 1.9, in which moist bare soil is considered (i.e. $\Delta Q = 0$) for a cloudless day. During the daytime, net radiation is directed downwards and promotes the upward fluxes of latent and sensible heat transporting moisture and heat away from the surface, while a fraction of net radiation continues to downwards in the shape of soil heat flux. When the net radiation is dominated by outgoing infrared radiation, i.e. during nighttime, the sensible heat flux becomes downward because of the Earth's surface radiative cooling, instead the latent heat flux becomes directed downward only if dew and frost form. Furthermore, the ground heat flux in these hours is upward because of the radiative cooling of the ground surface layer compared to the warmer deeper layers.

Influence of vegetation on the energy budget So far, a roughly representation of the land surface was considered, in which no element is situated between the surface and the atmosphere; however, for the purpose of this thesis some words must be spent on particular behaviors of the fluxes in the presence of vegetation. Whereas, considering plants the water balance can not be ignored because of crops and trees strongly influence the amount of available water for the evaporation.

In particular, according with the atmospheric conditions and the amount of water into the soil, the evaporation rate (and then the latent heat flux) can be controlled by the physiological mechanisms of the plants, that can limit the supply of water from the root layer into the atmosphere (passing trough the stomata) if the soil water is beyond a certain value needed for the survival of the plants. On the contrary, if there is a large amount of soil water into the root layer the evaporation rate is controlled by the atmospheric moisture content, because of the roots can not use all the water into the ground and what remains is available for the evaporation. Therefore, it comes out that also the soil, trough the field capacity of retain the water into the

root level of the ground, enters in the surface flux balancing.

Considering the situation in which vegetation controls the rate of evaporation, the soil water for pass from the ground to the atmosphere must necessary go through the plants. In this process soil water must overcome two resistance: the first related to the air inside the stomata during the travel to the surface of the leaves, the second one involves the passage from the surface of the leaves up to the roughness layer. The two resistance counteract the evaporation forcings that are referable to the net radiation (and then the energy available) and to the distance of air specific humidity from the saturation point.

Furthermore, not only the latent heat flux is influenced by the plant presence, even the sensible heat flux in particular occasion is modified. For example, a strong evaporation during the daytime leads the cooling of the ground (because of the upward latent heat flux) that can reaches a lower temperature than the air and resulting into a downward sensible heat flux during the daytime.

Therefore, it was seen that surface energy budget strongly changes in accordance with the presence of the vegetation. When this happens, an assessment of the plants efficacy to contribute to the budget, with particular attention to the evaporation rate (in this case, evapo-transpiration rate), is performed by the definition of the Leaf Area Index that is defined as the one sided green leaf area for unit ground area in broadleaf canopies, i.e. $LAI = \sum_i \frac{L_{A,i}}{A}$, where $L_{A,i}$ is the area of the $i-th$ leaf; following the definition, the use of the sum of the green leaf areas is used as a proxy for the number of stomata able to perform the evapo-transpiration. In fact it can be used for obtain the stomata resistance (r_s) in a unit ground area A: if r_{si} is the resistance of a single leaf, the total resistance can be obtained by parallel sum of all the leafs present in the ground area,

$$\frac{1}{r_{st}} = \frac{1}{A} \sum_i \frac{L_{A,i}}{r_{si}}. \tag{1.22}$$

For many applications this expression can be approximated as $r_s \approx r_{si}/LAI$ (Garratt, 1994). By the end, the Leaf Area Index is one of the parameters object of this thesis and will be investigated later.

1.4.3 Momentum exchange at the land surface

Having considered the surface energy budget, the heat exchange at the surface was taken into account, at least in a particular context where plants are present (others environments such as urban, desert or marine are not involved in this thesis and the exchanges are not investigated). Going on in the explanation of surface exchanges, the exchange of flux of momentum is now considered in land surfaces.

First of all, one can observe that this process is unidirectional because the ground can affect the atmospheric flows, but the opposite cannot have place. In particular, as said previously the ground acts as a trigger for the wind driven turbulence that forms by wind shear near the surface. Therefore, the vertical flux of momentum at the surface can be described in terms of eddy covariance quantities by means of the horizontal components of turbulent momentum flux $\overline{u'w'_s}$ and $\overline{v'w'_s}$, which enters in the definition of the velocity scale parameter called friction velocity

$$u_*^2 = \sqrt{\overline{u'w'_s}^2 + \overline{v'w'_s}^2}, \tag{1.23}$$

that is a measure of the surface stress.

According with the similarity theory[5], friction velocity enters in the calculation of the horizontal mean wind speed profile within the surface layer in neutral conditions of boundary layer. The profile follows a logarithmic behavior as a function of the quote and becomes zero close to the surface at the height z_0 called roughness length (which is the last parameter that will be investigated), as shown by the equation

$$\overline{U} = \frac{u_*}{k} \ln \frac{z}{z_0}, \tag{1.24}$$

where k is the Von Karman constant that value is between $k = 0.35$ and $k = 0.40$. Values of z_0 can vary between fractions of millimeters over oceans and few meters over centers of cities with high buildings. For non-neutral situations, the wind profile deviates slightly from logarithmic. One can note that given two observation of wind speed at different heights, the graphically extrapolation of z_0 can be performed and consequently the friction velocity (i.e. a measure of both momentum exchange and wind shear turbulence) can be calculated.

Influence of vegetation If surface elements, like tree or buildings, are interposed between land surface and atmosphere and if they are closed each other, the logarithmic wind speed profile can be shifted upwards, because these elements begin to act like a displaced surface (Stull, 1988); examples can be found considering forest (large amount of leaves), crops (dense package) or city centers. Vertical shift is described using the displacement distance d, which enters in the logarithmic argument as

$$\overline{U} = \frac{u_*}{k} \ln \frac{z - d}{z_0}, \tag{1.25}$$

now the mean wind speed becomes zero at the height $z = d + z_0$. However, values of displacement height does not correspond to the height of rough elements, but a percentage of them.

1.4.4 Water exchange at the surface

Last exchanges that have place through the Earth's surface are the water exchanges between the atmosphere and the surface below; the main characteristic of the flux of moisture between these system is that the closure of balancing cannot be observed within a limited Earth's surface region, but one must consider all the exchanges having place on global scale; in fact there are relevant horizontal moisture fluxes (such as atmospheric advection or water runoff) that cannot be neglected and that can move great quantities of water. Moreover, to close the global balancing all the interactions between land surface, terrestrial atmosphere, sea and marine atmosphere systems have to be discusses (i.e. evaporation, precipitations, advection, runoff).

However, to account for the purpose of this thesis the only water exchanges in a limited region are considered and depicted in figure 1.10; this help to comprehend

[5]The similarity theory is a large used theory that deduces empirical relationships between groups of dimensionless variables. It is used because the ABL usually shows repeatable characteristics that can not be described with mathematical equations but can be approximated by dimensionless relations.

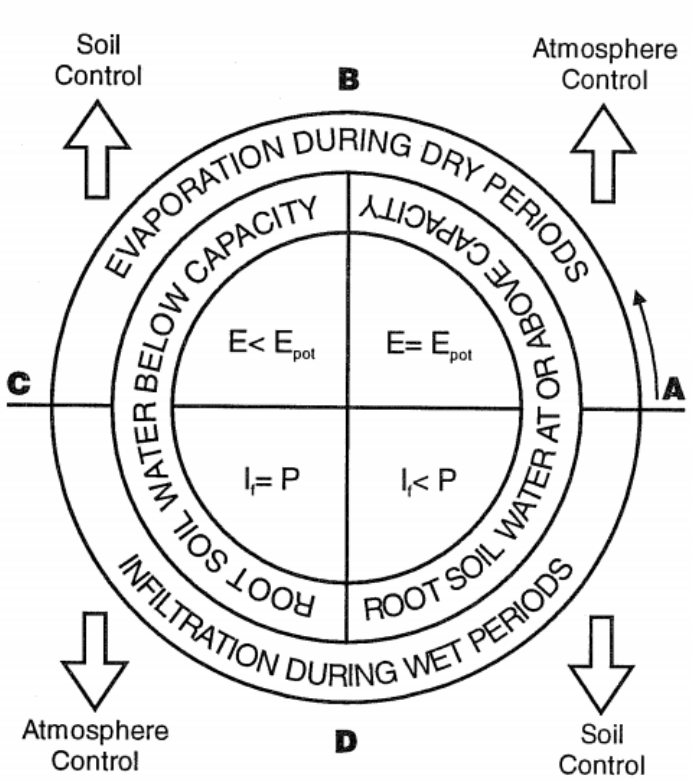

Figure 1.10: Scheme of the interaction between the soil hydrology and the atmosphere. From *A review of parameterization schemes for land surface process.* Viterbo P., 2002.

the mutual interaction between land surface and atmosphere that controls the moisture exchange. As will be described, the flux of water through the land surface is controlled periodically by atmosphere or by soil as a function of the soil moisture and of the weather precipitations. Starting from the point A in the picture and moving counterclockwise, a rainfall episode is just occurred and soil water is large available for evaporation, which is controlled by the atmospheric moisture content and occurs at the potential rate (i.e. as for a direct water source) until a certain threshold of soil moisture (point B of figure). When the threshold is reached, physiological mechanisms limit the supply of water from soil to the atmosphere, i.e. the soil controls the evaporation. At the point C a precipitation starts and the soil is able to collect the water by infiltration because it is dry enough to receive water from the outside (in this stage the passage of water from atmosphere to soil is controlled by atmosphere) until a threshold of soil moisture is reached (point D), this point represents the soil capacity to hold water. Beyond this values the soil returns to control the water exchange (in this case it avoids infiltration and permits surface runoff).

When plants are present at the land surface, there is a further element that help the water flux from the soil to the atmosphere in the case of wet soil, while in the case of dry soil the plants inhibit the same flux because they must hold water to survive

Chapter 2

Environmental modeling

Numerical environmental modeling is usually implemented by a collection of models and processors linked to each other to form a operational computing workflow. At the base of the chain there is the meteorological model, that acquires initial and boundary conditions to solve the fluid-dynamics equations of motion in the domain of interest; afterwards, several post-processors and modules are required to calculate the ABL quantities not provided by the previous model, to give a more accurate description of the land surface and to define the emissions of pollutant in the atmosphere. At the end of the chain there are the air quality models, that are of different types in accordance to the perfomed simulation; for instance the simulation of pollutant dispersion in atmosphere by punctual emission sources or the study of pollutant deposition and accumulation processes.

The environmental modeling operates within the coupled system atmosphere-Earth's surface; as one can suppose, the description of this system is not easy to implement due to the mutual exchanges saw in the first chapter which requires different computational steps. For instance plants over land surface supply water vapor to atmosphere that can be advected few kilometers away, where condenses in clouds releasing latent heat. Moreover, a further characteristic of environmental modeling to keep in mind is the different time scales involving each constituent of the system; however, according to the simulation time domain, one can decide to keep constant defined fields in order to simplify the complexity of the simulation, for example the temperature of the soil deeper layer.

Time scale of the deep soil (i.e. described by changes in temperature) is the largest among the time scales involved in the coupled system and can be greater than one year (depending by the soil type), whilst approaching to the Earth's surface the time scales of soil layers decrease rapidly until reach a order of magnitude between few days and one month. Whereas, considering the oceanic system, changes in physical properties varies monthly and seasonally as well as vegetation fraction over the land surface (with some variability related to human activity). Finally, the times scales of atmospheric system cover a wide range of magnitudes from hours to weeks, in accordance with the atmospheric phenomenon described (i.e. order of magnitude of thermal wind is the hour, while weather fronts have a time of occurrence close to one week).

Therefore, planning an environmental or atmospheric model the modeler must take into account the time range of simulations, in order to minimize the compu-

Forecast / System	Atmosphere	Soil	Ocean
Daily	Modeled	Parameterized	Parameterized
Seasonal	Modeled	Modeled	Parameterized
Climate	Modeled	Modeled	Modeled

Table 2.1: Overview of how the forecast models describe the systems accounting for their purpose. Note that this table would only be a indication based on system time scales, hypothetically a powerful calculator can simulate all the systems with a daily resolution.

tational time without making conceptual mistakes and provide suitable results for researchers or administrative agencies. Table 2.1 reports the three different time domains of numerical forecasts (i.e. daily, seasonal and climatic) associated to the sub-systems previously described (i.e. atmosphere, soil, ocean): it is shown how the models usually have implemented them. One can find that models can describe the physics of the systems in two ways: by means of computational methods (i.e. solving equations in time steps) and by parameterization through physical assumption, for instance that the surface sea temperature undergoes only small variations during one week or month.

2.1 Air quality modeling in CRMA

This thesis in written using the tools make available by the CRMA - ARPA FVG; among others services the air quality operational chain is provided, it produces both operative daily forecast and both a database of previous years simulations of meteorological and air quality quantities called analysis simulations.

The model used for simulate the meteorological fields (giving the start to the computational chain) is the Weather Research and Forecasting (WRF) limited area model, that is a numerical system designed for the prediction of mesoscale atmospheric phenomena. The model solves both the fluid-dynamics motion equations and the more complex interactions involving the ABL (e.g. friction velocity) for three spatial domains, starting from boundary and initial conditions provided by the European Centre for Medium-Range Weather Forecasts (ECMWF) every six hours. In particular, CRMA compiles the WRF model within three spatial domains (i.e. regional, national and continental) with different temporal and spatial resolution; for the implementation of air quality chain the smallest is taken into account to provide accurate information about environmental fields in the Friuli Venezia Giulia region. This region is at the center of the computational domain with a spatial resolution of 2 km ans a download time step of one hour.

The gridded meteorological fields is then provided to air quality models and their pre-processors, which prepare data and calculate ABL fields to feed air quality models. Summarizing, the tasks of processors are related to quantify the emissions from the Earth's surface to the atmosphere (i.e. Emma module), to give a suitable description of wind fields according to the land surface (i.e. Swift and Orogex) and to provide turbulence features in terms of scaling parameters (i.e. SurfPro, Landex and Turkey processors). The outputs are fields calculated over the same grid and with the same time steps of the meteorological model.

Air quality models are the final step of the computational chain; two models

are implemented by CRMA for the assessment of air quality in the Friuli Venezia Giulia region. Firstly, the SPRAY Lagrangian particle model can simulate the path of pollutant particles emitted by a source over the Earth's surface (e.g. factory plumes, farmings, blazes) to evaluate their dispersion in the atmosphere by means of ABL characteristics. For instance, the turbulence characteristics in the ABL (and in particular in the surface layer) determine the removal rate of pollutant chemical species from the lower atmosphere by deposition on the ground or by rising over the mixing height. The same features permit to another air quality model, the Eulerian photochemical model called FARM/F-AIR, to assess the pollutant concentrations over the whole Friuli Venezia Giulia knowing the estimates of all regional emissions (i.e. vehicles, industries, heating); pollutants species involved in the assessment are carbon monoxide, nitrogen dioxide, sulfur dioxide, ozone, PM10 and PM2.5.

As one can note, the entire air quality workflow could be affected from some inaccuracies made by one of the previous described steps and therefore is important validate the single sub-modules. This thesis would perform a first validation of the SurfPro processor making a comparison of its initialization parameters with both the corresponding measures in a specific site and the WRF outputs. Then the attention is payed on the functioning of the SurfPro meteorological processor.

2.2 SurfPro processor

As previously introduced, the tool designed to compute gridded Atmospheric Boundary Layer fields is the SurfPro[1] model (Arianet, 2011), a module of the CRMA air quality workflow that acquires as input the meteorological variables from WRF model and the land use information from CORINE database and finally provides turbulence parameters to actual air quality models,as shown in figure 2.1.

In the calculation of ABL quantities, SurfPro is strictly related to meteorological input; in fact, in addition to providing the atmospheric determinant, the metorological pre-processor dictates the time to proceed to the SurfPro model, included the sub-modules. Therefore, at each time step and for every computation cell of the domain, SurfPro reads from input meteorological fields all the needed variables and implements the operations in three stages process, corresponding to the three different modules.

Firstly, the terrain module is inquired for the definition of surface parameters on the basis of time, location and land-use class; these parameters will be used by the following modules and constitutes the object if these thesis (e.g. Bowen ratio, roughness length and albedo). Secondly, the solar radiation is computed taking into account perturbation aspects such as cloud cover, terrain slopes and topography shadowing effects; alternatively the solar radiation can be retrieved directly by meteorological model. Finally, the ABL scaling parameters are calculated applying surface energy balance, in accordance with entities within the computational cell (e.g. water bodies, crops, grass); this means that in each step the balancing is set up and no temporally energy storage can be described, for example within the canopy or the ground. Typical outputs of the SurfPro used by air quality models are the friction velocity, the mixing height and the convective velocity scale.

[1] SurfPro stands for SURFace-atmosphere interface PROcessor.

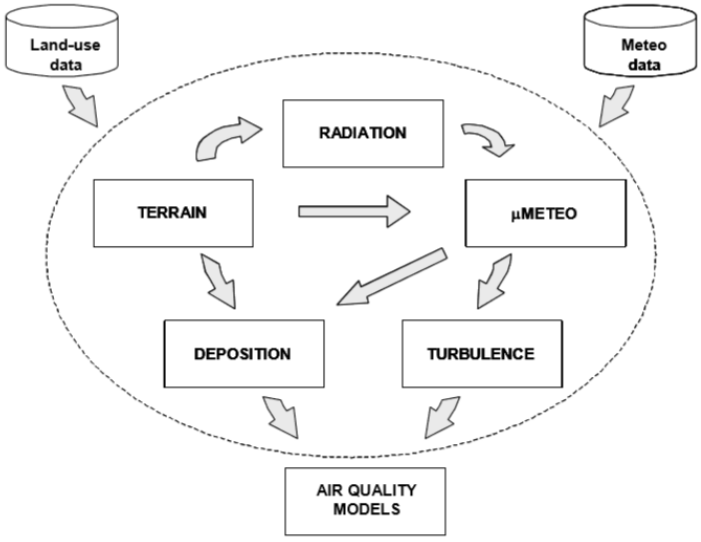

Figure 2.1: SurfPro processor logical scheme. Inputs needed are the meteorological fields and the land-use data in the spatial domain, internal modules can be activated according to the fields requested by air quality models.

2.2.1 Land use statically parameters

The validation process performed in this thesis involves the first stage of the SurfPro workflow, i.e. the definition of statically parameter of the simulation by means of input gridded land-use. In particular, one of the sources from which the processor can acquire information about the land use within the computational domain is the CORINE Land Cover data frame, that contains the land cover of the entire Europe collected by satellite data. Last update of this project dates back to 2012 (with time consistence 2011-2012) and contains 44 land use classes; however, not all the classes are implemented in the SurfPro classification, which reduces this number to 21 comprehending, among others, urban fabric, industrial units, arable land, permanent crops, pastures, bare rock and mixed forest.

Moreover, CORINE project provides land cover features on a 100 meters basis; that means a spatial accuracy better than the 2 km SurfPro grid. The land use class enters in the definition of the statically parameters, therefore, the matching between the grids is a delicate issue and is implemented in two ways that users can choose. First method specifies the land use class of computational cells in terms of CORINE prevailing class within them, and therefore the parameters will be evaluated only as a function of them. Whilst, the second method considers the percentages of all the classes within the SurfPro cells and calculates the parameters by weighted averages on them. Last one is set up in the CRMA air quality simulations of the year 2015.

Finally, it remains to introduce the land use depending parameters involved in the calculation of turbulence scaling parameters, which were meet in the first chapter and that are summarized in the following list.

- The *roughness length* is the height at which the logarithmic wind profile becomes equal to zero.

- The *leaf area index* describes the ratio between the one-sided green leaf per unit ground surface area.
- The *albedo*, defined as the ratio of shortwave incoming radiation to the reflected component.
- The *bowen ratio* is the fraction of sensible heat flux over the latent heat flux.
- The *soil heat flux* in percentage, defined as the fraction of net radiation absorbed by the ground.

2.2.2 Computing incoming solar radiation

Next step is the computation of incoming solar radiation flux through the parameterization of Holtslang and Van Ulden (1983) known the geographical position, the time and the solar elevation angle (φ); equations are

$$K_0^d = 141.91\varphi^{5.730}; \varphi \leq 10^\circ \tag{2.1}$$

$$K_0^d = 990 \sin\varphi - 30; \varphi > 10^\circ, \tag{2.2}$$

where the first expression is used for avoid negative values for small angles. Afterwards, the correction for cloud cover C (expressed in decimal as cover fraction) is applied

$$K_0' = K_0^d(1 - 0.75C^{3.4}). \tag{2.3}$$

Furthermore, shadow effects due to topography can be evaluated. However, a black mark of SurfPro model is that all these coefficients of the previous formulas are suitable for the site of Cabauw (Netherlands), according to Holtslang and Van Ulden measurements; they are extremely site-specific and dependent by the characteristics of aerosols in the air (i.e. concentration, type) and by the properties of clouds that can be found in that place (i.e. color, thickness). These parameters are re-calculated for $\phi > 10^\circ$ for the site of micrometeorological measures used to asses the statically parameterization of SurfPro processor (see appendix B).

2.2.3 Boundary Layer Scaling parameters

Having computed the incoming solar radiation and knowing the surface statically parameterizations, in the last step all the fluxes at the surface (i.e. net radiation, sensible heat flux, latent heat flux, ground heat flux and urban heat storage if necessary) are derived applying the surface energy budget (Holtslang and Van Ulden, 1983).

Afterwards, the boundary layer scaling parameters are calculated taking into account the land use of computational cells and ABL stability conditions. In the following, only the basic scaling parameters computed by the SurfPro module are reported, which are the Monin-Obukhov length, the friction velocity and mixing height, which also correspond to final outputs needed by the air quality models.

During daytime unstable conditions, friction velocity and Monin-Obukhov length (also called Obukhov stability parameter) are calculated in an iterative way knowing the air temperature T, the sensible heat flux H, the roughness length z_0 and the

wind speed at z-height U_z and applying the Monin-Obukhov similarity theory, which assumes stationary and horizontal homogeneous conditions. The equations that must be solved are

$$u_* = kU_z \left[ln\left(\frac{z}{z_0}\right) - \psi_M\left(\frac{z}{L}\right) + \psi_M\left(\frac{z_0}{L}\right)\right]^{-1} \tag{2.4}$$

$$L = -\frac{\rho C_p T u_*^3}{kgH}, \tag{2.5}$$

where k is the Von Karman constant, ${\psi_M}^2$ is the stability function, g is the acceleration of gravity, ρ the air density and C_p the specific heat at constant pressure. The iterative method starts solving the equation 2.4 with $\psi_M = 0$, the value of u_* obtained is putted into equation 2.5 to get L, which is used to obtain another estimate for u_*. To achieve an accuracy of 5% not more than three interactions are usually required (Holtslang and Van Ulden, 1983). Whilst, in the case of stable conditions (i.e. $L > 0$), the equations for the same scale parameters become

$$u_* = kU_z \left[ln\left(\frac{z}{z_0}\right) + \beta\frac{z}{L}\right]^{-1} \tag{2.6}$$

$$L = \beta z / ln\left(\frac{z}{z_0}\right), \tag{2.7}$$

where $\beta = 4.7$. Moreover, in ABL stable conditions Venkatram (1980) suggests an empirical equation between the two quantities, as $L = Au_*^2$, where $A \simeq 1.110^3 s^2 m^{-1}$.

Considering the mixing height h during the daytime, SurfPro module distinguishes convective and mechanical mixing height, it computes them in different steps, finally selects the highest between the two values. Firstly, convective mixing height is computed for unstable conditions following Carson (1973) and starting from the sensible heat flux and the potential temperature vertical profile (the first one is obtained applying the surface energy balance, previous step, and the second one by meteorological model). Then, convective mixing height is got by integration of the differential equation

$$\frac{\partial\Theta}{\partial z} h dt = (1 + 2A)\frac{H_0}{\rho c_p} dt. \tag{2.8}$$

Secondly, mechanical mixing height is calculated for ABL neutral conditions according to Venkatram (1980) from the friction velocity u_* and the Brunt-Vaisala frequency $B_\nu = \sqrt{g\frac{d\theta}{\theta}}$ (i.e the buoyancy frequency at which a parcel oscillates in a atmospheric stable conditions)

$$h_m = \frac{c_m u_*}{\sqrt{B_\nu}}, \tag{2.9}$$

where $c_m = 141$.

Finally, considering stable conditions the only mechanical mixing height is computed (i.e. convective turbulence has not place) using Venkatram (1980) as a main

[2]Stability function is defined for Obukhov stability parameter less than 0 (i.e. unstable atmospheric conditions) as $\psi_M(x) = 2ln\left(\frac{1+x}{2}\right) + ln\left(\frac{1+x^2}{2}\right) - tan^{-1}x + \pi/2$, where $x = \left(1 - 16\frac{z}{L}\right)^{1/4}$

reference (other references are used for near neutral conditions or considering a urban rural cover); he found the empirical relationship

$$h = c_n(u_*)^{3/2}, \tag{2.10}$$

where $c_n = 2400$.

As one can note, the mainly SurfPro outputs refers almost all to the Monin-Obukhov similarity theory valid within the surface layer and for dry air, in fact validations of the moisture influence on the previous equations are lacking (Foken, 2006).

2.3 WRF runs available for the analysis

Having described the SurfPro processor, now the focus is on what one can find at the base of the air quality computational chain, the WRF model, and on the produced simulations used in this thesis. The description of the 2015 WRF runs is important because the SurfPro statically parameters, calculated in accordance with CORINE data frame, are compared with both the on site measurements and the WRF outputs; with the purpose to verify if one of the two constitutes a better estimation of the reality. As introduced previously, starting from WRF model the CRMA provides operational weather and air quality forecasts within the entire Friuli Venezia Giulia region. In addition, a database of previous years meteorological simulations is going to be completed (Nausicaa project) with the aim of define a statistical base for model validations; moreover, this database of WRF simulations is what used in this thesis as a further comparison for SurfPro statically parameters.

The simulations of previous years (called WRF analysis) are the most realistic simulation of the meteorological quantities observed because they are implemented with the help of available measurements, that can be assimilated by model. Even the boundary conditions of simulations are an analysis product provided by the ECMWF, which collects measurements from different sources, i.e. from satellite, radar, station and many others. Following, the description of WRF analysis features are provided, taking into account that run settings can differ from those of the forecasts simulations (see table 2.1), in fact the analysis products cover a whole year, while forecast simulations work on five days; for this reason analysis and forecast products differ each other.

The main differences between the implementation of analysis and forecasts runs are related to the description of the Earth's surface behavior: considering annual simulations a detailed characterization of soil and sea surface temperatures is required because time scales of these systems are comparable to the period of simulations. In fact, considering a simulation over a whole year, the soil and sea surface temperatures cannot be fixed (as it happens in the forecast simulations, see table 2.1) and must be modeled during the computational time steps. In analysis runs, soil and sea surface temperatures are updated every six hours together with other surface properties such as soil moisture, snow cover, sea ice and vegetation fraction.

Different methods to update the quantities are implemente by the WRF model, for instance the sea surface temperature is supplied by the analysis of ECMWF, while the vegetation fraction is parameterized according to the day. In addition,

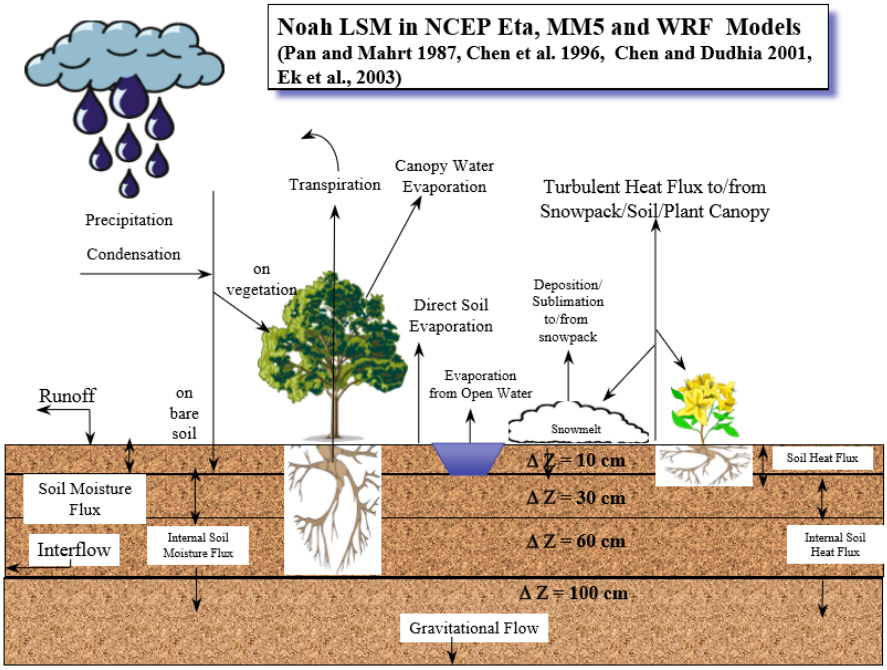

Figure 2.2: Summary of the physical process modeled by Noah land surface scheme. Moreover, soil layering is represented.

soil moisture and other quantitities ralated to the soil are updated in the analysis simulation through the Noah Land Surface model[3] (Niu, 2011), a WRF module for the description of physical interaction concerning the soil and its boundaries (with the surface layer and with the bedrock). In the context of this thesis, the Noah description of land surface plays an important role because it is involved in the computation of the quantities which will be used in the comparison with SurfPro staticallty parameters.

2.3.1 Noah land surface scheme

The purpose of Noah land surface model is to provide realistic descriptions of the quantities related to land surface-atmosphere interaction process such as heat fluxes, evapotranspiration rate and soil moisture. Noah is a multiparameterization model able to describe a widely range of physical processes like the vegetation canopy energy balance, the vegetation phenology, the interaction between soil moisture-groundwater and many others, as summarized in figure 2.2.

The global feature of Noah land surface scheme is the soil layering, that describes a total depth of 2 m through four layers of different thickness: the shallowest is 10 cm thicker, the below one is 30 cm and the the lasts two are respectively 60 cm and 100 cm thick. At the bottom of layering there is a "bedrock" that represents the boundary condition for soil heat flux and soil moisture. The boundary condition

[3] Noah is the acronym of the companies working on the model: N for National Centers for Environmental Prediction, O for Oregon State University, A for Air Force, and H for Hydrology Lab.

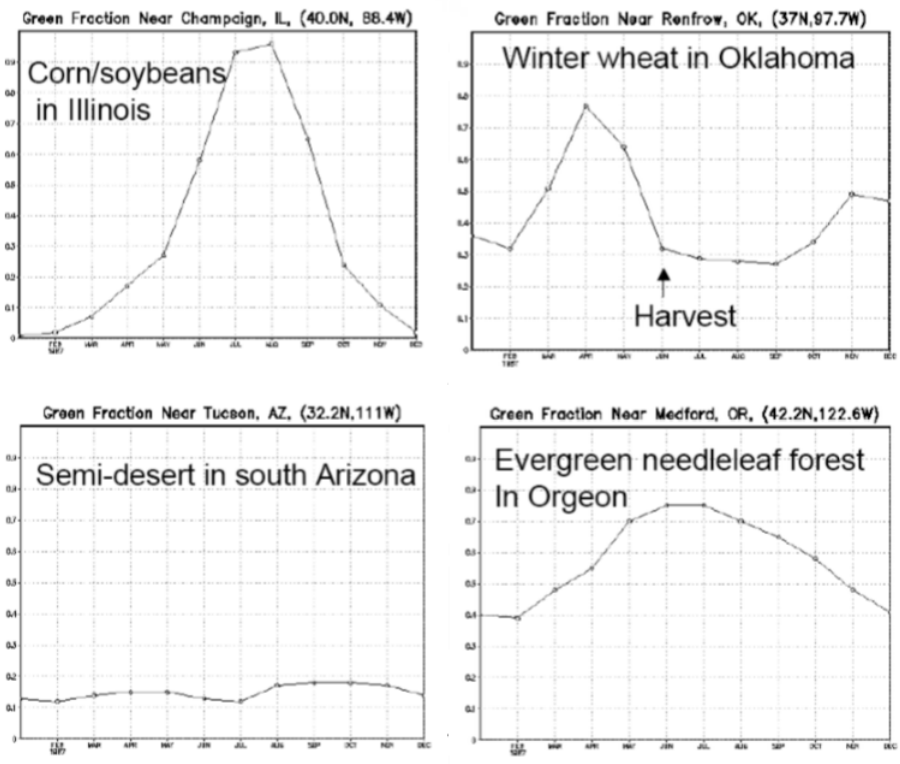

Figure 2.3: Examples of modeled leaf area index as a function of the land use class.

on soil moisture is depicted by the gravitational free drainage (a sort of aquifer); the drained water from the 2 m soil bottom should accumulate in its underlying soil during wet season, while during dry season water is able to be drawn back to the 2 m soil column by capillary forces.While, the boundary condition on soil heat flux is depicted as a thermal bath whose temperature can be modulated.

The Noah module requires three input parameters to start the routines: the land use type (with specifications about vegetation, if present), the soil texture and the terrain slope. The first two parameters are assigned for every computational cell from a list of classes; once the classes of land use and soil texture are assigned, the range of certain quantities to use in the flux estimates (i.e. roughness length, leaf area index, wilting point, soil capability) are consequently determined (figure 2.3). In addition to the three mandatory parameters, secondary parameters such as green vegetation fraction, albedo and maximum snow albedo, can be specified; otherwise they are derived from pre-compiled tables.

Soil energy transfer Entering in the details of the physical processes faced by the Noah scheme, the equations describing soil energy transfer and the soil water transfer are discussed, neglecting the coupling between them. Firstly, the Fourier law of diffusion is used to describe the prognostic equation for the soil temperature, i.e. the heat transfer through the soil in the vertical direction,

$$(\rho C)_S \frac{\partial T}{\partial t} = \frac{\partial}{\partial z}\left[\lambda_T \frac{\partial T}{\partial z}\right] \tag{2.11}$$

where T is the soil temperature, z is the depth, $(\rho C)_S$ is the volumetric soil heat capacity ($Jm^{-3}K^{-1}$) and λ_T is the thermal conductivity ($Wm^{-1}K^{-1}$). Last two parameters depend on the soil water content and the soil texture (percentage of clay, silt and sand), that determines essentially the amount of water that the soil can hold against the combined effects of gravity and pressure (Viterbo, 2002). The previous equation is solved for the layering previously depicted, with these boundary conditions: at the top it consists in the surface energy balance, while at the bottom is given by the temperature of "bedrock" (i.e. what is under the deepest layer). The annual WRF simulations are defined with constant "bedrock" temperature, which acts as boundary condition.

Soil water transfer Secondly, the Noah scheme models the vertical movement of water within the soil through Richard's equation (i.e. the equation of fluid transfer through a porous media) plus a source term. If Θ stands for liquid water content in the soil, the equation is

$$\frac{\partial \Theta}{\partial t} = \frac{\partial}{\partial z}\left[\lambda \frac{\partial \Theta}{\partial z}\right] - \frac{\partial \gamma}{\partial z} + S_\Theta, \tag{2.12}$$

where γ is the hydraulic conductivity (ms^{-1}), λ the hydraulic diffusivity (m^2s^{-1}) and S_Θ is the volumetric source term ($m^3m^{-3}s^{-1}$), the last one takes into account the root extraction of water from the root system up to the stomata and the phase changes of water (melting and freezing). If the terrain slope is relevant, the 2.12 must be associated with the equation of horizontal water transport. Unlike the heat flow equation, in which the forcing shows daily and seasonal periodicity due to net radiation at the surface (with a noise due to cloud cover), the forcing of 2.12 at the surface is mainly driven by the signal of precipitation with the infiltration and the evaporation that constitutes the boundary condition at the top (i.e. surface water budget). While, at the bottom boundary condition is constituted, at least in the run used, by an aquifer that can accumulate all the water by gravitational drainage, as seen previously.

Land surface evaporation Now the focus is on the top boundary condition of equation 2.12, represented by the surface water budget which is summarized as

$$d\Theta = P - R - E, \tag{2.13}$$

where P, R and E are respectively the precipitation, the runoff and the evaporation, with $P - R$ that represents the water infiltration on the ground. Among all these contributes, evaporation rate is the most complex to implement, and at the same time is what mainly affects mainly the evaluation of latent heat flux; soil moisture, vegetation type, depth and density of roots, green vegetation cover are all contributes to the total surface evaporation, that Noah land surface model implements as

$$E = E_{dir} + E_t + E_c + E_{snow}. \tag{2.14}$$

The equation shows the different contributes: the direct evaporation from soil, the transpiration through plant canopy, the evaporation from canopy intercepted rainfall and the sublimation from snowpack.

Firstly, the evaporation from bare soil is modeled by Noah model by means of a linear relationship that scales the maximum possible evaporation that could occurs over an open water surface under the existing atmospheric conditions (E_p, potential evaporation[4]) through a soil moisture availability parameter β; moreover an additional factor is devoted to exclude vegetation fraction σ_f within a computational cell from the calculation (Godfrey, 2010). The equation results

$$E_{dir} = (1 - \sigma_f)\beta^2 E_p, \tag{2.15}$$

where

$$\beta^2 = \left(\frac{\Theta - \Theta_w}{\Theta_{ref} - \Theta_w} \right)^2 \tag{2.16}$$

represents a normalized soil moisture availability term, with Θ_w wilting point, Θ_{ref} field capacity and Θ volumetric water content of the top soil layer.

Secondly, the evaporation due to canopy is described by two different mechanisms: the evaporation E_c of water intercepted by canopy leaves after a precipitation event or dew deposition, which has place in wet canopy conditions, and canopy transpiration E_t that has place in dry canopy conditions. The first mechanism is similar to what happens in the case of bare soil with the exception that water evaporates at the potential rate and that parameterizations are required to establish the fraction of the wet canopy and how long the water can evaporate at the potential rate (Viterbo, 2002).

On the other hand, the canopy transpiration mechanism is more complex because is controlled by both the plant physiology and the surface layer (aerodynamic) conditions. In fact, the water is firstly transported by plants from the root zone up to the stomatal cavities by means of stomata openings and closures as a function of plant needs (for instance, when soil moisture is low the stomata close to prevent the desiccation of the plant); afterwards, the atmospheric driven mechanism transports water from the stomata up to the air. In the case of dry conditions it results in the equation

$$E_t = \sigma_f E_p P_c, \tag{2.17}$$

in which the plant coefficient P_c is defined from thermodynamic (r and Δ are functions of the thermodynamic properties of the air at the lowest level) and aerodynamic (C_h, aerodynamic resistance) properties of surface layer and from canopy resistance R_c, as

$$P_c = \frac{r + \Delta}{r(1 + C_h R_c) + \Delta}. \tag{2.18}$$

In particular, canopy resistance (i.e. the plant resistance to the water flux from ground to atmosphere) is implemented by the Noah model as $R_c = \frac{R_{C,min}}{LAI * F_1 F_2 F_3 F_4}$, where $R_{c,min}$ is the minimal stomatal resistance for each vegetation type and factors F_1, F_2, F_3 and F_4 represent the effects of solar radiation, air temperature, humidity and moisture (as an example, hot atmospheric environment reduces plant transpiration). Otherwise, considering together dry and wet canopy, one must subtract

[4]Noah land surface model evaluation of potential evaporation involves energy balance, atmospheric stability and aerodynamic resistance; in this thesis the computation is not reported.

from the equation 2.17 the fraction of water intercepted by leaves (Godfrey, 2010) to obtain

$$E_t = \sigma_f E_p P_c \left[1 - \left(\frac{W_c}{S}\right)^{0.5}\right], \tag{2.19}$$

where W_c is the intercepted canopy water content and S is the maximum canopy water capacity. Finally, last contribute to surface evaporation is related to sublimation from snowpack if present (this contribute is not discussed in this thesis because it does not affect the analysis in a relevant way).

Chapter 3

Eddy covariance measurements

In order to perform the evaluation and validation of SurfPro statically parameterizations, direct observations of Atmospheric Boundary Layer quantities are required. Thanks to the collaboration between CRMA - ARPA FVG and the Department of Agriculture and Environmental Sciences of the University of Udine, micrometeorological data collected during the year 2015 by a an eddy covariance tower located on an agricultural field are available. Obliviously, the location where the data are measured establishes the route of the thesis in terms of the characteristics of ABL fields, in this case the focus is on a rural environment and particular attention is required on the presence of the plants and their life cycle, that are able to modify the surface energy budget, especially for what concern to the term of latent heat flux.

The supplied dataset collects measurements widely usable in many fields of environmental science, however their primary purposes involve agronomic studies, in particular about CO_2 emissions from maize crops (Alberti, 2010). This fact has an impact, as will seen, on the improvement of data quality and on the measurement availability during the plant life cycle compared to the worsening of data and measurement unavailability when crop is not present on the agricultural field and less attention was payed to collected data. For this reason, together with the eddy covariance measurements, also satellite observations are considered in order to perform the evaluation of SurfPro statically parameterizations.

Besides that, the eddy covariance tower which collects the Atmospheric Boundary Layer quantities refers to the European Eddy Fluxes Database Cluster, a network that would support standardization, integration and collaboration between different European databases with the aim to provide high quality data processing and sharing tools. Moreover, this database follows the FLUXNET global network standardization for the analysis of observations from micrometeorological tower sites; which operate on a long-term and continuous basis. As will be seen in this chapter, the international standard permits the evaluation of available micrometeorological data by means of quality flags that can be used to describe the suitability of tower data in the assessment of SurfPro model parameters.

Furthermore, a note is required on the fact that purpose of this work forces to use direct observations, therefore all the inferences about Atmospheric Boundary Layer quantities have to start only from available rough data collected by eddy covariance

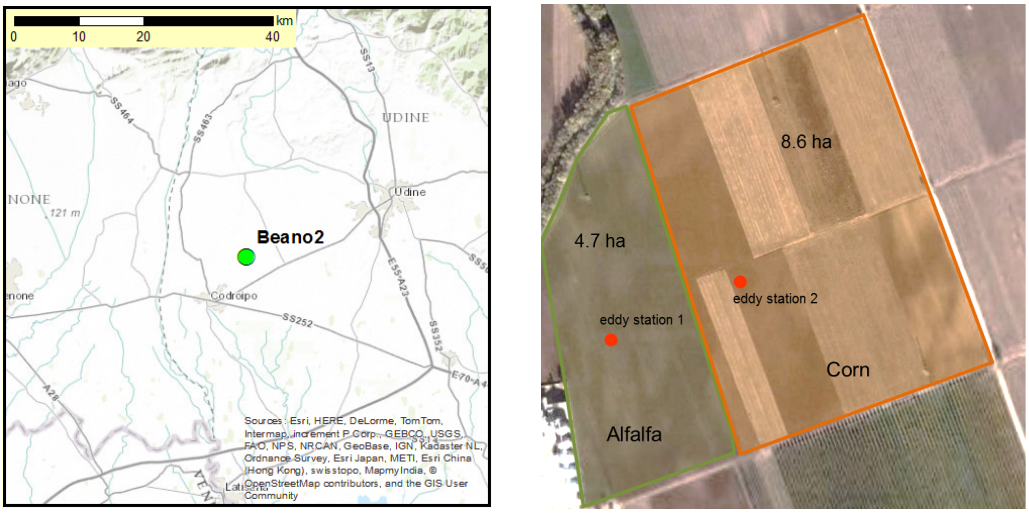

Figure 3.1: On the left-hand side the topographic map reports the site of eddy covariance experiment. While, on the right-hand side the micro-localization is reported.

tower without any gap filling[1] of data. In other words, theories and models widely accepted by the scientific community (i.e. similarity theory) can be used for the validation of parameters only if derived from the actual observations.

3.1 Site description

As was introduced, the available eddy covariance measurements are detected by an eddy covariance tower (and collected in the FLUXNET network) located on an maize field during the year 2015. In particular, the tower is sited in the agricultural neighborhood of Beano Village, in the Friuli Venezia Giulia plain (Italy, see figure 3.1), and the site is named IT-Be2 by the FLUXNET network.

In the table 3.1 are summarized the main information about Beano eddy covariance site: the firsts rows contain general information, after that the location is reported with some mean annual characteristics measured during the period of observation, finally the focus is on the type of agricultural land use and on the climate classification. In particular, the knowledge of the climatatological features related to a measurement site is fundamental for a correct evaluation of the available observations. However, for the purpose of this thesis the Köppen global climate classification is not sufficient to give complete information of the site, therefore a further division of the Friuli Venezia Giulia climate is considered. As said previously, the eddy covariance tower is sited in the Friulan plain which constitutes a climatic region in itself and can be explained considering the main meteorological quantities such as temperature, precipitations, solar radiation and wind (the description of how quantities are measured will be explained later in the chapter 6) reported in figure 3.2.

[1] The gap filling consists in the filling of data vacancies using standardized mathematical models. This post processing method is widely used in the evaluation of fluxes because unfavorable micrometeorological conditions and instrument failures can lead to several gaps in the data set.

General site information	
Site ID	IT-Be2
Site name	Beano 2
Country	Italy
Latitude	46.0043
Longitude	13.0278
Elevation (m)	30
Mean annual temperature (°C)	13.5
Mean annual precipitation (mm)	1216
Land use	Irrigated maize cropland with annual tillage
Climate classification	Warm temperate fully humid with warm summer

Table 3.1: Extract of FLUXNET information about the eddy covariance site used for the analysis; complete description can be found in the FLUXNET website, https://fluxnet.ornl.gov/site/4083. Climate classification is referred to Köppen system based on empirical observations; using its symbolism, Beano site corresponds to Cbf class. This classification sometimes leaves space to some arbitrary decisions according to the area considered, in fact with reference to OSMER (2014), the entire Friulan plain is classified with the symbol Cfa, warm temperature fully humid with hot summer.

3.1.1 Climatological features

Thanks to the position of the region between the Alpine chain and the Adriatic sea, temperatures in Friulan plain are not involved by considerable extreme values, in fact temperatures lower than $-5\,°C$ during the winter and higher than 32-33 °C during summer are rare to observe (OSMER - ARPA FVG, 2014); moreover, the mean annual temperature is between 13 °C and 14 °C. Beano micrometeorological tower is sited in the central area of the plain, where continental characteristics are highlighted, for instance relevant annual thermal excursion and daily thermal excursion. Instead in the Northern and in the Southern part of the plain slightly different climatological features are caused respectively by lower winter temperatures and by the mitigating effect of the sea on thermal excursions.

Considering the precipitations, the whole Friuli Venezia Giulia Region (and also the Friulan plain) is characterized by a large number of days involved in precipitations and by a relevant amount of them over the whole year, with high storm occurrence during the hot season. In particular, the eddy covariance tower is situated in a site where 40-45 days of the year are affected by storms, whilst those attendances increase to 97-98 days considering all the precipitations those numbers increase to 97-98. Moreover, if the amount of precipitations is considered, a quantity between 1300-1400 mm falls in the plain non uniformly distributed during the year: on average over the period 1961-2013, February is the less rainy month (60-90 mm on the plain) and November is the most rainy month, with 150 mm. Moreover, few words are devoted to the rain origin: during the months between October and May the precipitations are mainly due to synoptic circulation that leads Southern humid fluxes to the region, while during other months the precipitations are mainly due to convective motions conditions that cause local storms.

Talking about solar radiation, figure 3.2 shows that the annual average value of about $4800\,\mathrm{MJm^{-2}}$ is recorded on the plain, with a seasonal pattern that detects lower values on February (closed to $5000\,\mathrm{kJm^{-2}}$) and highest on July (just below $25\,000\,\mathrm{kJm^{-2}}$) with a mean of 10 hours of sunshine in a single day. These values are mainly dependent to the latitude and to the presence of atmospheric aerosols, but an important source of non uniformity is the recursive presence of clouds in some parts of the region in particular periods of the year (e.g. formation of clouds over Alpine area during the summer months).

Finally, the winds blowing in the region are determined by the configuration of the territory and mainly come from North and North-East, this is true also for the Friulan plain climatological area; however, some local winds and breezes are present in front of the main river valleys. Therefore, wind magnitudes can widely differ according to the kind of wind (i.e. synoptic, breeze) and to the morphology, however for the purpose of the thesis the previously cited main features are adequate.

3.1.2 Soil and land use features

Having studied the climatological features of the chosen site, now the focus is on the characteristics of the Beano ground and on what is above. Firstly, according with the FAO soil type classification, the soil can be classified as a Chromi-Endoskeletic Cambisol, that are relatively young soils with moderately profile development, a red hue and a relevant presence of gravel or other coarse fragments; the ability of these soils to hold the water makes them a good agricultural land and widely used.

Particular attention is paid on two soil properties strictly connected with the eddy covariance fluxes and in particular with the latent heat flux: the soil field capacity and the soil wilting point. The soil field capacity is defined by the Soil Science Glossary Terms Committee (2008) as the content of water, on a mass or volume basis, remaining in a soil 2 or 3 days after having been wetted with water and when free drainage is negligible; on the other hand the wilting point corresponds to the maximum amount of water, on a mass or volume basis, that soil can hold back without that roots of plants manage to absorb it, and plants will wilt. In Beano site these values are respectively equal to 23% and 12%.

By the point of view of what is above the surface, as previously mentioned the eddy covariance tower is sited on an agricultural field of 13.3 ha, where irrigated maize was cultivated since 1976 (Alberti et al., 2010). In particular, considering the maize crop during the year 2015, main events are summarized: the seeding took place on 1^{st} April, during the period between the end of May and the end of August the field was watered, finally the harvest has been made on 10^{th} September. The practice of irrigation obviously modifies the water balance between atmosphere and land surface (therefore the latent heat flux) and could be a problem for our study. However, it is a widely used agricultural treatment that must be considered in designing an atmospheric boundary layer model; as an example, during the year 2011 the 77.8% of horticulture fields in Friuli Venezia Giulia region are regularly been watered and for another 7.9% of them the watering was sometimes used as a support technique to the crop (Cattivello, 2013).

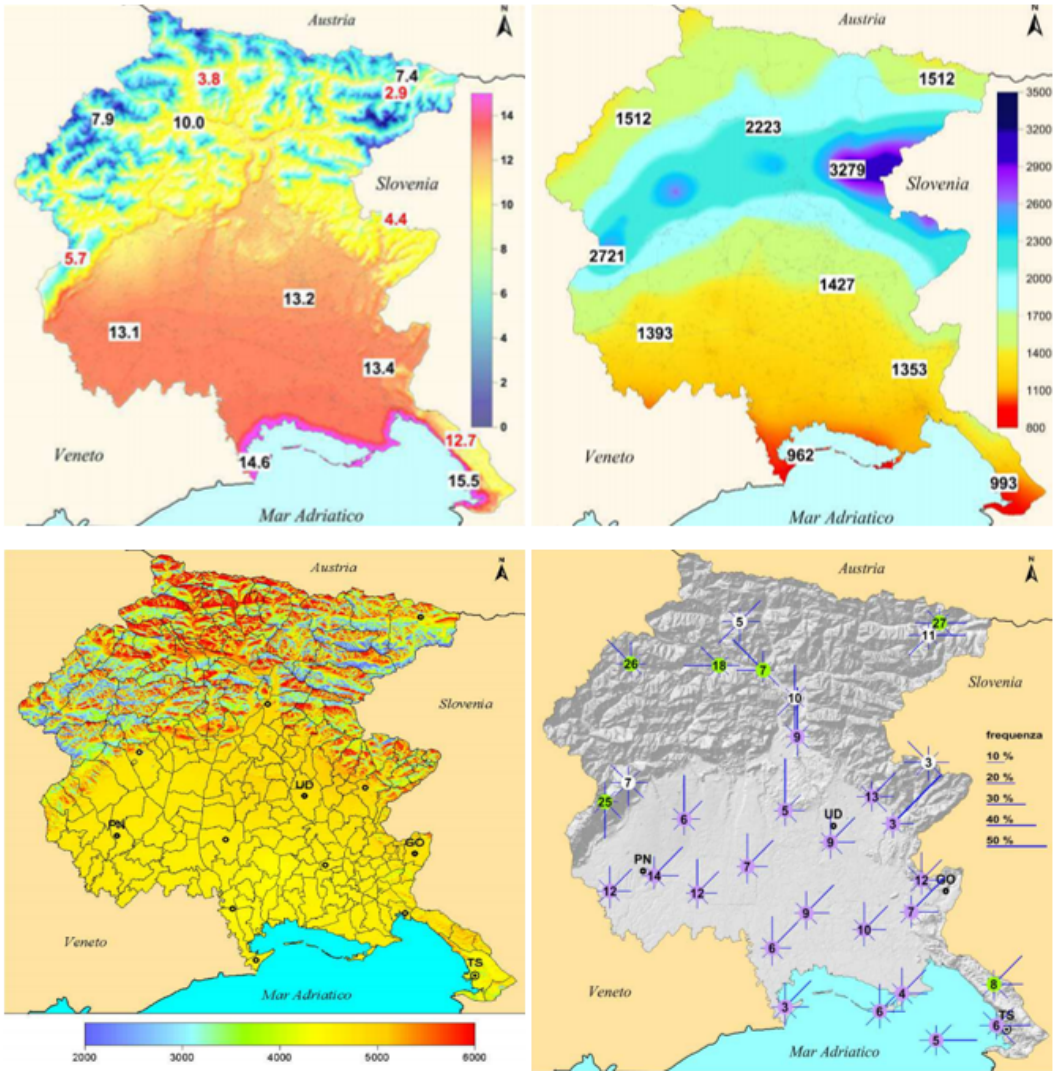

Figure 3.2: Climate features of Friuli Venezia Giulia region from OSMER (2014): starting from the top on the left-hand side, mean annual temperature, mean annual precipitation, mean annual solar radiation and percentage of wind occurrence are reported. Temperatures are evaluated during the period 1993-2013 and reported in °C; precipitations during the period 1961-2013 and measured in mm; incoming solar radiation in the decade 1995-2005 and reported in MJ/m^2; finally, the wind speed and horizontal direction during the period 1999-2013, the numbers indicate the occurrence in percentage of wind down ($v < 0.5\,\mathrm{m/s}$).

3.2 Eddy covariance method

Tower measurements are widely used to evaluate the exchange of heat, water, momentum and trace gases, such as carbon dioxide, close to the Earth's surface; in the context of field measures these fluxes must be measured applying the eddy covariance method. As saw in the first chapter, the mathematical context of the Atmospheric Boundary Layer and related fields is based on statistical analysis, as a natural consequence the practical implementation must provide a large amount of high frequency measurements to the data processing tools, in order to build up usable dataset.

The purpose of the eddy covariance method based on tower measurements is to estimate the vertical turbulent transport of quantities to and from the Earth's surface, by measuring the vertical turbulent velocity and the turbulent part of quantity affected (set of equations 1.12-1.14). As an example, the comparison between a situation in which there is not water exchange through the surface and a situation in which the molecules of water vapor pass from the surface to the atmosphere is taken into account. Considering the first case, micrometeorological tower detects the water vapor molecules carried over the measured area by horizontal mean flow and perturbed roundly by turbulent swirls; due to circular motion, the same amount of water is carried upward and downward and the net water flux is null. Conversely, in the second case, if the ground surface provides water vapor to the atmosphere, the eddy covariance tower detects more molecules moving upward than downward because the downward moving molecules are carried away by the mean flow; therefore the vertical water vapor net flux is different from zero and is directed upward.

What just explained is the physical essence of eddy covariance measurements, by the practical point of view, vertical velocity and interested quantities (e.g. water vapor) are surveyed over averaging periods of 10-60 minutes, their turbulent parts are extracted and multiplied each other, finally the average of the product determines the vertical turbulent flux associated to the time domain. As one can imagine, this method requires very sophisticated instrumentation, in fact turbulent fluctuations happen very quickly and respective changes in concentration, density or temperature are quite small, and therefore must be measured both very fast and with some accuracy (Burba, 2013); in particular, for a suitable description of turbulent fluctuations a time sampling of 10-20 Hz is required.

Besides of the assumptions which allow for the covariant formulation of the turbulent fluxes, such as the split representation of flow in mean and turbulent part, the fulfillment of steady state conditions (i.e. all statistical parameters do not vary over the averaging time), the incompressible fluid approximation and the assumption of a negligible mean vertical flow, planning an eddy covariance experiment additional evaluations are required to know. Firstly, the terrain where the tower is placed must be horizontal and uniform, in addition the flux is assumed to be fully turbulent (most of the net vertical transfer is done by eddies); finally the measurements at a point can represent an upwind area and the measured fluxes result from meteorological condition joined to the characteristic of the ground region around the tower called flux footprint.

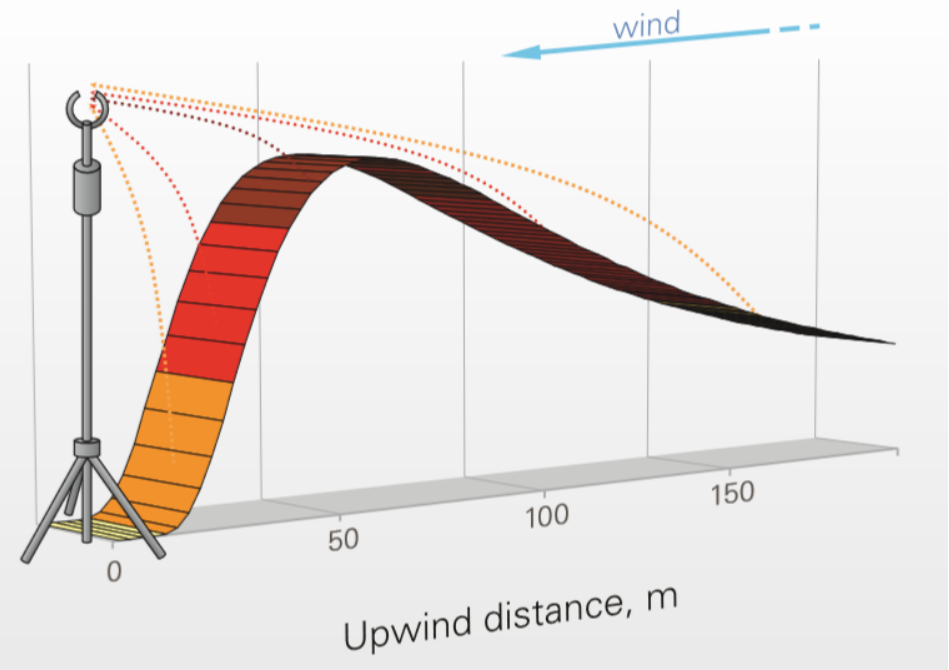

Figure 3.3: An example of flux contribution according to the upwind distance from the station. Larger contribution is coming from the intermediate area of the flux footprint; around the tower lower contribution can be noticed. By Burba G. (2013), *Eddy Covariance Method for Scientific, Industrial, Agricultural and Regulatory Applications.*

3.2.1 Flux footprint

This area can be described in the simplest way as the area seen by the instruments on the tower, or in other words the area that affects the flux measurements, and can be described using the *fetch*, the upwind distance of footprint borders from the tower. However, the portions of the footprint area do not contribute in the same way to the final flux evaluation and a radial pattern of the contribution can be observed, as shown in figure 3.3, that behavior is due to different factors, such as measurement height, elements on the field and atmospheric thermal stability. For near-neutral conditions Schuepp et al. (1990) modeled the cumulative normalized contribution to flux measurement (CNF) as

$$CNF(x_L) = -\int_0^{x_L} \frac{U(z-d)}{u_* k x^2} e^{-\frac{U(z-d)}{u_* k x}}, dx = e^{-\frac{U(z-d)}{u_* k x_L}}, \tag{3.1}$$

where x_L is the distance from the station, U the mean wind speed, z the measurement height, u_* the friction velocity, d the displacement length and k the Von Karman constant.

Considering the variation of footprint according to the measurement height, it is straight that the peak contribution is closed to the tower when the measurement height is lowered. Moreover, the increasing of the measurement height leads to the definition of an area around the station that does not affect the evaluation of the flux (i.e. a flux footprint with a hole in the center is obtained). Secondly, the effect of terrain roughness is evaluated: the presence of rough elements leads the footprint

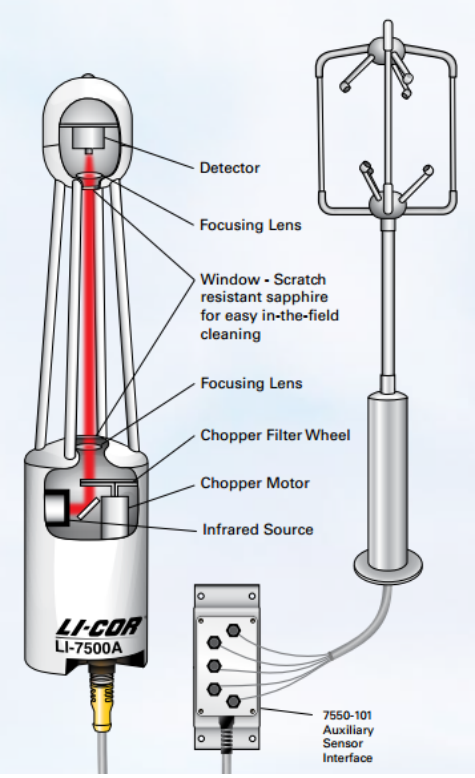

Figure 3.4: Scheme of the eddy covariance instruments: the open path infrared gas analyzer on the left-hand side and the sonic anemometer on the right-hand side.

to became less extensive than in smooth ground; however in this case the footprint near the station is less affected by roughness and the blind area (i.e. hole in flux footprint) is smaller than in the previous dependence. Even if the effects on flux footprint are qualitatively similar, the empirical distributions of the contribution to fluxes according to measurement height and terrain roughness are quite different and vary with the chosen configuration.

Furthermore, for the same measurement height and terrain roughness, atmospheric instability constitutes a further element of variability: atmospheric instability tends to make the footprint less extensive, whilst stability increases it, but at the same time creates a blind zone near the station. As one can deduce, the three contributions make the evaluation of the flux footprint extremely variable with widely changes during the sampling domain.

Usually, to account for the large variability of the flux footprint, a control flag is introduced in the post-processing protocol: if the tower detects fluxes from an area with different characteristics than the studied region, the control flag results negative and the measurement must be discarded (there are different footprint quality flags for the various fluxes). However, for the purpose of the thesis strictly conditions on flux footprint are not required, even in the worst case the area detected by the tower is inside the integration domain of the SurfPro computational cell (with the contribution to the flux that rapidly decreases over 250 m). As will be seen in the final section of this chapter, most important condition to realize is the evaluation of measurement usability, and consequently the definition of their limitations.

3.3 Experimental equipment

Having explained the principles of eddy covariance method, now the features of the micrometeorological station and the instrumental characteristics are treated noting that the Beano measurement site is implemented with an eddy covariance flux system associated to a weather station to take into account environmental measurements.

3.3.1 Eddy covariance system

For what concerns the evaluation of turbulent fluxes, the measurement height is 2.5 m and the system comprehends a sonic anemometer and an open path infrared gas analyzer, both of them record data at a frequency of 20 Hz (Alberti et al., 2010); after the acquisition, fluxes are obtained by eddy covariance processing over 30 minutes. Figure 3.4 shows the two instruments used, which constitute the easier example of eddy covariance station; in order to take into account the same air mass the horizontal distance between them should not exceed 20 cm, whilst to avoid the reciprocal distortion of the natural flow the gas analyzer is usually positioned slightly below the sonic anemometer level.

The sonic anemometer measures the three wind speed components (from which the orthogonal component to the advection plane is obtained) using acoustic signals, usually ultrasound wave burst (Burba, 2013). It is composed by two sets of three non-orthogonal transducers supported by a rod, every transducer is coupled with one of the other set and the acoustic signals travel between them. The time taken by the acoustic signals to travel between opposite traducers (e.g. from A to B) is equal to the distance traveled over its velocity, that is the sum between the speed of sound[2] (c) and the wind speed,

$$t_{A-B} = \frac{d}{c + w_s}; \tag{3.2}$$

Instead, the acoustic signal travels the reverse path (e.g. from B to A) with another velocity, resulting by the difference between the speed of sound and the wind speed, so the travel time results

$$t_{B-A} = \frac{d}{c - w_s}. \tag{3.3}$$

Therefore, the wind speed is computed from the difference in time it takes for an acoustic signal to travel the same path in opposite directions,

$$w_s = \frac{d}{2}\left(\frac{1}{t_{A-B}} - \frac{1}{t_{B-A}}\right). \tag{3.4}$$

In addition to the turbulent wind speed, sonic anemometer can also be used to compute the sonic temperature starting from the speed of sound by the equation

$$T_s = \frac{c^2}{y_d R_d} - 273.15, \tag{3.5}$$

[2]The well-known value for the speed of sound in dry air at 20 °C (343 m/s) must be corrected to account for air temperature, humidity, air density and pressure

where $y_d = \frac{c_p}{c_v}$ is the ratio between specific heat at constant pressure and constant volume and R_d is the gas constant for dry air. However in the evaluation of sensible heat flux ($H_0 = \frac{1}{\rho C_p}\overline{w'\theta'}$) the virtual potential temperature is needed, to get it two further steps are required. Firstly, the presence of water vapor must be considered, it is measured by the gas analyzer (as will see later) and permits to obtain the virtual temperature via a corrective factor function of the specific humidity (q),

$$T_v = T_s \frac{1 + 0.61q}{1 + 0.51q}. \tag{3.6}$$

Secondly, the conversion from virtual temperature to virtual potential temperature is performed (as shown in appendix) to evaluate the changes in pressure and brings to the final expression

$$\theta_v = T_s \frac{1 + 0.61q}{1 + 0.51q} \left(\frac{p}{p_R}\right)^{-\frac{R_d}{c_p}}. \tag{3.7}$$

The other fundamental instrument in an eddy covariance tower is the gas analyzer, a device that measures gas content in the air. In Beano micrometorological tower is installed the widely used *Li-7500* open path infrared gas analyzer suitable for the analysis of CO_2 and H_2O fluxes, nevertheless in this thesis the only eddy covariance latent heat flux is used. This optical instrument is based on the physical process of light absorption by gas (or vapor) molecules in a sampling volume; in addition, to reach the purpose of detecting CO_2 and H_2O densities the appropriate light must be infrared, because these molecules absorb in a spectral band centered respectively at 4.26 nm and 2.59 nm.

The main components of the *Li-7500* are the infrared source, the detector and the chopper wheel; the last one is a sort of filter equipped with different windows that permits to modulate the sent beam to distinguish the detection process of the different molecules. As an example, if the gas analyzer have to measure the water density, the chopper wheel only allows light at the 2.59 nm spectral band to pass through and the detector will measure how much of known light is absorbed only by water molecules, in the next step the result will be calibrated using a reference band to provide the actual density measure of the water. Afterwards, the chopper wheel rotates to consider the carbon dioxide. Finally, because of the eddy covariance flux equations are based on mixing ratios the densities q_c must be converted accounting for temperature T, pressure p and water vapor mole fraction X_w,

$$s = q_c \frac{RT}{P(1 - X_w)} \tag{3.8}$$

with q_c the measured density.

Moreover, the sonic wind speed will be used in the evaluation of roughness length and friction velocity (already defined in section 1.4.3) starting from the vertical flux of horizontal momentum, which can be obtained from the measured fluctuations of wind speed.

In conclusion, in the context of this thesis eddy covariance experiment allows for the measurements of vertical eddy fluxes of momentum, sensible heat and latent

heat; through the set of equations

$$\begin{aligned} \tau_{zi} &= \overline{\rho_d}\ \overline{w'u_i'} \\ H &= \overline{\rho}\ C_p \overline{w'T'} \\ L_v E &= L_v \frac{M_w/M_a}{\overline{P}}\ \overline{\rho_d}\ \overline{w'q'}. \end{aligned} \tag{3.9}$$

3.3.2 Environmental measurements

Together with the eddy covariance system, a weather station is placed on the measurement site. In the context of this thesis, environmental measures are fundamental to employ a measure of how much representative are the measurements performed in Beano site; in addiction, these kind of measure will be important in the quality assessment of some model outputs (e.g. soil content).

The weather station is equipped to measure different meteorological and environmental quantities for a wide range of purposes, to facilitate the text reading the only measurements used in the thesis are reported. Firstly, the station detects the precipitations having place in the site, secondly it measures air temperature, air humidity and incoming solar radiation flux, in addition wind speed and direction are measured, and finally it estimates two quantities related to the soil, such as the soil heat flux and the soil water content in the first 30 cm from the surface.

3.4 Quality control of eddy covariance measurements

As previously reported, the eddy covariance method must satisfy specific conditions related both to the experimental design (i.e. tower placed on horizontal surface) and to the covariant assumptions (i.e. flows as mean part plus turbulent part, steady state conditions, footprint). The first ones are unchanged during the time of experiment, while the second ones vary in accordance with the atmospheric conditions and can reduce the accuracy of eddy covariance measurements when the theoretical conditions are not met. To account for this, the CarboEurope network standardizes data quality assessment using two test which verifies the fulfillment of theoretical requirements and provide a uniform classification of measurements (Mauder and Foken, 2004).

Steady state test The first test considered by the European standardization is the steady state test (remember that steady state hypothesis assumes that over the averaging time the statistical parameters remain unchanged), that would compare the statistical parameters determined for the averaging period and for short intervals within this period. As an example, the covariance of vertical wind speed and virtual potential temperature is considered (i.e. sensible heat vertical flux) and an averaging interval of 30 minutes is considered, the result is simply denoted as

$$\overline{w'\theta_v'}. \tag{3.10}$$

If the averaging time is divided in 6 intervals of 5 minutes and if the steady state condition is satisfied, the covariance over the 30 minutes can be computed averaging

Steady state test (%)	ITC test (%)	Quality control flag
< 30	< 30	0
< 100	< 100	1
> 100	> 100	2

Table 3.2: Definition of quality control classes using the results of steady state and integral turbulence characteristics tests.

the covariance of the subsets within this period (lasting 5 minutes) and is denoted with the subscript that indicates the steady state hypothesis

$$\left(\overline{w'\theta'_v}\right)_{ss} = \frac{1}{6}\sum_{i}^{6}\left(\overline{w'\theta'_v}\right)_i . \tag{3.11}$$

The comparison between the obtained values is actually performed through the relative bias

$$RN_{cov} = \left| \frac{\left(\overline{w'\theta'_v}\right)_{ss} - \overline{w'\theta'_v}}{\left(\overline{w'\theta'_v}\right)_{ss}} \right|, \tag{3.12}$$

and a time series is considered to be steady state if the value is lower than 30% (Foken and Wichura, 1996).

Integral turbulence characteristics test The second test is devoted to asses the development of turbulent conditions and is based on the flux-variance similarity; this similarity means that the ratio of standard deviation of a turbulent parameter and its turbulent flux is nearly constant or function of the stability. This ratio is both measured and modeled with a parameterization[3] function of the stability parameter, afterwards the relative bias between the two is computed as

$$ITC_\sigma = \left| \frac{\left(\frac{\sigma_X}{X_*}\right)_{model} - \left(\frac{\sigma_X}{X_*}\right)_{meas}}{\left(\frac{\sigma_X}{X_*}\right)_{model}} \right|. \tag{3.13}$$

A well developed turbulence can be assumed if ITC_σ assumes values less than 30%.

Overall flag system Taking into account the two just described tests, the CarboEurope network has defined a quality control flag system that comprehends three classes described by a number from 0 to 2 and reported in table 3.2. Highest quality data are included in class 0, good quality data in class 1, while class 2 comprehends questionable data quality that must be discarded.

[3]The definition of parameterizations used in the model and of the model itself would require further explanations that fall outside the theoretical basis explained in chapter 1.

Chapter 4

Measures representativeness

Having described the available dataset from eddy covariance measurements, next step consists in the definition of their spatial and temporal representativeness; this means that an assessment of the operative limits of measures made by Beano eddy covariance tower is performed. At the end of the analysis, a limit radius from Beano site will be defined, within that the comparisons between measurements and simulations are allowed. The importance of performing this analysis is the definition of potential local peculiarities of the site, both spatial and temporal, correlated with the possibility for the simulations to reproduce the reality measured by Beano station; in fact, it could be possible that models can not be able to take into account some site characteristics.

To achieve this goal, Friuli Venezia Giulia OSMER[1] network for meteorological observations is considered, the stations within a 35 km radius from Beano site are selected and observation of some variable are correlated with meteorological available measurements by eddy covariance tower. Correlation was performed for the year 2015 considering global radiation, humidity precipitation, temperature and wind speed during the different seasons, to take into account the temporal variability; this analysis offers us the possibility for a quick digression about Friuli Venezia Giulia meteorology, the base for this representativeness evaluation.

Before proceeding, it is remarked that the primary aim of the following section is the validation of Beano site measurements with some statistical significance, that can vary according to season and to variable considered. In order to do that, it is necessary to provide to the reader some information about the OSMER meteorological observation network.

4.1 The OSMER meteorological network

The OSMER meteorological network is the Friuli Venezia Giulia network for the meteorological monitoring, and is one of the tools used for the daily weather forecasts and for the understanding of meteorological phenomena. To achieve its goals, OSMER collects observations from networks of automatic meteorological stations, radars and hailstorm panels placed in meteorological and climatological interesting areas.

[1] Osservatorio Meterorologico Regionale, regional meteorological observatory.

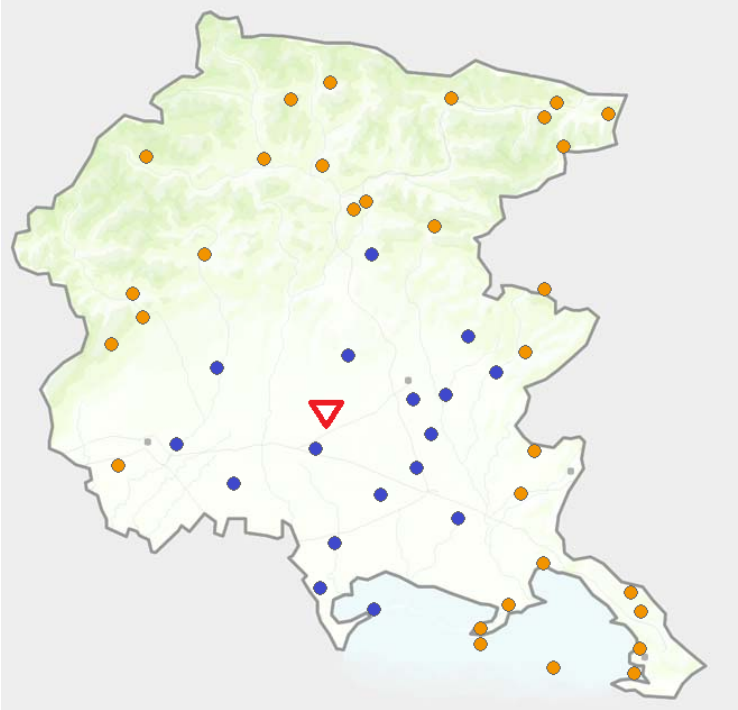

Figure 4.1: Map of OSMER meteorological monitoring network in Friuli Venezia Giulia region. Blue circles define stations within 35 km radius from Beano eddy covariance tower represented by red triangle.

By the point of view of the validation of the eddy covariance tower measurements, the OSMER meteorological network fits the statistical requirements: it is composed by 51 stations situated in the region (figure 4.1) that satisfy World Meteorological Organization (WMO) standards to ensure adequate uniformity in the storaged data. In particular, these standards involved the site definition and it representativeness, the frequency and timing of observations, and the meteorological variables to collect.

Where stations are used for several purposes (e.g. aviation, synoptic and climatological purposes), the most stringent requirements involve the exact location of the observing sites and their sensors. Following WMO publications (2008, 2015), synoptic and climatological stations in a regional or national network must be placed on ground covered by short grass or over a representative surface of the locality. In addition, there should be no steeply sloping ground in the vicinity, the distance of any obstacle (e.g. trees, buildings, walls) from the raingauge should not be less than twice the height of the object and it must be satisfactory to avoid that obstacle obstructs the horizon of the sunshine recorder. Finally, adequate distances between installations are required, according to their features and purposes. A special meaning is required for coastal and special stations (e.g. situated near volcanoes), whom must fit particular conditions not treated in this context.

Talking about time sampling, WMO recommended the meteorological variable should be sampled continuously or repeatedly over suitable time in order to obtain both representative means and extreme values. The averaging time should be short compared with the time scale of discontinuities such as fronts or squall lines, which usually delineate air masses with different characteristics. For the purpose of the

thesis one hour sampling is considered, for which the observations are the averages over the last 10 minutes of every hour; this is valid for the measurement of solar incoming radiation, humidity, temperature and wind speed. Whereas, measurements of precipitation are cumulative observations over the same time interval.

4.1.1 Meteorological variables

Last concept permits us to face the practical question of the WMO standardization of the used observations. First of all, global radiation is considered, it is defined as the solar radiation received from a solid angle of 2π on a horizontal surface, and includes radiation received directly from the sun's disc, as well as diffuse sky radiation that has been scattered in traversing the atmosphere. The instrument used for measuring global radiation is the pyranometer, that must meet among others the requirements of sensitivity, stability, linearity and have to be calibrated according to environmental factors. For its purpose, it measures radiation confined to the spectral range from 300 to 3000 nm (short-wave radiation), with a standard deviation at most of 0.4 MJm^{-2}.

Continuing with the description of variables, humidity is proposed as the quantity suitable for defining water vapor contained in a mass of air; however there are different definitions for its estimation at the Earth's surface (e.g. mixing ratio, specific humidity, relative humidity). Friuli Venezia Giulia OSMER network provides moisture in the air as relative humidity, that specifies the ratio of the observed vapor pressure over the water vapor saturation pressure at the same air temperature and pressure, it is expressed as a percentage and target accuracy for high quality data is 1%. At the end, different types of hygrometers can be used for measurements, as long as they reach the accuracy target.

Furthermore, the amount of precipitation shall be the amount of liquid precipitation and the liquid equivalent of solid precipitation over the time sampling, this definition includes all the products of condensation of water vapor deposited from air onto the ground, e.g. rain, hail, snow, dew, rime and fog precipitation. The unit of measure is the linear depth, usually in millimeters, defined as the ratio between the volume of precipitation detected and the area of ground considered; for daily amounts of precipitation (and then for more frequent sampling), WMO recommends at least a resolution of 0.2 mm. At the end, raingauge is the instrument used for the measurements and must be designed to minimize the effects of wind, evaporation and splashing, that are the most frequent sources of error.

Next quantity taken into consideration is the air temperature, the physical quantity characterized by the mean random motion of molecules into an air parcel. Going into details, for meteorological purposes WMO (1992) defines air temperature as the temperature indicated by a thermometer exposed to the air in a place sheltered from direct solar radiation, and obviously the International System of units is complied for the definition of scale and unit. Moreover, WMO leaves the choice of the instrument used (e.g. liquid-in-glass thermometer, resistance thermometer, thermocouples) but defines its height from the ground to obtain representative air temperature measurements, varying from 1.25 to 2.00 m, and the accuracy requirements according for the operational range, e.g. for ordinary temperatures (in a range between $-30\,°C$ and $45\,°C$) maximum error less then $0.2\,°C$ is required.

Observation	Unit	Absolute maximum error
Global radiation	Jm^{-2}	$\pm 1 Jm^{-2}$
Relative humidity	%	$\pm 1\%$
Precipitations	mm	± 0.1 mm
Air temperature	°C	± 0.1 °C
Wind speed	ms^{-1}	$\pm 0.1 ms^{-1}$

Table 4.1: OSMER network meteorological observations used for representativeness evaluation of Beano eddy covariance measurements.

Finally, surface wind speed is defined as the modulus of the three-dimensional vector defining wind velocity. However, surface wind is considered a two-dimensional vector quantity specified by speed and direction; while the wind velocity still remains the vector modulus, the direction is described by the horizontal angle of wind from the North, in clockwise direction. Measurements of these quantities are made, respectively, by anemometer and by a tape installed into a goniometric reference frame. However, for the purpose of this section, only wind speed are considered because of the great variability of wind direction according to local properties of the site.

Meteorological quantities considered for the evaluation of the correlation coefficients with Beano eddy covariance measurements are summarized in the table 4.1, associated with some accuracy estimates that can eventually improve WMO requirements.

4.1.2 OSMER network meteorological stations

To achieve the goal, 17 stations within 35 km radius from Beano eddy covariance tower are selected and reported in table 4.2. As Beano measurement site, most of them are situated in Friulian plain; exceptions are the coastal station sited in Lignano Sabbiadoro and the stations sited onto hilly areas (i.e. Cividale del Friuli, Faedis and Gemona). The coastal station site is characterized by the moderate ventilation and by the influence of Adriatic sea on humidity and air temperature, instead meteorological variables measured by the second ones are mainly driven by local valley effects. In spite of peculiarities, these stations are still considered in the analysis because of a larger statistical sample is preferred and because they permit reveal the peculiarities of the region.

4.2 Statistical Analysis

For listed variables and for selected stations, the observations during the year 2015 are considered, and statistical significance of Beano eddy covariance measurements is evaluated using correlation Pearson test. Generally, correlation is a technique for investigate the relationship between two variables; in particular, Pearson correlation coefficient is a measure of the linear dependence between them. It is defined as the ratio between the covariance of the two variables and the product of their standard deviations; defining x and y the variables, it is

$$r = \frac{cov(x,y)}{\sigma_x \sigma_y} = \frac{\sum (x - m_x)(y - m_y)}{\sqrt{\sum (x - m_x)^2 \sum (y - m_y)^2}}. \tag{4.1}$$

Station	Code	Position (lat, lon)	Distance (km)
Codroipo	COD	45.95, 13.00	5.995
Fagagna	FAG	46.10, 13.07	11.701
Udine	UDI	46.04, 13.23	15.860
Talmassons	TAL	45.88, 13.16	16.789
Bicinicco	BIC	45.93, 13.24	18.787
San Vito al Tagliamento	SAN	45.90, 12.81	18.803
Lauzacco	LAU	45.98, 13.27	18.942
Pradamano	PRD	46.04, 13.30	21.415
Vivaro	VIV	46.08, 12.77	21.484
Palazzolo dello Stella	PAL	45.81, 13.05	22.038
Pordenone	POR	45.95, 12.68	29.504
Gorgo	GRG	45.74, 13.02	28.288
Faedis	FAE	46.13, 13.35	29.057
Cervignano del Friuli	CER	45.85, 13.34	29.504
Gemona del Friuli	GEM	46.26, 13.12	29.587
Cividale del Friuli	CIV	46.08, 13.42	31.533
Lignano Sabbiadoro	LIG	45.70, 13.15	34.782

Table 4.2: OSMER network stations within 35 km radius from Beano measurments site. For every station name of stations, codes, positions and distances from Beano tower are reported.

Pearson correlation coefficient could vary in a range from the extreme values of -1 and 1; that respectively indicate maximum anti-correlation (data lie on a perfect straight line with negative slope) and maximum correlation (perfect straight line with positive slope), while 0 means that no linear relationship involved the two set of variables.

However, correlation coefficients are not calculated between simple time-series of variables. First of all the time-series are divided into seasons, to account for the variability of the observations during the year and for avoid the correlation being dominated by the annual patterns (e.g. hot in summer, cold in winter). Afterward, starting from seasonal time-series, the bias with respect the seasonal averages are calculated and used for the calcuation of Pearson correlation coefficients.

After the assessment of the correlation coefficients, they are displayed according to the distance of measurement site from Beano eddy covariance tower; this representation permits the definition of decreasing trend in which correlation threshold can be selected and associated to a representative radius. To achieve the goal a threshold of 0.75 is selected, this is a strictly condition because it have to comes out from two dataset that collect measurements every hour for a whole season. Therefore, given the great number of available measurements (meteorological data measured by Beano eddy covariance tower are not affected by relevant defections), a correlation coefficient of 0.75 corresponds to a p-value less than 0.001, calculated by t-test[2]. It means that correlation between variables is statistically significant.

[2]T-value corresponds to $t = \frac{r}{\sqrt{1-r^2}}\sqrt{n-2}$, with n number of observations, in this case corresponds to hourly seasonal measurements.

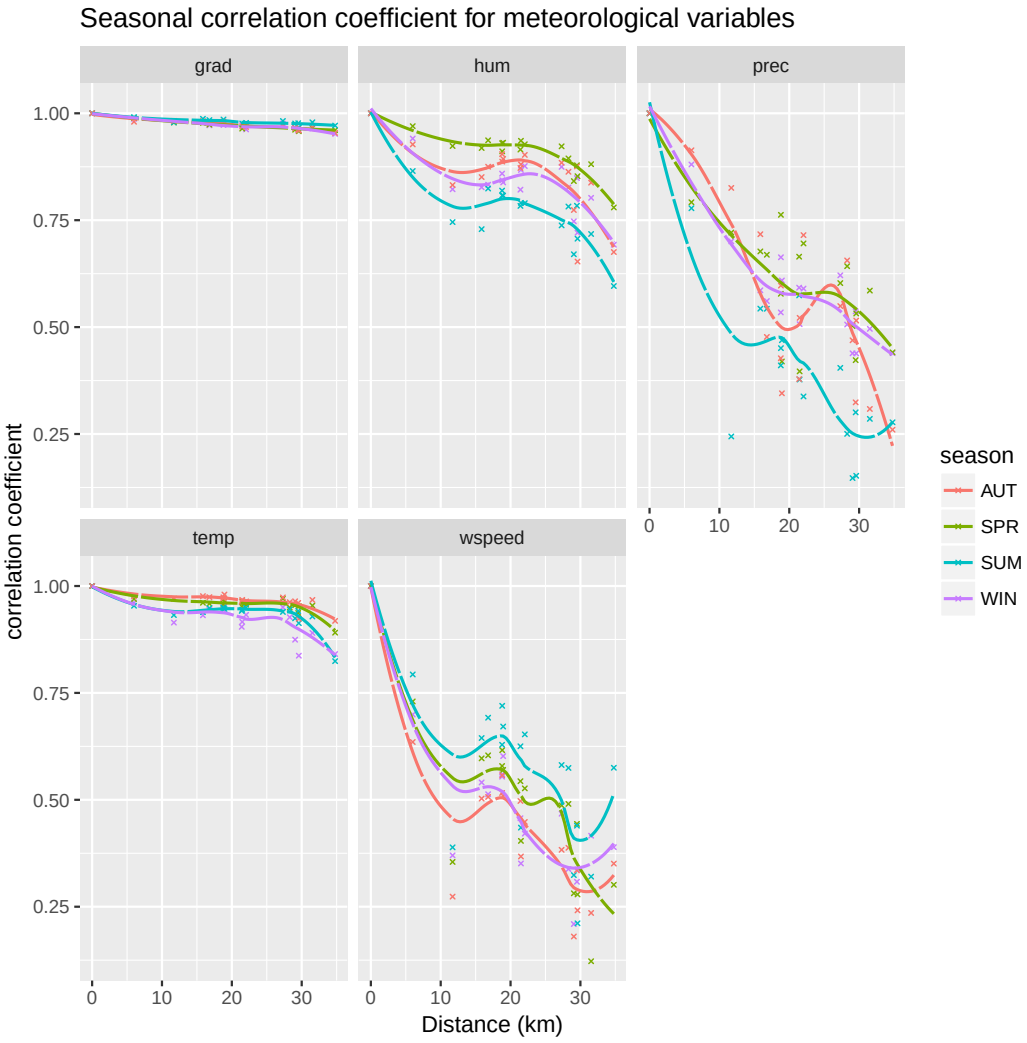

Figure 4.2: Seasonal Pearson correlation coefficient according to distance from Beano eddy covariance site and displayed separately for solar global radiation, relative humidity, amount of precipitation, air temperature and horizontal wind speed. Correlation are calculated using 2015 available measurement and fits are made by polynomial smoothing.

4.3 Correlation analysis results

Before discussing the results, some words are devoted to summarize main features of the analysis. First of all, the purposes are the description of peculiarities of the Beano site and the estimation of the limits for general meteorological model to reproduce the reality measured in Beano. Last aim means, for every variable listed above, the definition of a limit ray from Beano site within which comparisons between measures and simulations are allowed. To account for the intrinsic variability of the meteorological quantities, the correlation analysis is divided into seasons and for each of them different representative rays are evaluated.

Results are displayed in figure 4.2 grouped by meteorological variable and filtered to seasons; interpolations are made using a polynomial non linear fit calculated by R statistical software[3] (Cleveland, 1992); it was preferred to linear fit to take into account for some station site peculiarities. It is easy to see that all patterns follow a trend that indicate the decreasing of correlation respect the distance from reference station, with some exceptions related to some peculiar stations that could create depressions in drawing the fit, e.g. Fagagna station located 11 km away contributes to lower the correlation related to relative humidity and precipitations in summer, and related to wind speed in every season. For suitable analysis, deductions are made considering separately the meteorological variables.

Firstly, global radiation and air temperature are strictly correlated among them (i.e. mainly due to diurnal cycle), this brings to comparable patterns of correlation. They differ essentially for the spread of correlation among seasons that involves air temperature, caused by the presence of peculiar stations situated onto hilly areas[4], that detected lower temperatures with respect to plain stations, especially during winter (purple line). In both cases and for every season, correlation coefficient threshold is overtaken by whole stations considered, therefore every quantity strongly linked to solar radiation (as is the temperature) measured in Beano site is representative for an area delimited at least by 35 km radius, or at least for rural, WMO-compliant sites incuded in that area.

Secondly, relative humidity is a site-specific meteorological observable, in fact it strongly depends from geographically position of station and to features around it (e.g. woods, urban environment). Patterns of the seasonal correlation detect this characteristic and delineate well-marked distinctions among the seasons, i.e. saddle shape is reproduced in every season with different coefficient magnitudes. In particular, during summer the correlation related to relative humidity is constantly lower than other seasons, due to convective phenomena formation, such as storms, and to potential presence of wood and rivers closed to Osmer stations; the last contributes to provide more water vapor to atmosphere by evaporation, and therefore local effects are incremented (blue line shows less correlation then other seasons). To assess the representativeness radius for relative humidity the worst case is considered, as a consequence it can be defined in 25 km length; to taking into account for some error associated to polynomial smoothing.

In addition, horizontal wind speed is considered; for every season correlation

[3] For further information, see https://www.rdocumentation.org/

[4] As said previously, stations onto hilly areas are Fagagna (12 km away from Beano site), Faedis (29 km), Gemona del Friuli (30 km), and Cividale del Friuli (32 km).

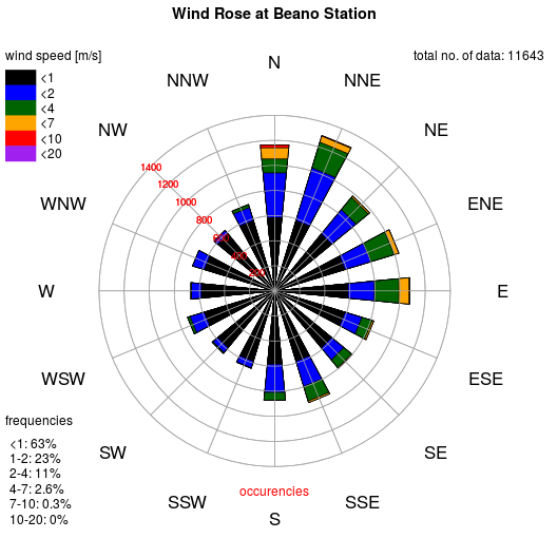

Figure 4.3: Wind Rose for Beano site considering the year 2015. Red scale describes the occurrences for every sector of the rose, while bars colors indicate ranges of wind speed; on the bottom left frequencies of wind speed are summarized. Regional North-North-East pattern of wind direction is visible (Bora), while winds coming from South-South-East are also frequent (Scirocco).

decreases quickly than previous observables. Two aspects drive this pattern, on the one hand the analysis comprehends some OSMER network stations sited in different climatological areas of Friuli Venezia Giulia region[5] with respect Beano site (e.g. plain area), this brings to consider at the same time strongly windy regions and areas characterized by wind depressions. For example, Fagagna station 11 km away from Beano eddy covariance tower is sited in the hilly climatological zone and low correlation is detected; while a cluster of stations from 15 to 20 km away from Beano station is part of the plain climatological area (i.e. as Beano site) and correlation reaches a local maximum. On the other hand, measurements of horizontal wind speed made in Beano detect the influence of the near Tagliamento valley, that provides local micro-scale winds of the order 7-10 m/s from the North (red bar in figure 4.3) which features are different during the river trail. Moreover, a further explanation of the lower correlation patterns could be linked to the fact that during a seasonal time domain, most of the observations made by OSMER network are comparable with the instrumental sensitivity, this can bring to unidentifiable behavior of correlation in according with the distance. Therefore, spatial representativeness for horizontal wind speed is defined by a 3 km radius; within it no remarkable differences come out considering the different seasons.

Finally, hourly precipitations are considered, taking care to remove the watering from Beano measures. As already seen for wind speed, climatological zones play a relevant role in correlation analysis; in fact, stations sited into hilly areas measure

[5]The definition of climatological areas follows *Il clima del Friuli-Venezia Giulia*, Stefanutto L., 2003.

more precipitations than all the others (Stefanuto, 2003), this happens especially during summer when convective precipitations (i.e. rainstorms) are mainly detected. This comes out in the summer fit, in which low correlation coefficients beyond 5 km from Beano site can reflects the dimensions of convective cells, few kilometers wide; on the contrary, during other seasons precipitations are mainly due to synoptic and mesoscale movements that involve wider areas. Therefore, considering the summer worst case, a radius of 5 km delimits the spatial representativeness for the amount of precipitation measured by Beano micrometeorological tower; hypothetically, if the study considers only a season different from the summer, this ray can be extended to 10 km.

4.3.1 Conclusion

Having considered the correlation between Beano eddy covariance measurements and observations detected by Friuli Venezia Giulia OSMER network, spatial representativeness of the firsts can be extracted. Summarizing, it was observed that global radiation and air temperature are the less stringent variables (i.e. largest representation radius), relative humidity has a strongly site-specific feature, and amount of precipitation representativeness is dependent from the season. Moreover, horizontal wind speed is influenced by different factors that cause that it constitutes the most stringent variable for the definition of spatial representativeness. Finally, considering at the same time all the observables, Beano eddy covariance measurements are representative for a ray of 3 km.

Considering that SurfPro spatial resolution is 2 km, Beano measurements are able to represent the computational cells immediately closed to it. In other words, the SurfPro cells having the center within a 3 km radius from Beano can be chosen to performing a comparison between measures and simulations.

Chapter 5

Remote sensing data

Another source of measures employed in this thesis to evaluate SurfPro initialization parameters is provided by remote sensing measurements based on elaborations of satellite images; in particular this kind of measurements is used for the comparison of albedo and leaf area index (LAI) parameterizations. The reasons why the remote sensing data are explored concern the lack of direct measurements of the leaf area index for the maize field over which the micrometeorological tower is sited, and the uselessness of the measures from the pointed downward radiometer (see appendix C).

The satellite data used are provided by the *NASA Earth Science Data and Information System* via the *Land Processes Distributed Active Archive Center* (LP-DAAC), that distributes a set of measures referred to land surface quantities detected by the MODIS instrument. Even if at the base of remote sensing measurements there is a model (sometimes not trivial to understand) which elaborate the received signals, the conjecture that these data can be used as good quality description of the reality is supported by the extensively validation that satellite and MODIS products meet (Cescatti, 2012, Liu et al., 2009 for albedo products and Garrigues, 2008, Wang et al., 2016 for LAI products).

5.1 MODIS overview

MODIS is the acronym for *Moderate Resolution Imaging Spectroradiometer*, an instrument which operates aboard the Terra and Aqua satellites, that are NASA scientific research satellites in a Sun-synchronous orbit around the Earth. Thanks to this kind of orbita the two satellites goes over a point of the Earth at the same local time[1] each time; Terra passes over all the places in the Earth at 10:30 a.m. while Aqua at 1:39 p.m. at about the same altitude of 705 km and with a period closed to 99 minutes.

Therefore, MODIS instrument aboard satellites views the entire Earth's surface every day, acquiring data using an optical system composed by four refractive objective assemblies (one for each of the following spectral regions, visible, near infrared, shortwave and medium wave infrared, and finally long wave infrared), that allow to cover the spectral range from 0.4 to 14.4 µm. Globally, the detectors measure

[1] The *local time* statement refers to the mean solar time.

36 spectral bands with three different spatial resolutions (250 m, 500 m and 100 m), which change as a function of the band wavelength range.

Due to the detailed spectral resolution, MODIS remote sensing measurements are able to describe many aspects of the land, oceans and lower atmosphere (such as surface temperature, ocean color, cloud properties, aerosols and many others) that are currently used for studying global processes and dynamics.

5.2 LAI measures

The MCD15A23H version 6 data from MODIS are employed to extract a leaf area index time series for the whole year 2015 within the SurfPro computational cell which includes the Beano site of measurements. Summarizing the characteristics of dataset, LAI MODIS products are provided for consecutive 8-day time windows with spatial resolution of 500 meters. Terra and Aqua satellites record daily values of leaf area index, from which an algorithm chooses the best pixel available from all the acquisitions of both the satellites within the time window, and associates it to the first day of it; this post-processing would avoid the use of inaccurate measurements affected by the presence of clouds, which can act as shield for radiation. Following, a description of the data acquisition is reported.

MODIS data are based on a typical inversion algorithm that converts the detected spectral information in the vegetation absorption bands into evaluations of canopy status. In particular, the wavelength affected by vegetation absorption are the red (648 nm) and near-infrared (858 nm) spectral bands and therefore MODIS detects the surface reflectance within these spectral bands to obtain information about plant status. Input to the algorithm are the just introduced remote surveys and the land cover classification, associated to an expected vegetation type, that permits to define a suite of canopy structures usable in the algorithm. The suite is represented as a cloudy-like distribution of points associated to values of leaf area index and of reflectance at near-infrared and red spectral bands (figure 5.1A).

Once defined the distribution of samples, the MODIS radiance retrievals at NIR and red spectral bands can be plotted into the graph to obtain a single point associated to the uncertainly ellipse obtained by standard deviations related to each spectral band. In order to match the requirement that MODIS LAI measurements must have the same statistical properties of LAI ground based measures, all the points within the ellipse are considered acceptable solutions of the inverse problem. Finally, for each detected pixel the MODIS algorithm plots the density distribution function to obtain the mean leaf area index and it dispersion measured in standard deviation (figure 5.1B). Nevertheless, in the case of dense canopies (e.g. forests) the reflenctance saturate, and therefore MODIS can be weakly sensitive to changes in canopy properties; in this situations the algorithm exploits an indicating flag.

For all the acquisition pixels, the just described procedure is repeated every day; however, in order to ensure a sufficient data quality another parameter is daily detected, the fraction of photosynthetically active radiation absorbed by vegetation (FPAR) that is defined as the fraction of incident photosynthetically active radiation (400 - 700 nm) absorbed by the green elements of a vegetation canopy. Within 8-day time windows, the highest value of FPAR is identified and used to select the suitable leaf area index value for the description of the final intervals; in fact, the highest

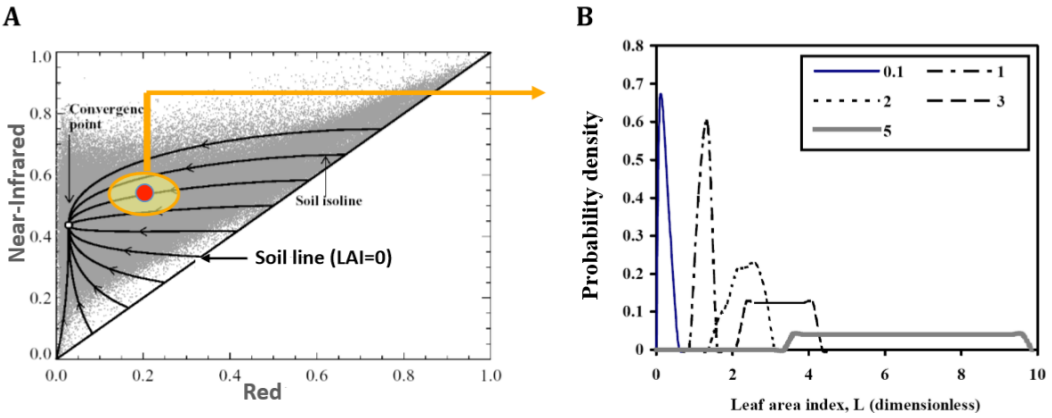

Figure 5.1: Panel A: Distribution of vegetated pixels detected by Terra MODIS instrument in accordance to their reflectances at NIR and red spectral bands. Red point indicates an hypothetical measurement and yellow circle the associated standard deviation. Lines represent LAI values. Panel B: Density distribution function of acceptable solutions for five different measurements. From Y. Knyazikhin et al., *MODIS Leaf Area Index (LAI) and Fraction of Photosynthetically Active Radiation Absorbed by Vegetation (FPAR) Product (MOD15) Algorithm Theoretical Basis Document*, 1999.

values of FPAR indicates that the least part of incoming radiation is absorbed by clouds or aerosols. Despite of the apparently low time resolution, this procedure can be applied because the leaf area index is a variable that change smoothly during the time; finally the LAI time series with time resolution of 8-days is provided by the Nasa LPDAAC.

Furthermore, considering spatial resolution of the MODIS LAI measurements (500 m), one can noticed that it is more accurate than the SurfPro computational grid (2 km). To make them comparable, the 16 pixels of MODIS mesh within every SurfPro cell are averaged to extract a single value and its standard deviation. In addition, applying this procedure a further control on measurement quality data is performed excluding measures with extremely high associated standard deviation.

5.3 Albedo measures

The evaluation of ground surface albedo (ratio of reflected radiation over incoming radiation) by remote sensing measures is more complex than what previously explained for the leaf area index; in fact, different nature factors must be considered such as atmospheric effects (due to cloud cover and aerosol presence) and geometrical effects which comprehend solar angle, satellite view angle and geometrical characteristics of the surface affected by solar radiation. All these contributing elements must be taken into account when satellite measures of albedo are performed.

Measures of ground albedo used in this thesis have passed several steps to be defined in a suitable way for the study of surface energy balance. The procedure starts from the MODIS acquisition of reflectance that takes into account land surface geometrical characteristics, it continues with the elaboration made by the *Copernicus Atmosphere Monitoring Service* (CAMS) that inserts, among others, the atmospheric effect, and finally the procedure ends with the punctual ground albedo time

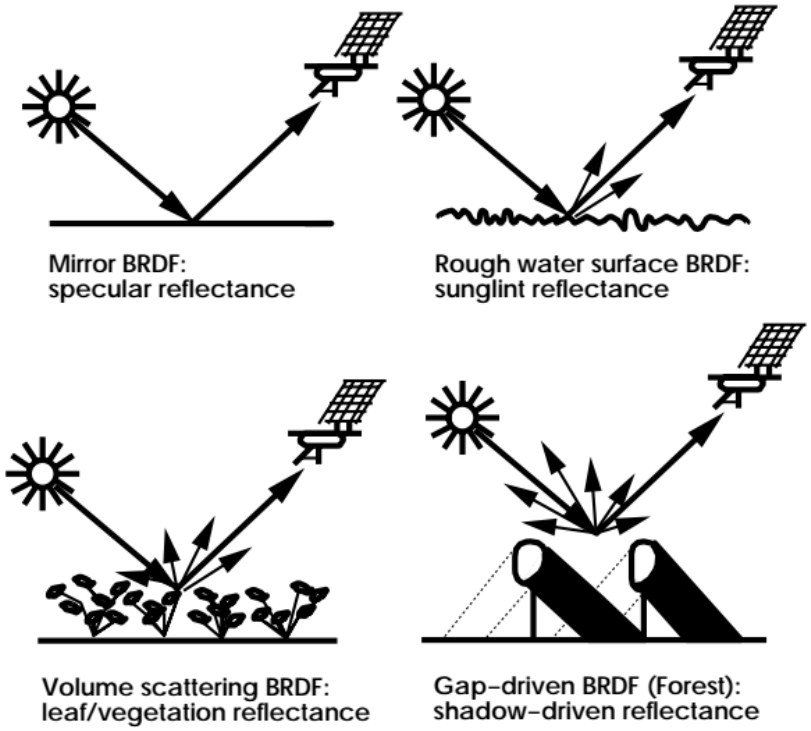

Figure 5.2: Examples of land surface reflectance anisotropy. Reflectance schemes for flat surface, water surface, leaves of plant canopies and forest are reported. From *MODIS BRDF/Albedo Product: ALgorithm Theorethical Basis Document Version 5.0.*, by Strahler A.H. and Muller J.-P., 1999.

series provided by the same structure with a time resolution of 1 minute.

Before starting the description of the albedo measures, it is better underline that models we will use are widely known in the field of remote sensing and are widely validated by scientific community (Hu et al., 1997; Hoyer-Klick C. et al., 2008; Liu et al., 2009; Cescatti et al., 2012).

Finally, two concepts are here anticipated to make the dissertation more readable: firstly, the black-sky albedo is defined as the albedo in absence of a diffuse component and is a function of solar zenith angle (i.e. all the incident radiation is due to direct solar beam); on the contrary, the white-sky albedo is defined as the albedo in the absence of direct component when the diffuse component is isotropic, and therefore there is no dependence on solar zenithal angle.

5.3.1 Geometrical aspects of albedo remote sensing measures

The first feature to consider is the dependence of albedo on the geometry of the system consisting of the sun, the reflector and the viewer satellite, i.e. how the ground reflectance depends on satellite view and solar angle. For instance, if the reflector is a flat surface an isotropic reflectance is expected, while if the incident radiation is reflected by a rough surface the outgoing radiation cannot be isotropic distributed and a further analysis of the signal viewed by satellite is needed.

Evaluating the albedo by remote sensing techniques, this behavior is described by

the bidirectional reflectance distribution function (BRDF), a function that provides land surface reflectance explicitly in terms of its spectral, directional, spatial and temporal characteristics. It is extremely important because it describes anisotropy in land surface reflectance, which deviates far from the linearity the relationship between albedo and reflectance observed by a satellite in a given direction; it is a sort of correction needed in remote sensing measures to account for the view and illumination angle effects.

Summarizing, the BRDF gives the reflectance of a target as a function of illumination geometry and viewing geometry and is determined by the structural and optical properties of the surface, for instance shadows, terrain tilt, surface elements and facet characteristics. Figure 5.2 reports the basic reasons for the surface reflectance anisotropy, the picture on the top at the right-hand side shows the reference scheme of bidirectional reflectance, while other pictures report the reflectance as a function of the land characteristics. One can note that the reflected light detected by the radiometer aboard the satellite changes considering the different cases in accordance, among others, with the surface roughness and its spatial distribution, and with the presence of shadows that is related to sun position and that leads the reflected radiation to return towards the sun. In natural systems, all types of reflectance can simultaneously occur.

Therefore, different types of scattering provides different contributes to the reflectance observed by the satellite at a certain position and the BDRF can be considered as a superposition of the scatter models. This assumption equals to the spatial distinction of the models or to the negligible interaction between them, and permits a linear expansion of the BRDF in the λ waveband of acquisition,

$$R(\theta, \vartheta, \phi, \lambda) = \sum_k f_k(\lambda) K_k(\theta, \vartheta, \phi) \tag{5.1}$$

where $K_k(\theta, \vartheta, \phi)$ is the BRDF kernel that describe the scatter models and $f_k(\lambda)$ are the coefficients containing the reflectance observations within the spectral bands made at angle $(\theta, \vartheta, \phi)$. Moreover, $f_k(\lambda)$ can be obtained as analytical solution of the minimization of $\partial e^2 / \partial f_k = 0$ at least-squares error function

$$e^2(\lambda) = \frac{1}{d} \sum_l \frac{(\rho(\theta_l, \vartheta_l, \phi_l) - R(\theta_l, \vartheta_l, \phi_l, \lambda))^2}{w_l(\lambda)}, \tag{5.2}$$

where $w_l(\lambda)$ is the weighted given to each observation.

The general case of equation 5.1 can be modeled in different ways as a function of the number of considered scatter models and of their complexity, which are reflected on the characteristic of the kernels $K_k(\theta, \vartheta, \phi)$. However, the linear develop implemented in MODIS is the widely used and widely validated Ross-Li model (Roujean et al., 1992; Wanner et al.,1995; Schaaf et al., 2002; Lefèvre et al., 2013, Blanc et al., 2014; Lucht, 1997). As said previously, theoretical basis of this implementation require that the land surface reflectance is modeled as a sum of kernels representing basic scattering types, in this case three scattering types are considered: the isotropic scattering (ideal case), the radiative volumetric scattering as from horizontally homogeneous leaf canopies, and the geometrical-optical surface scattering as from three-dimensional objects that cast shadows for which $K_k(\theta, \vartheta, \phi)$ are known.

Therefore, the following expression for the BRDF can be derived,

$$R(\theta, \vartheta, \phi, \lambda) = f_{iso}(\lambda) + f_{vol}(\lambda)K_{vol}(\theta, \vartheta, \phi) + f_{vol}(\lambda)K_{geol}(\theta, \vartheta, \phi). \tag{5.3}$$

The analytical expressions of the kernels are not the reported in this thesis, however must know that values of f_{iso}, f_{vol} and f_{geo} (which contain the measure information from MODIS) permit to obtain the BRDF. These three parameters are what MODIS passes to CAMS project for the evaluation of the surface ground albedo, taking into account the atmospheric effects. Before proceeding, an example of how the albedo depends on BRDF is reported considering the previous defined black-sky and white-sky albedo.

To do this, the kernels $K_k(\theta, \vartheta, \phi, \lambda)$, which depend only by model characteristics, must be integrated on the angular domains of black-sky and white-sky albedo. For the directional hemispherical reflectance (i.e. black-sky albedo) the integration involves only the angles (ϑ, ϕ), while for the bihemispherical reflectance (i.e. white-sky albedo) the kernel is integrated also on the solar zenithal angle θ. Therefore one can obtain

$$h_k(\theta) = \int_0^{2\pi} \int_0^{\pi/2} K_k(\theta, \vartheta, \phi) sin(\vartheta) cos(\vartheta) d\vartheta d\phi, \tag{5.4}$$

for the direct component and

$$H_k = 2 \int_0^{\pi/2} h_k(\theta) sin(\theta) cos(\theta) d\theta \tag{5.5}$$

for the diffuse component. To obtain the expressions respectively for black-sky and white-sky albedo the coefficients derived by measures must be considered,

$$\alpha_{bs}(\theta, \lambda) = \sum_k f_k(\lambda) h_k(\theta) \tag{5.6}$$

$$\alpha_{ws}(\lambda) = \sum_k f_k(\lambda) H_k. \tag{5.7}$$

To complete the part concerning MODIS data, the way to convert the spectral to broadband albedo is reported. As other remote sensing instruments, the MODIS sensor acquires reflectances within spectral bands (seven in the case of albedo), to evaluate all the shortwave energy reflected by the surface, a spectral-to-broadband conversion must be applied using appropriate band-dependent weighting factors, which depend by aerosol optical depth and solar zenith angle and must be empirically determined from computational simulations (Liang, 1999),

$$\alpha(\theta) = \sum_i c_i \alpha(\theta, \lambda_i). \tag{5.8}$$

5.3.2 CAMS analysis

The *Copernicus Atmosphere Monitoring Service* (CAMS) acquires from MODIS the values of the parameters f_{iso}, f_{vol} and f_{geo} to give a proper evaluation of the ground surface albedo in the European states accounting for grid spatial interpolation and atmospheric effects. To implement this, CAMS derived the climatological monthly

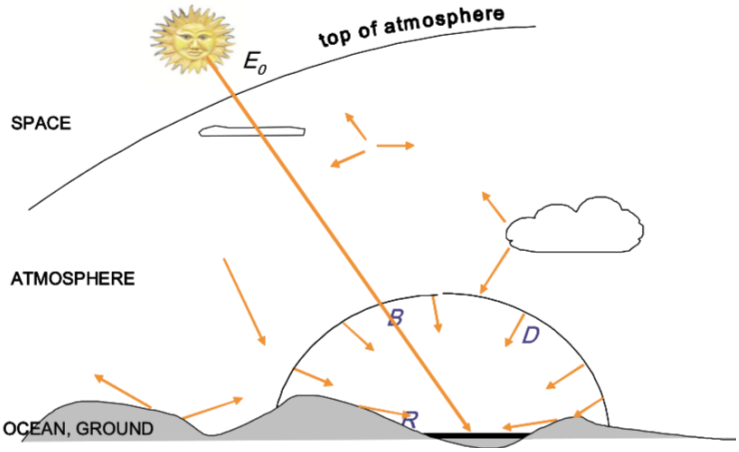

Figure 5.3: Scheme of the incoming radiation at a point in the ground. The radiation at the top of the atmosphere is described with E_0, letter B depicts the direct solar beam, D the diffuse contribution and R the radiation reflected by topographical effects. From *Copernicus Atmosphere Monitoring Service* user guide.

means of the three parameters describing the isotropic and anisotropic part of the BRDF from the MODIS MCD43C1 and MCD43C2 products. These products provide information on spatial resolution of 0.05° (i.e. in Friuli Venezia Giulia region about 5 km in latitude and 4 km in longitude) with a 8-day temporal scale but produced with 16 days of acquisition, in a way as leaf area index acquisition.

Once the CAMS has stored the information about the climatological BRDF components (i.e. the three parameters) it creates a database that can be used for the extraction of the parameters in a specific European site; moreover, a linear interpolation calculates the parameters within the MODIS grid, bringing to zero the spatial resolution. With this procedure, CAMS is able to define a climatological base for the bidirectional reflectance distribution function $R(\theta, \vartheta, \phi, \lambda)$ in the whole Europe, that can be used for the albedo evaluation once known the atmospheric dependence of it.

As previously showed, if the coefficients f_k are known, the black-sky and the white-sky albedo can be calculated using the equations 5.6 and 5.7 remembering that $h_k(\theta)$ and H_k are known model-dependent functions.

5.3.3 Effect of the atmosphere on albedo

However, black-sky and white-sky albedoes depict the extreme cases of completely direct and completely diffuse albedo, whilst the actual albedo is a value in the middle between the two components that depends on atmospheric characteristics (cloud cover, aerosol types and its optical length), that modulates the total incoming radiation on a ground site (figure 5.3). With the purpose of finding a relation between the components, the ratio of the direct radiation over the global radiation that affects a site is defined as

$$K^{dir}(\alpha) = \frac{E^{dir}}{E^{glo}(\alpha)}, \tag{5.9}$$

where the dependence of global incoming radiation on albedo can be explained referring to the figure 5.3. Therefore, the ground surface albedo can be written as,

$$\alpha(\theta) = \alpha_{ws} + K^{dir}(\alpha(\theta))(\alpha_{bs}(\theta) - \alpha_{ws}). \tag{5.10}$$

At this point, the major difficulty for CAMS in the retrieving a value of albedo knowing black-sky and white-sky component is the evaluation of the coefficient $K^{dir}(\alpha) = \frac{E^{dir}}{E^{glo}(\alpha)}$ because it depends itself by the ground albedo. Fortunately, according to Lefèvre et al. (2013) only one solution of K^{dir} can be found at a specific time using the Monte Carlo technique to randomly select 100000 samples. Therefore, ground albedo can be evaluated in a selected point for each minute of the day using the equation 5.10 and consequently provided for a wide range of purposes.

Finally, a time series of the ground surface albedo is extracted for the whole 2015 at the center of selected SurfPro computational cell in order to perform the comparison with the statically parameterization of the model.

Chapter 6

Global features of the comparison

The evaluation of SurfPro parameters using eddy covariance measurements can be performed in an area bounded by the representative radius of measures, that was defined in chapter and it is about 3 km. On the contrary, the satellite measures which will be used for the same purpose does not find the same problems and rather an equalization of the meshes must be performed, for instance LAI remote sensing data are provided with a spatial resolution of 500 m, less than SurfPro grid. Therefore, the choice of the SurfPro grid point (that corresponds to a computational cell) for the evaluation will be achieved taking into account the position of the eddy covariance tower and its representative feature, while the satellite data are extracted with reference to the previously defined SurfPro cell.

Moreover, another topic to be faced before starting the comparison is the issue of inhomogeneous annual distribution of available measurements, in fact some instrumental issues could be rise during the entire year of surveys. Clearly, this issue is related only to the eddy covariance measurements because remote sensing data are provided already validated all year long.

In this chapter the answers to this questions are provided, with a particular attention to the factors that could affect the eddy covariance measures.

6.1 Definition of extraction points

While the position of measurements is clearly defined by geographical coordinates, as well as the area within which they are representative (i.e. the circular region delimited by the representativeness radius), the extraction of variables from the grid data frames of models could constitute a source of inaccuracy. Moreover, for the purpose of this thesis this element would represent a relevant mistake because the choice of a particular grid point compared to another could lead to a different description of land use and therefore a different parameterization of related quantities. Minimization of the distance between micrometeorological tower position and grid points around it is the easiest procedure for the definition of the computational cell to use in the comparison measurements-models; note that it can be applied only if the distance results less than representativeness radius of measures.

This method is used for the definition of the suitable grid point to use in the comparison of Surfpro statically parameters with Beano measurements; it is found

	SurfPro
Cell A	Arable land, non-irrigated and permanently irrigated
Cell B	Heterogeneous agricultural area
	WRF
Cell A	Dryland, Cropland and Pasture
Cell B	Dryland, Cropland and Pasture

Table 6.1: Prevalent land use of the selected computational cells for SurfPro and WRF model.

a grid point that summarizes the features of a computational cell within which the prevalent land use is described by CORINE land scheme (see paragraph 2.2.1) as *Arable land, non-irrigated and permanently irrigated* land use, from now it will be called cell A. We remark that prevalent land use is what mainly affected the calculation of statically parameters within the computational cells. Furthermore, to take into account for possible peculiarities in the land use nearby the measurements site, a second grid point with different prevalent land use description is considered, this grid cell will be referred as cell B and its prevalent land use is defined by CORINE land scheme as *Heterogeneous agricultural area*.

In the following, besides the comparison between measurement and SurfPro statically parameters, the comparison between SurfPro quantities and WRF model outputs will be performed, in order to evaluate if the SurfPro processor (by means of statically parameterizations implementations) actually improves the quality of environmental modeling chain. Therefore, also the extraction grid points for the WRF model must be fixed; this is done matching the two computational domains: so the two WRF grid points are selected choosing the computational cells closest to the SurfPro previously selected; in other words within the modeling chain SurfPro selected cells acquire meteorological information from the selected WRF cells). Performing this procedure, the prevalent land use of both of the two found WRF computational cells is *Dryland, cropland and pasture* land use. Table 6.1 provides a summary of the computational cells for each model.

6.2 Availability of eddy covariance measures

In order to perform the evaluation of models using on field measures, first of all one must provide an assessment of the data set quality, in terms of data availability, standardized quality flags and possible sources of errors in measurement processing. The knowledge of the characteristics of the measures and the limits in their usage allows to perform a fair comparison with the model; as an example, if the annual series of temperature is built by measurements taken every noon, it cannot be compared with a modeled time series consisting of every hour temperatures, because different features of the same variable are described by the two time series.

As saw previously, the implementation of an eddy covariance experiment must take into account several conditions such as the eddy covariance assumptions, the terrain flatness, the flux footprint; furthermore, some practical aspect must also be considered in the evaluation of final data set. One of the most important source that

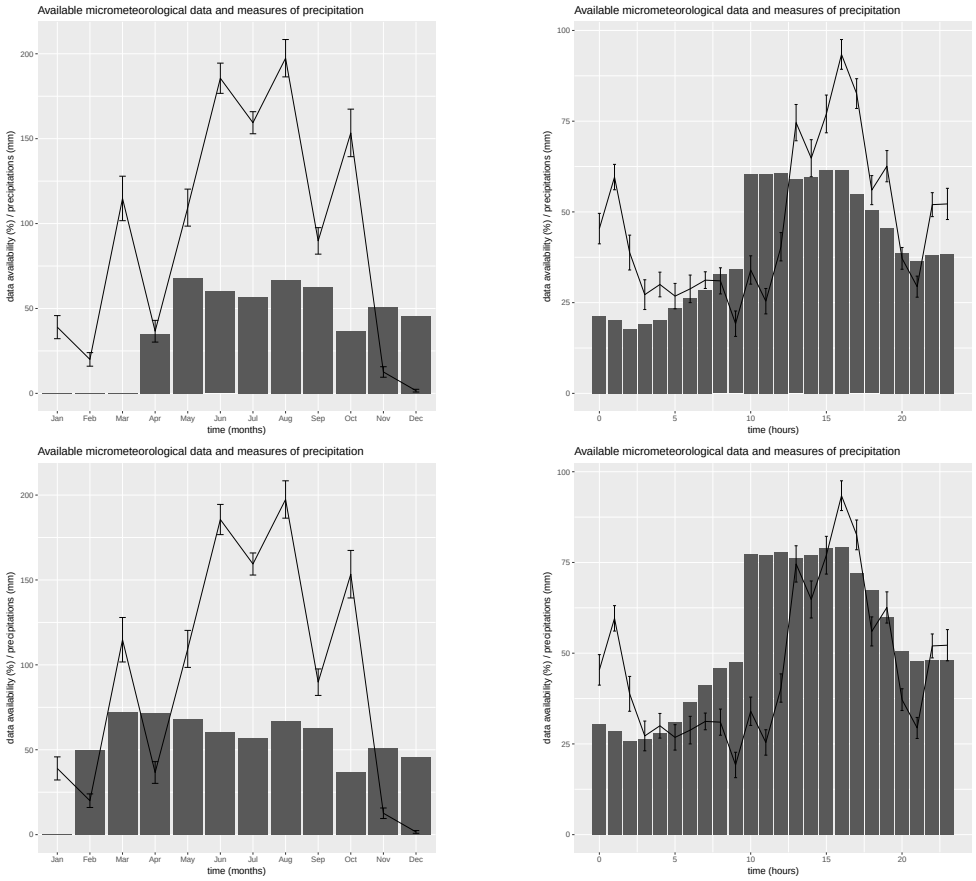

Figure 6.1: Availability of eddy covariance measurements of sensible (top) and latent (bottom) heat flux related to the cumulative precipitations measured by pluviometer in Beano station. On the left-hand side monthly distributions are reported, while on the right-hand side one can find the hourly distributions. Cumulative precipitations are reported as the sum of all the water detected on ground derived by all sources, i.e. rain, snow, frost, dew and watering; while hourly distribution follows local time (CEST).

can affect the quality of data is the presence of a quantity of liquid water on the sonic anemometer transducers, that may change the path length used to estimate speed of sound, leading to small or large errors depending on instrument features and to data interruptions (Burba, 2013); furthermore gas analyzer *Li-7500* is even more sensible to water presence. Water on instrumental apparatus can be due to both precipitation events (e.g. water and snow) and on land water state transitions (e.g. dew and frost). Data affected by the presence of water on the instruments are automatically flagged with low quality index and therefore have been discarded from the dataset of analysis.

The dataset provided by the Department of Agriculture and Environmental Sciences of the University of Udine is preliminary tested to assess the potential relationship between measurements made in disadvantageous conditions and availability and quality of data. As just said, unfavorable conditions are determined by the presence and water on the instrumental apparatus, in the case of Beano measurements they happen both during previous cited atmospheric conditions and during the watering

of crop field.

To perform this preliminary analysis the measure qualities of sensible heat flux and latent heat flux are taken into account, the second ones are the most restrictive because require measurements of both sonic anemometer and gas analyzer. The study is performed on monthly and hourly basis considering the percentages of available measurements over the total number of possible half-hour measures that could be taken at the same month or at the same hour during the entire year. Then, in figure 6.1 the hourly and monthly availability are reported by the bar charts related to the total amount of precipitations detected by the raingauge. An initial remark is on the fact that pluviometer collects all the water derived from different sources (i.e. rain, dew, watering) that can be detected on the ground; in this study we do not care about the water origin, we are only interested in the assessment of potential fails of the instrumental apparatus. The net amount of precipitations over the months or over the hours are reported in appendix D together with a brief evaluation of the WRF capability to simulate precipitations over Beano site.

Considering the monthly availability patterns (i.e. the bar charts on the left-hand side in figure 6.1), one can note that measures of sensible and latent heat flux (at the top and at the bottom of figure, respectively) are available with the same occurrence starting from May and presumably since mid-April, before that time sensible heat flux measurements are not collected and no considerations can be made. From an overview, one can evince that the critical months for the number of measures are February (only for latent heat flux), October and December, when less than 50% of possible measurements are collected; for the other months the measurements cover a range from 50% to 75% of the potential measures.

Even analyzing the graphs on the right-hand side of the figure, in which the hourly availability during the entire year are represented, one can find the same pattern for the two quantities; in particular, eddy covariance measures are successfully taken at the central hours of day, with a plateau of 75% between 10 to 15 local time. In the previous hours, and in particular before sunrise, the minimum of availability is detected and it reaches the 25% of potential measures. Then, considering the annual average day there is a greater number of available measures during the daytime.

Now, the amount of water detected by the pluviometer is putted in relation with the availability of flux measures: both in annual and daily time domain, there is not any anti-correlation between the two variables; which could have ratified the negative effect of the water on availability of micrometeorological measures (i.e. large amount of precipitations and low levels of data).

However, one cannot completely exclude that water is able to affect the availability measures, but only says that water on instruments is not the prevalent cause of the measurement availability; this is because the low occurrence of measurements take with precipitations, watering or dew than measures taken without it. Therefore, one can conclude that the main feature which contributes to the availability of eddy covariance measures is the fulfillment of the eddy covariance method requirements, which happen predominantly when convective turbulence is created by heating of the land surface (i.e. central hours of day).

Found out that strong anti-correlation between water on instruments and availability of eddy covariance data is not shown by figure 6.1, now the hypothesis that they can affect the quality flag of measures (see section 3.4) is evaluated. To reach

SHF Quality flag	0	1	2	NA
No precipitations	3675	2476	641	4950
Precipitations	69	165	49	650
Precipitations NA	2	1	0	842
Precipitations for quality flag (%)	1.8	6.2	7.1	10.1

Table 6.2: Contingency table of sensible heat flux (SHF) quality flag and Boolean precipitations, numbers in table report the number of measurements for each contingency. Last line reports the percentage of measures collected with precipitations as a function of quality flag.

LHF Quality flag	0	1	2	NA
No precipitations	4282	3652	1012	6792
Precipitations	74	230	80	549
Precipitations NA	4	2	1	838
Precipitations for quality flag (%)	1.7	5.9	7.3	6.7

Table 6.3: Contingency table of latent heat flux (LHF)quality flag and Boolean precipitations, numbers in table report the number of measurements for each contingency. Last line reports the percentage of measures collected with precipitations as a function of quality flag.

the purpose, contingency table of precipitations (defined as previously) and quality flag values are reported in tables 6.2 and 6.3 for sensible and latent heat flux. Focusing on the two highest quality classes (i.e. avoiding the quality flag 2 related to questionable data which can be affected by several errors), one can note that passing from measures without precipitations and measures taken during precipitation the proportion between highest quality data (i.e. quality flag equal to zero) and medium quality data (i.e. quality flag equal to one) dramatically changes: in fact without precipitations there is a ratio of $4282 : 3645$, while with precipitations the same ratio is $74 : 230$. Then, high quality data are related to lack of water on instruments, while medium quality data can be associated to data of medium quality.

Therefore, as said before precipitations does not affect the availability of eddy covariance measurements; however, precipitations can affect the quality of measures, in particular they are able to worse them.

Chapter 7

Analysis of the parameters

In this chapter the analysis performed to make SurfPro parameters comparable with the available measurements and with the WRF model quantities are reported; while the statistical comparison between them will be reported in the next chapter to not weight down this chapter. As a matter of fact now are showed different methods to compare the variables as a function of the role of each parameter within the SurfPro processor.

Then to make easier the reading, this general scheme is followed in the rest of chapter for each parameter: firstly a general recall of the parameter definition is provided with a description of how SurfPro parameterization implements it, then the study of available measurements is implemented to get a time series comparable with SurfPro parameterization, afterwards the same study is performed for WRF model if needed, and at the end eventually developments of the study are taken into account. However, this scheme may be subject to some changes or expansions according to the complexity of parameter.

7.1 Bowen ratio

Bowen ratio is the first SurfPro statically parameter considered, as shown it is defined as the ratio between sensible and latent heat fluxes at the surface,

$$\beta = \frac{H_0}{L_v E_0}. \tag{7.1}$$

Therefore, it is smaller over moist surfaces, where most of the energy makes available from net radiation goes into evaporation, and larger over dry surfaces, where the large amount of energy goes into sensible heating. According to Stull (1988) typical values range from 5 over semi-arid regions, 0.5 over grasslands and forests, 0.1 over the sea, to negative values over oasis. Moreover further variability is due to time (i.e. hour of the day and season), weather, soil properties and plant status over the considered site.

SurfPro uses the bowen ratio to define the partitioning of net radiation (net of soil heat flux and anthropogenic storage) between sensible and latent heat flux according to land use, season and a climatic index related to soil moisture. In fact, for each land use it provides a parameterization defined by seasonal values of Bowen ratio, these values are determined by the weighted average computed over

	Dry					Neutral					Wet				
	SP	SU	FA	WI	WS	SP	SU	FA	WI	WS	SP	SU	FA	WI	WS
Cell A	1.0	1.5	2.0	2.0	2.0	0.3	0.5	0.7	0.7	1.5	0.2	0.3	0.4	0.4	0.5
Cell B	1.2	1.0	1.8	1.8	2.0	0.5	0.4	0.8	0.8	1.5	0.2	0.3	0.4	0.4	0.5

Table 7.1: Seasonal Bowen ratio values for two CORINE land use corresponding to prevalent land use of the two chosen SurfPro cells: grid cell A corresponds to *Arable land, non-irrigated and permanently irrigated*, while grid cell B to *Heterogeneous agricultural area*. WS indicates the presence of snow over the ground during winter.

the cells. Moreover, the setting up of climatic flag permits to define these values taking into account the climatic index, which would represents *wet*, *neutral* and *dry* environmental conditions. However, this flag has not worked in the 2015 SurfPro runs and the environmental conditions are left to *neutral*. As an example, table 7.1 shows an extract of the initialization SurfPro table in which the Bowen ratio for two land uses are reported taking into account the three climate index; the two land use correspond to the prevalent land use of the two chosen SurfPro grid point, i.e. *Arable land, non-irrigated and permanently irrigated* and *Heterogeneous agricultural area* respectively for grid cell A and grid cell B. As one can note, Bowen ratio values decrease from dry to wet climate index; while during the entire year they increase passing from spring to winter.

7.1.1 Eddy covariance measurements

Comparing SurfPro seasonal parameterization of Bowen ratio and measurements collected by Beano eddy covariance tower different aspects must be taken into account, such as the highly variability of this quantity, that SurfPro waives to describe. In fact, a seasonal parameterization is not able to take into account fluctuations that occur with a period shorter than months; therefore the comparison between measures and model should be performed in a suitable way, not too strictly neither too permissive for SurfPro parameterization. For this reason a detailed analysis of Bowen ratio measurements is required starting from the study of fluxes of heat which composed it.

Study of turbulent heat fluxes Keeping in mind the availability of heat fluxes data (reported in section 6.2), now the evaluation of average daily fluxes is considered and plotted in figure 7.1, in which one can immediately see vacancies in the first period of the year and in the firsts days of October, due to unavailability of data. Furthermore, before proceeding with considerations the reference system must be fixed, in this case the figure reports positive fluxes as the fluxes related to a movement from Earth's surface up to the atmosphere, on the contrary negative fluxes describe movement from atmosphere to the Earth's surface.

Considering the latent heat flux, an evident annual modulation can be shown: minimum values are detected during cold months (i.e. November and December), while the maximum is reached during the summer with a peak observed in July. Maximum values are strictly linked to the growth of maize plants, which are able to produce a high evaporation rate. Drops of latent heat flux in summer period (June and August) are due to days in which the air is near the saturation (with presence

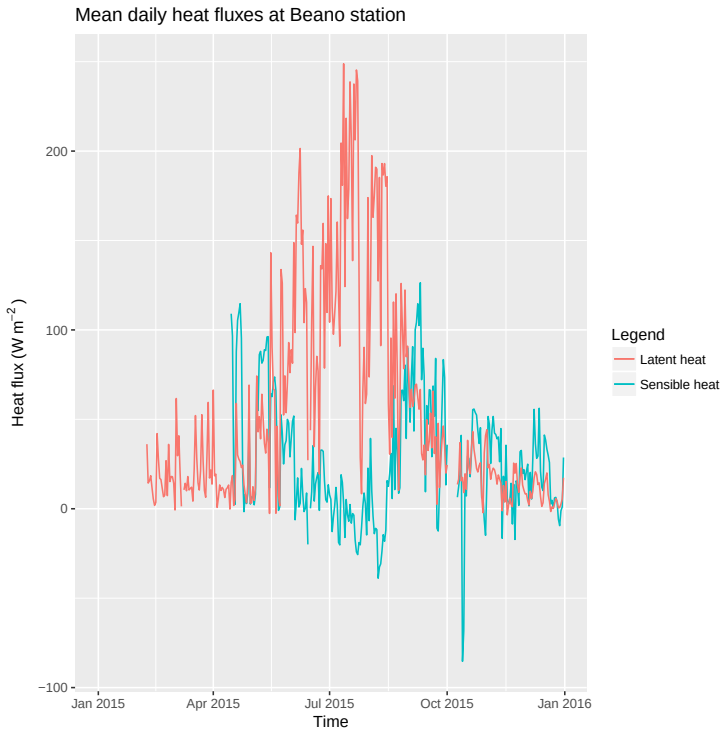

Figure 7.1: Daily average latent heat flux (red) and daily average sensible heat flux measured by Beano eddy covariance tower during the year 2015.

of cloud cover) and the evapotranspiration process is less effective; these days are accompanied by risings of sensible heat flux (in August is more visible) that is an evidence of positive heat flux from warm ground to cool atmosphere (i.e. passage of weather front that brings humid and cold air). Moreover, the daily average of latent heat flux is always positive, that means that evapotranspiration processes, which bring water vapor from the Earth's surface up to the atmosphere, are more effective than reverse processes, constituted by the formation of dew and frost during the nighttime.

On the contrary, the sensible heat flux shows the minimum values during the summer (apart from a single spike in October that comes just after a period of vacancy of data and probably represents an instrumental failure) and maximums during May and September. Minimum values of sensible heat flux are negatives (i.e. flux from warm air to cool surface) and together with positive latent heat flux depict the oasis effect, that describes the situation in which large evapotranspiration due to maize plants results in latent cooling close to the ground and negative sensible heat flux can have place (i.e. from the atmosphere to the ground surface). Instead, maximum values of sensible heat flux are due to different process in accordance to the month when they are found: during the autumn, maximum positive values are related to the fact that ground is still warm since summer and cooled air lies above; whilst during the spring, the progressive warming of the system atmosphere-land surface can be perturbed by advection of cooler air (i.e. weather front), resulting in a positive values of sensible heat flux.

Now, the behavior of heat fluxes during the day is investigated taking into ac-

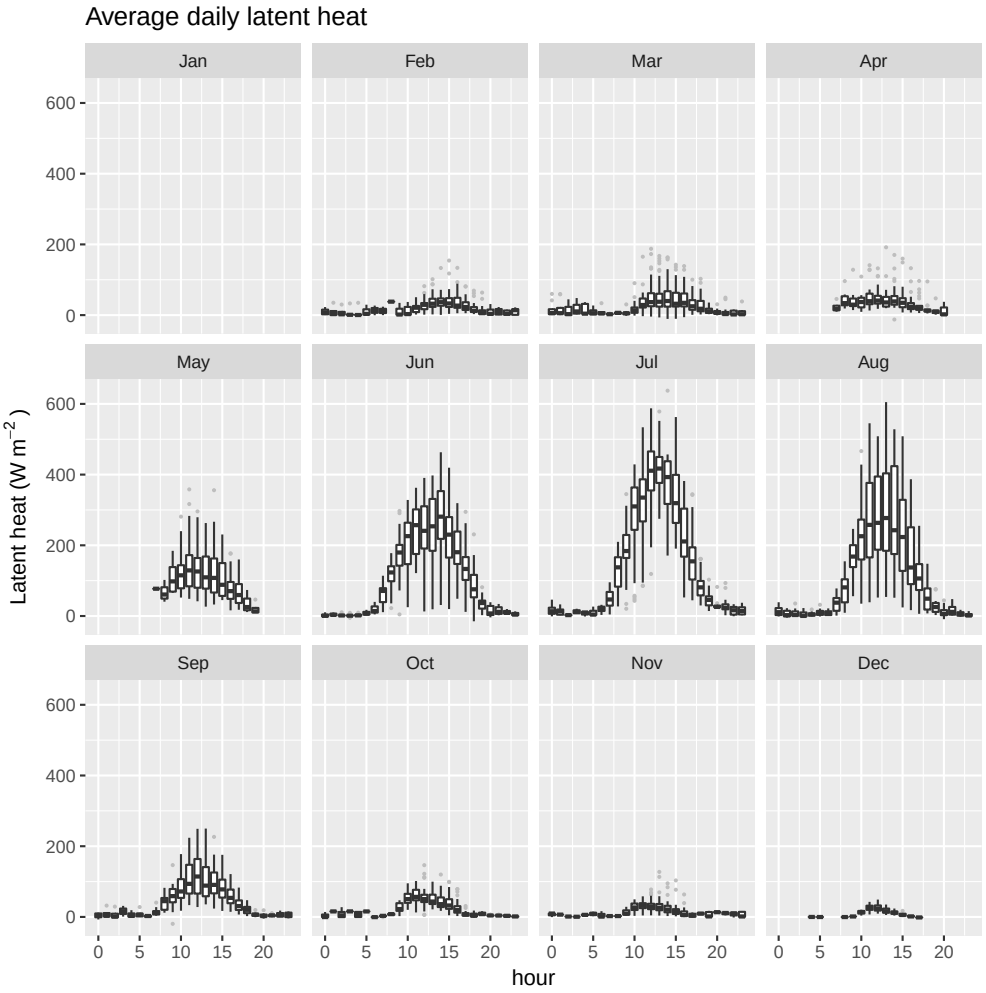

Figure 7.2: Average monthly day for latent heat flux. Boxplots represent the median as a line within the boxes, the boundary of boxes correspond to 25 and 75 percentiles and bars delimit the 5 and 95 percentile; finally, the points outside are the outliers of the distribution. Data are measured by Beano eddy covariance tower during 2015, hours refer to local time (CEST). Whenever a box is not plotted the data is not available.

count the average monthly day, in order to distinguish when the presence of plant plays an important role in the sensible and latent heat fluxes. To provide an effective visualization of the average monthly day, figures 7.2 and 7.3 report the boxplots of monthly distributions of latent and sensible heat fluxes, respectively.

Firstly, the average monthly day of latent heat flux confirms what previously seen in figure 7.1: the presence of the plant increases considerably the flux of latent heat from the surface up to the atmosphere, at least until the growth period. In fact, passing from July to August, a decrease of the peak is observed together with a spreading of the boxplot, these observations imply that plants are going toward the final stages of their life and transpiration is less effective. Moreover, September includes ten days with old maize plants and twenty without plants, this fact reflects in a flattering of distribution which in following months results more evident; moreover, the flattering is still visible also in the months before the plant growth. Then,

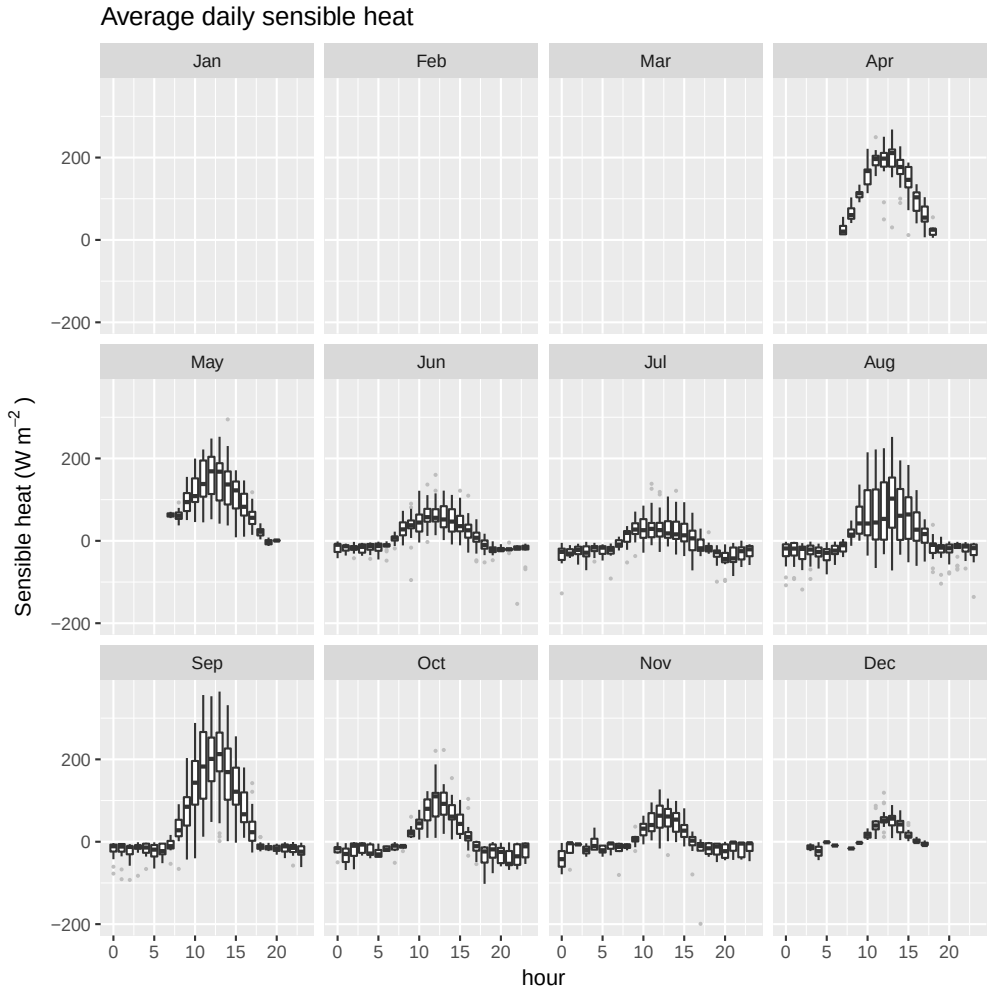

Figure 7.3: Average monthly day for sensible heat flux. Boxplots represent medians as lines within the boxes, the boundary of boxes correspond to 25 and 75 percentiles and bars delimit the 5 and 95 percentile; finally, the points outside are the outliers of the distribution. Data are measured by Beano eddy covariance tower during 2015, hours refer to local time (CEST). Whenever a box is not plotted the data is not available.

when there are no plants over the surface, the latent heat flux is determined by the evaporation of water from the bare soil, which strictly depends on the soil moisture that is affected by occurred precipitations, soil texture and other soil properties.

Finally, another aspect of figure 7.2 remains to be considered: the widely observed increase of latent heat flux during the central hours of the day, even if it concerns different magnitudes as a function of months. This suggest that both the evaporation and the transpiration are encouraged by diurnal atmospheric conditions, in which generally a greater distance from saturation point is detected; as an example, the plant transpiration occurs both during the daytime and the nighttime, but with different efficiency.

On the other hand, considering the average monthly day of sensible heat flux (figure 7.3), the main feature is that plant cover acts as a resistance for the heat flux passage from Earth's surface to the atmosphere, as can be seen during the

daytime of June, July and August, for which the daily peaks are less evident than others months. As opposed to of the latent heat, the sensible heat flux during the nighttime goes to negative values in all the months for which data are available; therefore this is a common behavior that delineates the passage of sensible heat flux from the atmosphere to the Earth's surface, due to warmer air over cooler surface.

Eddy covariance measurements As seen previously, the purpose of SurfPro parameterization is to provide a seasonal parameterization of Bowen ratio, without taking into account the description of daily changes, that can also be large (e.g. figures 7.2 and 7.3). Therefore, the daily variations observed, which produce direct consequences on the Bowen ratio, cannot be used to compare measurement and models. Instead, the comparison can properly be performed when the Bowen ratio is rather constant, that is during the central hours of the day (Wang, 2008), i.e. when latent and sensible heat fluxes are not close to zero.

Therefore, hours between 9 and 16 local time are selected and the median monthly day of Bowen ratio is considered and compared with SurfPro actual parameterization and with the three different settings (dry, neutral and wet) of cell A prevalent land use class (i.e. *Arable land, non-irrigated and permanently irrigated*); figure 7.4 reports them and permits to define a suitable climate index for each months taking into account that the number of hours in which Bowen ratio is almost constant is changeable through the months, i.e. during winter the hours of solar illumination decrease and stability of Bowen ratio is observed for a short range of time. Furthermore, a remark is made about the availability of data: April and October are months poorer of measurements for sensible heat flux than other months (figure 6.1) and therefore are excluded from the considerations.

The graphs show that for the months between May and September the measured Bowen ratio (gold line) during the day is rather constant. In particular, for the months at the end of this interval, the measured Bowen ratio assumes values comparable with the dry setting of SurfPro parameterization for the prevalent land use in the cell A (red line). Instead, in the period from June to August, measured Bowen ratio is comparable with the wet setting of SurfPro parameterization for cell A (purple line); this behavior is strictly related to the presence over the field of well-developed crop which promotes the latent heat flux from soil to atmosphere, as seen previously. Finally, November and December measurements of Bowen ratio are less constant than other months, this can be due to the minor hours of incident sunlight or to the less availability of data (figure 6.1); anyway the best description of the measured Bowen ratio is provided by the dry setting of SurfPro parameterization, as for May and September.

Summarizing, one can conclude that the Bowen ratio is strongly influenced by the presence of plant cover over the field: when maize plants are absent the Bowen ratio assumes values that can be described by SurfPro dry parameterization, while when the crop is on the field, SurfPro is able to describe the Bowen ratio by a wet parameterization. Therefore, an immediate result can be evinced at least for the area of Friulan plain cultivated with corn, an improvement of Bowen ratio parameterization can be performed choosing the suitable climate index for each months, which corresponds to dry environment when the plants are absent or not developed and to wet environment when the plants are well-developed and provide a relevant

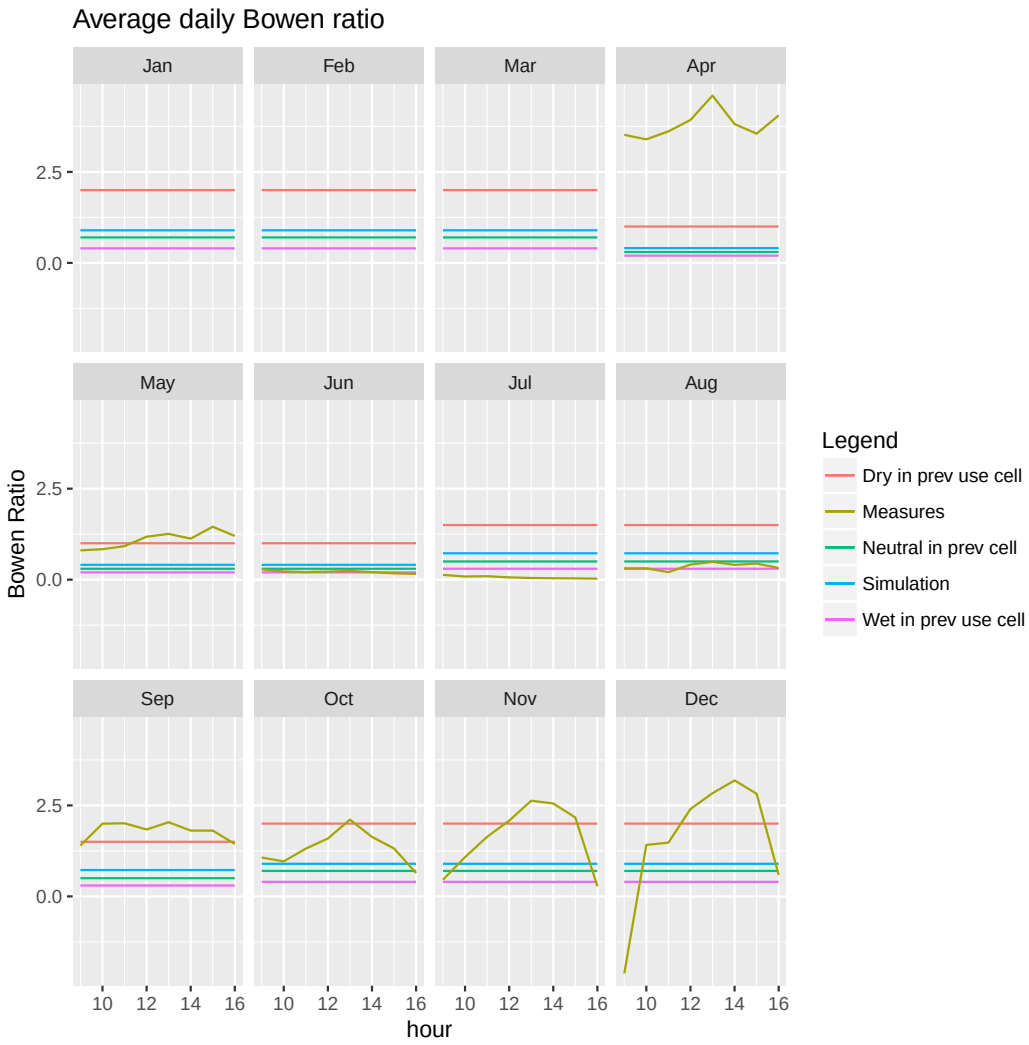

Figure 7.4: Average monthly day for measured Bowen ratio compared with SurfPro parameterization for the same year and with three values of Bowen ratio in accordance to the climate settings for *Arable land, non-irrigated and permanently irrigated* land use (i.e. grid cell A). Data are measured by Beano eddy covariance tower during 2015, hours refer to local time (CEST). Data of measured Bowen ratio are not available for the firsts three months.

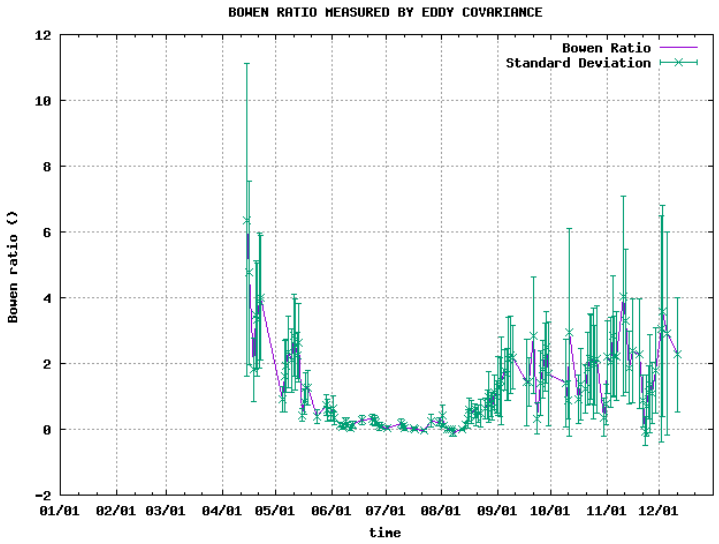

Figure 7.5: Time series of Bowen ratio measured by eddy covariance tower in Beano site of measurements during the year 2015.

contribute to evapotranspiration rate. However, this hint can be applied only for the areas with similar soil properties to the Beano region, in fact when there are not plants over the ground the soil texture and soil moisture determine the ground capability to hold the water.

Time series of measured and WRF Bowen ratio From the previous analysis it immediately follows that the definition of the measured time series of Bowen ratio (that will be used for the comparison between model and measurements) must be defined starting from the average day fluxes within a time window containing the central hours of the day; this must be done to avoid the diurnal variability of Bowen ratio. As we saw, Bowen ratio changes a lot during the day, it is rather stable during the daytime but presents visible fluctuations during the nighttime when the ratio rapidly decreases.

To account for these features, the hours between 9 and 16 local time of each day are selected for the computation of Bowen ratio. Moreover, the only days containing at least the 70% of available measurements of latent and sensible heat fluxes are selected for the calculation of mean daily Bowen ratio, this condition avoids that days with few measurements affect the time series with non physically fluctuations. Final annual time series of Bowen ratio are constituted by measurements made in 122 days starting from April, associated with a standard deviation calculated through the errors propagation law, figure 7.5.

The same procedure is applied for the definition of WRF time series, which is calculated starting from hourly outputs of latent and sensible heat fluxes and therefore needs for the same treatment.

7.1.2 Comparison between measurements and models

Having defined a well-balanced analysis for the evaluation of SurfPro model, and consequently the time series usable for it, now the graphical comparison between measurements and models is proposed in figure 7.6 for the two extraction points.

The SurfPro parameterization pattern for Bowen ratio would simulate the annual variability during the day time, considering lowest values for spring and highest values for autumn and winter; the idea of this parameterization is that latent heat flux (denominator of the ratio) increases in accordance with the crop growth, when the plants reach the maximum growth the latent heat starts to decrease (i.e. from spring to summer in extraction point A) and Bowen consequently ratio increases. Moreover, during autumn and winter the Bowen ratio assumes the highest same value; therefore all the considerations lead to the conclusion that SurfPro takes into account only the plant behavior for the parameterization of Bowen ratio. The influence of the environment enters only if the climate index flag is activated; in the 2015 SurfPro runs used in this work the climate index option is not activated and the Bowen ratio is parameterized only with land surface features.

Instead, following Viterbo (2002), evaporation is not guided only by plants: two environmental factors compete to the evaporation flux, the advection term and the energy term. The first is proportional to the saturation deficit at the screen level height and the second is proportional to the net radiation minus the soil heat storage. If vegetation is present (as in this case), both of the terms must be scaled by a factor that described also the aerodynamic and stomata resistance to the passage of water vapor molecules from plants to the atmosphere. During the year, one of the two terms can dominate, for example during the winter the advection term dominate, while during summer the energy term can dominate due to the increase of net radiation.

Studying Bowen ratio for agricultural ground, the focus is on the latent heat because the sensible heat does not depend directly on the plants (in the sense of stomata or transipration); however, the canopy contributes to the decrease of Earth's skin temperature with respect to the atmosphere temperature, this results in a rather zero Bowen ratio. Furthermore, sometimes during summer (i.e. maximum plant cover) negative daily bowen ratio can be observed.

Therefore, the analysis of Bowen ratio measured by eddy covariance tower can be split in two periods according with the impressing presence of plants and with their absence (remind that seeding took place on April 1st and the harvest on September 10th). During the period of plants growth the measured Bowen ratio shows on average the lower values of the whole year; this is what expected because of both latent and sensible heat competes in this sense. Specific features is noted when the plants stop to grow (in the middle of August), at that time plant transpiration decreases and consequently Bowen ratio rises until the harvest, when it reaches magnitude 2. As seen previously, even SurfPro tries to parameterize the behavior of plants, however it simulates that the crop growth has place during the spring instead of the summer, i.e. low Bowen ratio with reference to grid cell A.

While, if the period immediately after the seeding or the period after the harvest is considered, the main forcings of the Bowen ratio are the meteorology and the soil properties; in particular, observed fluctuations of the Bowen time series involved

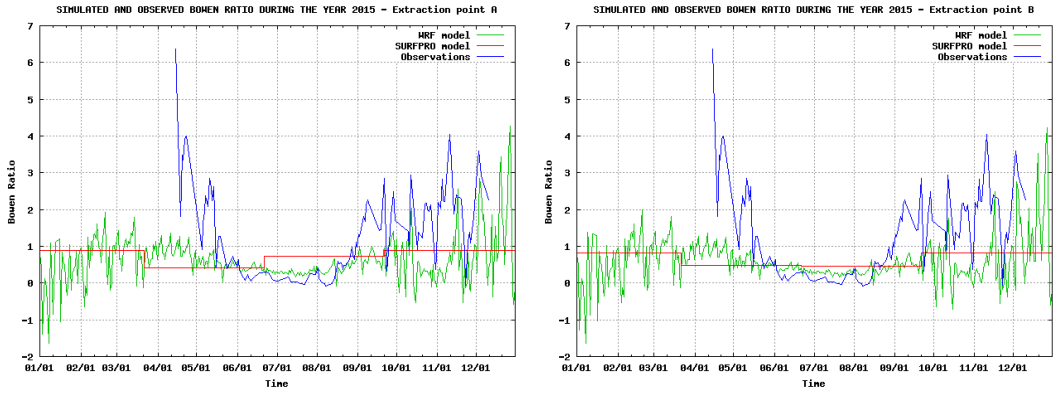

Figure 7.6: Bowen ratio measured by Beano station, parameterized by SurfPro and modeled by WRF for the year 2015. Two extraction points are selected, grid cell A and grid cell B.

atmospheric time scales. For example in the middle of April the advection of a mass of warm air over the cold land surface led to the increase of sensible heat and consequently to a peak in Bowen ratio. Therefore, Bowen ratio in these months (i.e. in absence of plant cover) is strongly dependent to atmospheric events.

On the other hand, SurfPro statically parameterization of Bowen ratio can be compared with the outputs of WRF model, remembering that the same procedure of measurements (selection of 9:00-16:00 time interval and calculation of average) is applied for obtain the WRF time series (i.e. daily Bowen ratio). One can note in figure 7.6 that for the both computational, WRF agrees better than SurfPro with the measurements during the period between the end of May and the end of August, that corresponds to the period when the plants are well-developed. Whilst, during other months the underestimation of Bowen ratio with respect the measurements can be observed, as shown in the following this behavior is related to an overestimation by WRF of the soil moisture in the same months, which contributes to the increasing of latent heat flux at the denominator of the Bowen ratio.

7.1.3 WRF simulation of soil moisture

Figure 7.7 shows the comparison between soil moisture measured in Beano site (within a layer from 0 to 30 cm) and soil moisture simulated by WRF within three different soil layers; the soil moisture quantity is defined as the ratio of volume of water over the total volume of the wet terrain.

First of all, a remark is made on the fact that the thickness of layers within which the soil moisture is calculated and simulated are different, however this does not affect the analysis because the content of water within the simulated soil layers is rather the same and one can suppose that it remains the same even considering corresponding depth layers.

Starting with the analysis, measurements related to the first months (not reported) are affected by some errors that were corrected starting from April; in addition, the soil moisture detects the watering of the maize field in the period from 25th May to 25th August. However, the watering results in the soil moisture as a peculiar pattern defined by a well-defined spike caused by the high evapotranspiration rate

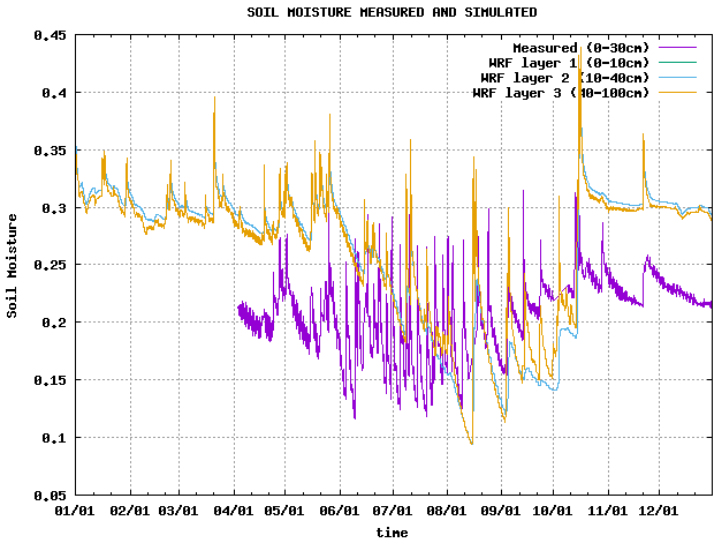

Figure 7.7: Time series of soil moisture measured by Beano station and simulated by WRF model within three different soil layers during the year 2015.

that permits a fast leak of the water from the ground; instead, the precipitation results in the soil moisture as a non-symmetrical spike having an elongated right tail dependent by different factors such as soil texture, plant presence, distance from saturation point.

For what concerns the Noah Land Surface model implemented in WRF, there are not large differences between the soil layer's moistures, in fact the patterns are closed each other or overlapped, as said previously. Excluding the period affected by watering (that WRF model cannot simulate), main differences between measured and simulated soil moisture are found in the period when the crop is not present over the surface or during its growing period, i.e. autumnal months or April and May, when one can find an overestimation of soil moisture. Therefore, Noah Land Surface model is able to simulate the evapotranspiration of the plants with some accuracy, whilst the description of the bare soil does not match the characteristics of the selected site.

The reason of this failure is attributable to a non-suitable description of the Beano soil type; in fact, WRF model (through the Noah scheme) defines it as *loam*, a soil composed mainly by silt with widely variable portions of clay and sand. Its characteristics related to the soil moisture are reported in table 7.2 together with the real observed values; soil field capacity is defined by the Soil Science Glossary Terms Committee (Soil Science Society of America, 2008) as the content of water, on a mass or volume basis, remaining in a soil 2 or 3 days after having been wetted with water and after free drainage is negligible, while the wilting point corresponds to the amount of water, on a mass or volume basis, that is held by the soil matrix that plant roots cannot absorb and a plant will wilt.

As was expected there are some differences between real and parameterized values that reflect in the modeling of the water soil content. Moreover, these discards are relevant and a new definition of the soil type for the Beano site and for the parts of Friulan plain closed to it is recommended. Unfortunately, among the soil types

Soil type	Field capacity m^3/m^3	Wilting point m^3/m^3
WRF loam modeling	0.329	0.066
Beano site	0.23	0.12

Table 7.2: Soil characteristics in Beano site of measures modeled by WRF (as a *loam* soil type) and reported by Alberti et al. (2010).

implemented by the Noah scheme, there is not a type that fit the observed values of soil field capacity and soil wilting point in Beano site (figure 7.8): soil field capacity is comparable to sand, while the wilting point to silty clay loam or silty clay loam. The sandy clay soil type could be used in place of the *loam* soil type, since it is the most similar to observations, as shown in figure 7.2.

As a consequence, the overestimation of soil water content affects the WRF evaluation of Bowen ratio and therefore the portioning of net radiation between latent and sensible heat flux; when the Noah Land Surface model overestimates the soil water content (i.e. April, May, second part of October, November, December), consequently the WRF model underestimates the Bowen ratio.

7.2 Roughness length

Roughness length is a parameter related to momentum exchange at the surface an cab be obtained through the similarity theory in statically neutral boundary layer conditions (paragraph 1.4.3) by inversion of the logarithmic horizontal wind speed profile (equation 1.25); the expression obtained for roughness length, and that will be useful computing to define the measured time series, is

$$z_0 = (z - d)\, e^{-\frac{Uk}{u_*}}, \tag{7.2}$$

where z is the measurement height, d is the displacement length dependent by the elements over the surface, k is the Von Karman constant (which values is between 0.35 and 0.40, in this thesis $k = 0.40$ is used), U is the wind speed in horizontal direction and u_* is the friction velocity defined by equation 1.23. The variables in equation 7.2 are U and u_*, while z_0 is a parameter of the equation that can be obtained in neutral or unstable conditions, according with Monin-Obukhov similarity theory.

Studying roughness length equation, one can observe that it is strongly dependent on the surface elements through the displacement height, moreover there is a dependence on the boundary layer conditions, by means of the horizontal wind speed measured at the height z and by friction velocity, both of them contribute to describe the status of wind shear generated turbulence.

As for Bowen ratio, even for roughness length SurfPro provides a seasonal modulation that takes into account only the characteristics of land use. Then, roughness length is lower when the field is plowed or seeded, during winter and spring, after it suddenly increases passing from spring to summer (with a high step) and finally it goes down during the winter, when the field is not worked. The pattern just described is well defined for the extraction cell A, where the prevalent land use is

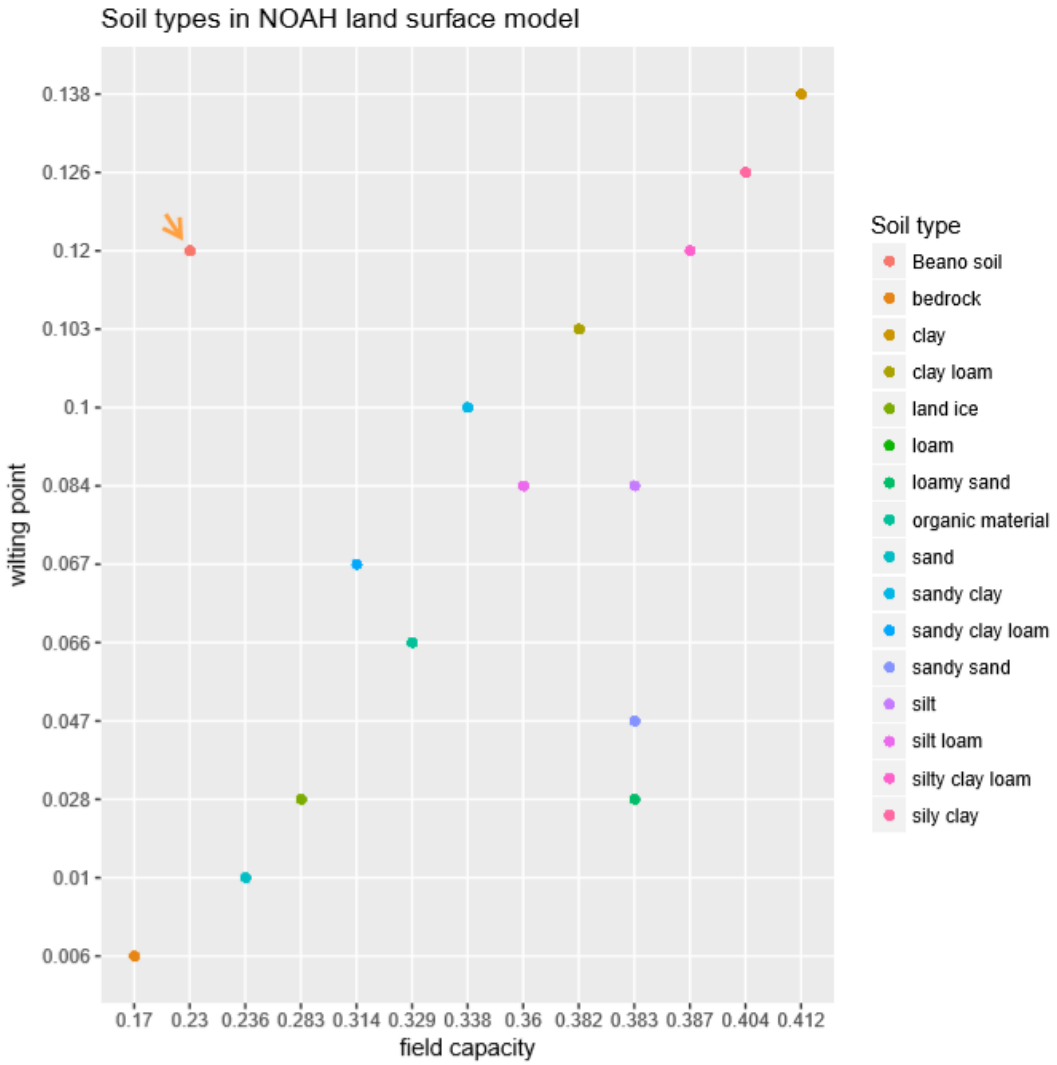

Figure 7.8: Scatter plot of soil type classes implemented by NOAH mode according to soil field capacity and soil wilting point. The values of soil field capacity and wilting point are used for the definition of the position of actual Beano soil (underlined by the orange arrow).

Arable land, non-irrigated and permanently irrigated, whilst for cell B, *Heterogeneous agricultural area*, the pattern is definitely flatter and difference between seasons are minimal.

7.2.1 Eddy covariance measurements

Aerodynamic roughness length Performing an eddy covariance experiment, in which the measurement height is known, the unknowns in equation 7.2 are the displacement height which varies in accordance with the plant cycle, the horizontal wind speed and the friction velocity. Lasts two quantities are measured by Beano eddy covariance tower using the sonic anemometer; while the first one was not measured during the 2015 and a model of plant growth will be used to obtain it. However, first step towards the definition of the measured roughness length time series for 2015 is the definition of a filter to select the measurements that satisfy the statically stable boundary layer conditions.

The filter is applied on the stability parameter z/L, which is made available by the eddy covariance measures dataset: values of z/L close to zero indicate statically neutral conditions of boundary layer, while more positive and more negative values indicate respectively stable and unstable conditions. The stability parameter is defined as

$$\frac{z}{L} = -kzg\ \frac{(\overline{w'\theta'_v})_s}{\overline{\theta_v} u_*^3}, \tag{7.3}$$

in which a positive value of parameter is obtained if the buoyancy term $\overline{w'\theta'_v}$ at the surface is negative, and is a negative value if the buoyancy term is positive. Instead, if the friction velocity (i.e. wind shear driven turbulence) prevails over buoyancy term (i.e. thermal driven turbulence), neutral conditions of boundary layer are delineated and parameter results close to zero. Moreover, statically neutral conditions of boundary layer are selected choosing a widely used threshold value for stability parameter equals to one tenth of measurements height (in this case 2.5 m, that leads to $|z/L| < 0.25$).

After the application of filter, a first evaluation of roughness length (called aerodynamic roughness length) is calculated using a simplified formula in which displacement height is "incorpored" within z_0, that is

$$z_0 = z\ e^{-\frac{Uk}{u_*}}. \tag{7.4}$$

This equation permits to obtain a first estimation of roughness length that can be used to make considerations about the availability of data and the quality of filter applied. The time series obtained is shown in figure 7.9, where a moving average with a window length of 21 measures is applied; some features can be easily observed. Firstly, the measurements are available starting from the end of April (remark that to compute the roughness length both the measures of friction velocity and sonic wind speed must be taken); secondly, the roughness length increases in accordance with the crop development and sharply decreases in correspondence with the harvest (early Septemper); finally, there is an increase of roughness length starting from October until the end of the year, this part is associated with a large standard deviation.

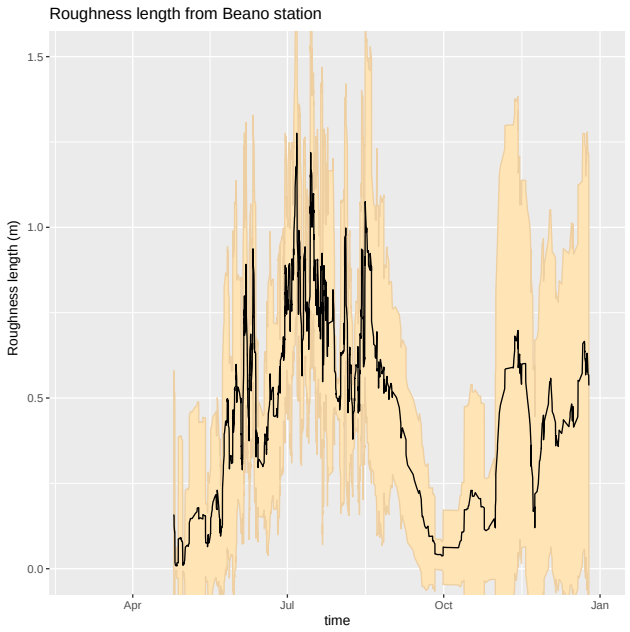

Figure 7.9: Aerodynamic roughness length with standard deviation measured by Beano eddy covariance tower during 2015.

	APR	MAY	JUN	JUL	AUG	SEP	OCT	NOV	DEC
Measures	299	969	897	931	988	882	528	772	672
Filtered	52	150	363	467	315	50	40	66	56

Table 7.3: Number of available half-hour measurements before and after the application of neutral stability filter. Availability before the filtering is driven by the contemporary presence of sonic wind speed and friction velocity measurements. Second row refers to only boundary layer statically conditions.

These large values in absence of the plants could be counter intuitive and therefore should be carefully analyzed. During lasts months of the year the crop is not present on the field and the rising is only due to boundary layer statically conditions; in particular, these months of year 2015 are affected by strong stability that had place in a large portion of Europe, as shown by figure 7.10.

Strong stability leads to two main consequences related to roughness length: the first one is that Monin-Obukhov similarity theory is not widely applicable and only few measurements pass the filter on neutral stability conditions, leading to a less robust estimation (see table 7.3 that shows the number of half-hour available measurements before and after the filtering); while the second one is that when a measurement passes the filter, the values of measurements are close to the sensitivity of the sonic anemometer and therefore large uncertainty is associated. Moreover, another factor that affect the roughness length evaluation in the last months of the 2015 was the presence of fog, which may have influenced the sonic anemometer measures, as seen in chapter 6 eddy covariance instruments are sensitive to water on them.

In conclusion, the lack of neutral boundary layer conditions (which are the base

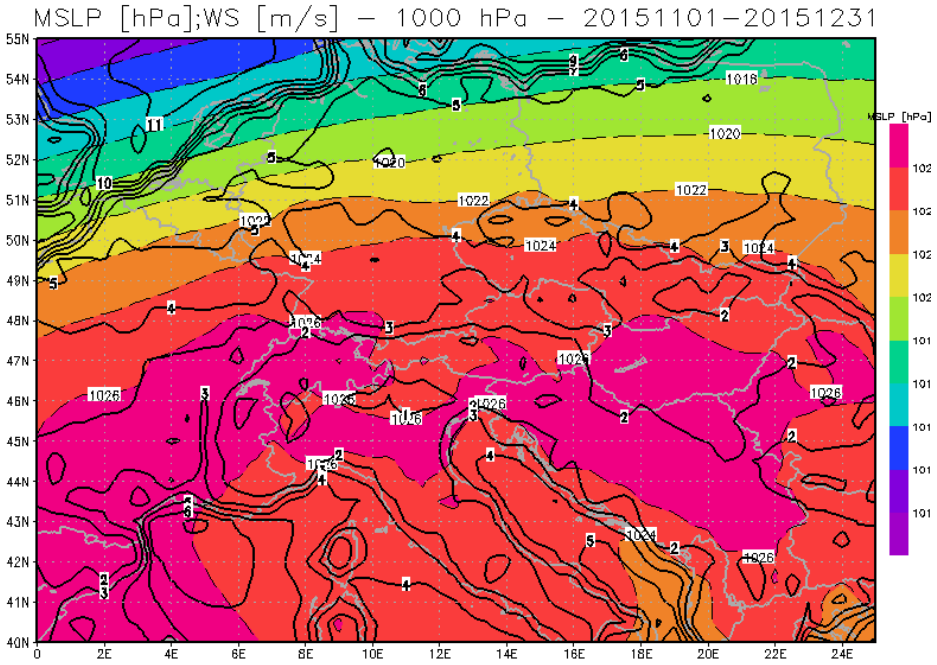

Figure 7.10: Synoptic map of mean sea level pressure (colors with dotted contours) and mean wind speed (bold line) during the months of November and December 2015.

for the applicability of similarity theory) during the last three months of the year has got a direct consequence in the number of available measurements in that period; therefore it is decided to remove from the time series these months, considering in the comparison with SurfPro parameterization only the roughness length when the crop is present over the agricultural field.

Roughness length Last step consists in the definition of roughness length time series net of displacement height. To make it possible, the height of crop must be inserted in the roughness length evaluation, not being aware of the exact plant evolution during year 2015, a model of plant growth based on measurements performed on the same crop cultivated on the same field during the years 2007 and 2008 is used. This model is shown in figure 7.11 and is built by extrapolation over the number of days from the seeding. Considering the year 2015, the crop management is not changed compared to previous years, proof of this is the number of the days of plant life cycle, that is 162 compared to 160 of 2007 and 2008. Therefore, model of the plant growth during 2007 and 2008 can be used for the 2015 scaled for the day of seeding.

Being aware of the plant height time series, with reference to Yu et al., 2017 the displacement height can be estimated through $d = 0.67h$ (where h is plant height) and can be used to receive the roughness length comparable with SurfPro parameterization. Moreover, an honest evaluation of SurfPro roughness length parameterization requires that the comparison is performed with measurements that parameterization can able to detect. For example, a seasonal parameterization (such

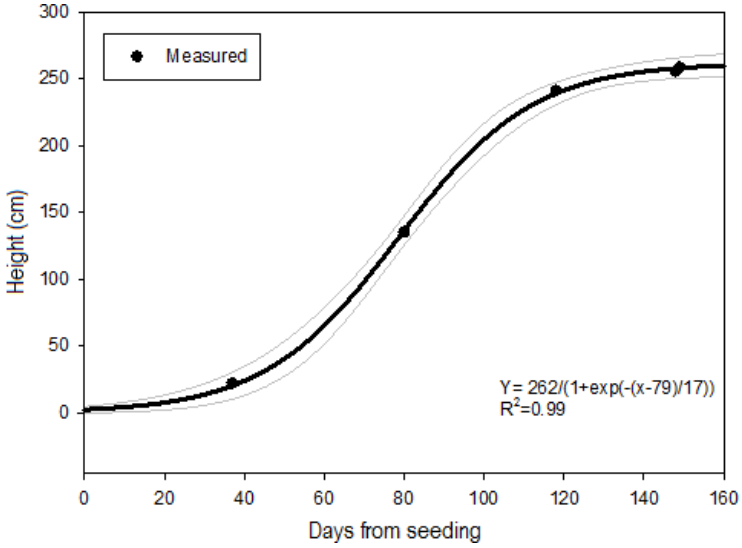

Figure 7.11: Plant growth model derived by measures of the height of plants during the years 2007 and 2008 for the same maize plants cultivated in the same agricultural field.

as what performed by SurfPro) cannot detect diurnal or weekly fluctuation; therefore, to perform a suitable comparison the moving median of roughness length is considered with a time window of 1 week. Moreover, only high quality data are used (quality flag related to momentum flux equals to zero). In addition, to avoid median estimations derived by few measure, a further condition on data availability is applied. A filter is performed through a count of the available measurements within the moving window, if the moving median is calculated with less than 10% of possible measurements it was discarded. To summarize, estimations of median roughness length over a weekly moving window are reported in figure 7.12 associated with the 0.25th and 0.75th percentiles (remember that the only period with the crop over the ground is considered).

Feature of the new time series is that roughness has got low values until the end of May, afterwards a visible peak is detected, and finally a rather constant value of roughness length can be observed, when the growth of plant was stable.

Uncertainly on the estimation of the roughness length are greatest during the period of fast growth of the plant (i.e. over the start of June) and they are associated to the fitting of the plant growth model with eddy covariance measurements. In particular, the uncertainly in this period shows that if the model was shifted forward or backward by few days the roughness length could result rather different.

Anyway, performing the statistical evaluation of time series, the uncertainly associated to the measurements will be taken into account and therefore the peak between the end of May and the beginning of June will not matter much in the global evaluation of SurfPro parameterization.

7.2.2 Comparison between measurements and models

Having defined a suitable measured time series of roughness length, now the comparison between models ad simulations can be plotted in figure 7.13 for the two

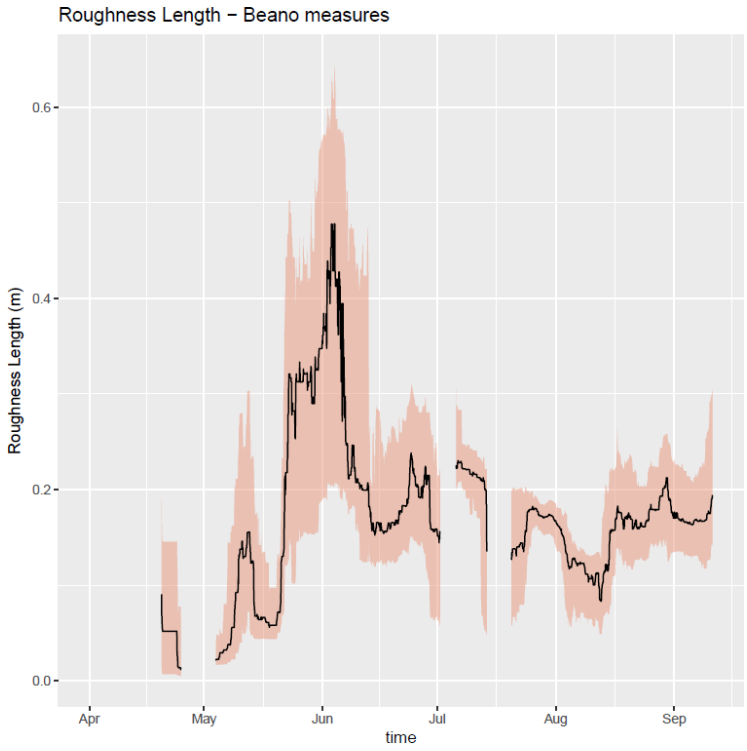

Figure 7.12: Median roughness length for year 2015 determined within moving windows of one week, shaded region of plot is determinated by 1st and 3rd quartiles.

extraction sites noting that also WRF provides the roughness length as output and further calculations are not needed.

Firstly, considering the two SurfPro cells (red lines) one can observe that the statically parameterizations made by the processor are considerably different: for the grid cell A there is an evident modulation that try to follow the life cycle of the crop, while for the grid cell B the seasonal modulation is rather disappear and the difference between seasons tend to zero, as said previously. However, considering that site extraction cell A is the closest to the tower one can expect slightly differences moving away from the site of interest. However, the reference site for statistical evaluations in further chapter is the extraction cell A.

This difference is not found in the WRF model, that describes the roughness length in the same way within the two cells; in comparison with the grid cell A of SurfPro, the roughness length modeled by WRF (trough NOAH land scheme) does not present steep values but a smooth function that does not reach the SurfPro maximum value during the summer and the minimum value during the winter.

Moreover, considering also the measured roughness length (during the period of maize cultivation) one can note that the growing period (picturing that the peak vanishes with a more suitable model of plant growth) was simulated better by WRF model than SurfPro parameterization. While the observed summer peak is positioned in the middle between the values of roughness length provided by the two models.

Finally, in paragraph 7.2.1 it was seen that for the last months of 2015 the equation 7.2 for roughness length (derived by the equation of logarithmic wind profile)

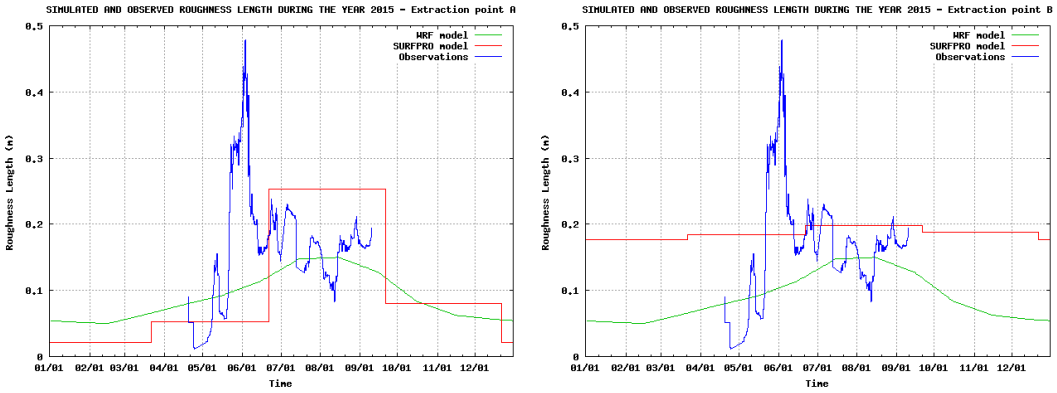

Figure 7.13: Roughness length measured by Beano station and parameterization by SurfPro and WRF (trough Noah scheme) for the year 2015. Two extraction points are selected for the models.

is often not applicable (table 7.3) because similarity theory conditions are not meet. However, both SurfPro pre-processor and WRF model do not consider that logarithmic function is not a suitable description for the wind profile in stable conditions of boundary layer, recent studies are currently faced this topic (Optis et al., 2014) and in the future could lead to improvements in air quality modeling.

7.3 Leaf Area Index

Leaf area index is one of the quantities related to canopy difficult to observe with measurement on field (it is defined as the one sided green leaf area for unit ground area in broadleaf canopies), and usually is determined through satellite measures. Even in the context of this thesis, the on field leaf area index measures of the maize crop are not available and data from MODIS project is taken into account. The description of these kind of measures together with some technical details are already explained in section 5.2, therefore in this part of thesis only few recalls are considered performing the comparison between measurements and models.

SurfPro parameterization of leaf area index is a seasonal parameterization that would define the agricultural cycle of maize crop; and is built by a flat winter minimum and a flat summer maximum linked by two segments during spring (positive slope) and autumn (negative slope), as will see below.

7.3.1 Remote sensing measures

NASA provides leaf area index data with a spatial resolution of 500 m and time step of 8 days, i.e. 46 measures over the entire year. On the other hand, spatial resolution of SurfPro grid is 2 km, this means that if the two meshes were exactly overlappable, 16 MODIS cells describing leaf area index subtend the same SurfPro computational cell. This issue must be taken into account in the comparison; in fact, a simple extraction of leaf area index from the nearest neighbor MODIS grid point leads to compare each of the two SurfPro selected cells with an arbitrary MODIS extraction related to one of the 16 cells which enter into the bigger SurfPro cell.

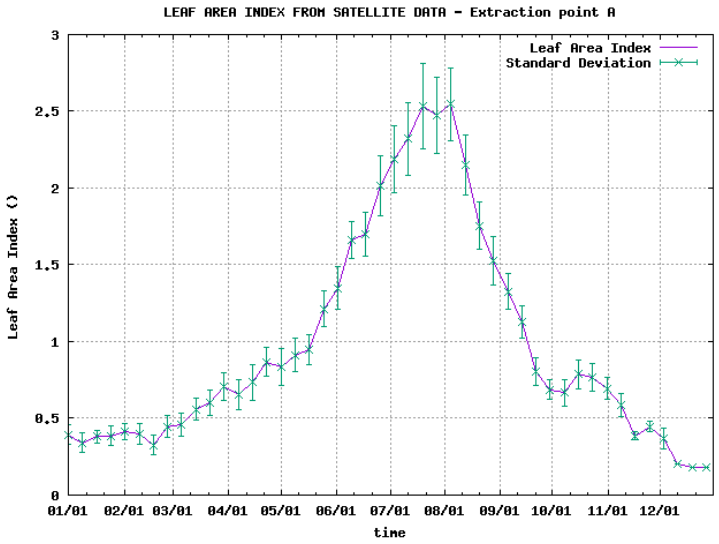

Figure 7.14: Leaf area index detected by MODIS project in the extraction cell A for the year 2015.

Therefore, the proper use of MODIS data is to average the cells whose center enters into the spatial domain of each of the SurfPro selected computational cell (i.e. cell A and cell B). Doing that, one avoids that SurfPro parameterization is compared to time series related to smaller spatial resolutions, which elements cannot be detected due to SurfPro spatial resolution. Moreover, the averaging operation was just described is similar to the operation that SurfPro performs when it defines the statically parameters of the computational cells of domain in accordance to land use of the sub-cells from CORINE database.

For instance, figure 7.14 reports the extraction of MODIS leaf area index in correspondence of the grid cell A of SurfPro model. A remark is made on the number of cells averaged, that is 15 (one is lost due to staggering between the different grids) for both the SurfPro extraction points. Moreover, maximum and minimum values of plot (which occur in July and December) are coherent with Bousetta et al. (2014), that indicates that crops and grass regions show pronounced seasonal cycles with leaf area index varying between 0.2 and 2.7, that is comparable with MODIS measures. In addition, one can note that the slope on the left side of the time series is less steep than what observed in the right side, this reflects that the drying of the plants and the following harvest have place in a shorter time than the plant growth. Clearly, a vertical collapse of the leaf area index following the harvest can not be observed due to the presence of other agricultural fields within the spatial resolution of MODIS data, and to the fact that cut plants are usually left on the ground after the harvest.

7.3.2 Comparison between measurements and models

Besides SurfPro parameterization and remote sensing measures, also the WRF parameterization of leaf area index is reported in figure 7.13. As seen, the leaf area index is a quantity that shows a remarkable seasonal modulation that could be easily described knowing maximum and minimum values; however, the figure shows

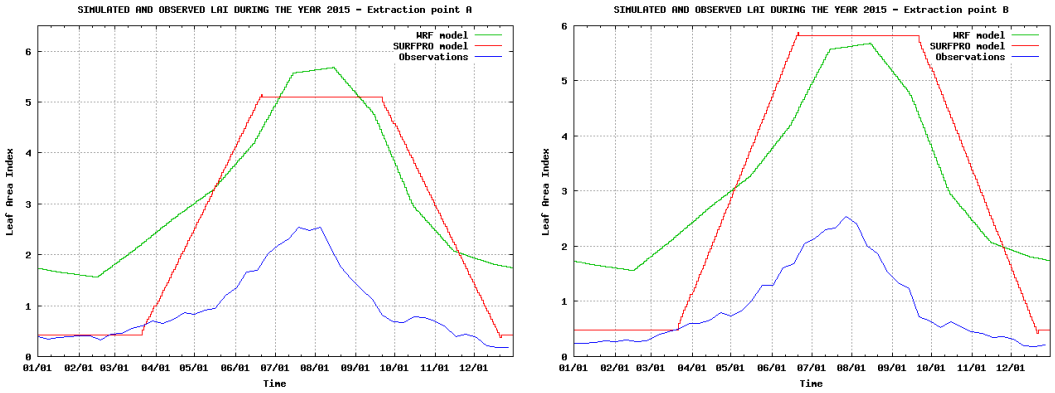

Figure 7.15: Leaf area index measured by MODIS project and parameterized by SurfPro and WRF (trough Noah scheme)for the year 2015. Two extraction points are selected for the models, in this case also the remote sensing measures are extracted for the two points.

that SurfPro is able to describe LAI in an acceptable manner only during winter, while the maximum is greatly overestimated (it reaches values that can be observed for forests, Bousetta et al., 2014). Moreover, SurfPro does not take into account thesudden drop of the LAI due to the harvest of the crops and consider at the same manner the growth and the decrease of plants.

On the other hand, WRF model is able to describe the seasonal pattern (i.e. the shape) of leaf area index with good quality. However, for the entire year WRF provides (by means of NOAH land surface scheme) a systematically overestimate of leaf area index.

7.4 Ground albedo

Ground albedo (also referred as surface albedo) is the variable that estimates the quantity of shortwave solar radiation (direct and diffuse) that does not enter in the surface energy balance, but is reflected towards the space by the Earth's surface. In spite of the simple physical definition, ground albedo is the only SurfPro statically parameter that is not dependent only on the surface characteristics and on the boundary layer quantities (e.g.stability parameter).

In fact, ground albedo is not an intrinsic property of a surface (Coakley J.A., 2002), and for any surface it depends on two factors that enters in the process of measure or in the process of modeling, that are the spectral and angular distributions of the incident light, which in turn are governed by the atmospheric composition and by the direction of the beam of light from the sun (i.e. the solar position).

Spectral dependence (i.e. first factor) is usually simplified in terms of wavelength intervals for which the surface reflectance is rather constant, within the visible and near-infrared spectral intervals. On the other hand, the angular distribution is described by dividing the incident light into two components, the direct beam from the sun and the diffuse component composed of sunlight that has been scattered from atmospheric particles and clouds, and therefore affects the surface with different angles (note that also the reflected beam can undergone scattering and return towards Earth's surface). These components are respectively the black-sky and white-sky

albedo described in section 5.3.

Due to these peculiarities, according to the usage within the code, models could not implement the albedo in the same way. For instance, SurfPro seasonal statically parameterization takes into account only the characteristics of the surface, neglecting diurnal and annual dependence to solar position. On the other hand, WRF model output reports the surface albedo taking into account the dependence to solar zenith angle[1]; this makes the two models not directly comparable.

For that reason, starting from the ground albedo obtained by remote sensing measures (data acquisition is described in section 5.3) two time series are derived: the first one to perform the comparison with SurfPro statically parameterization and the second one to perform the comparison with WRF albedo. However, the two time series derive from the same satellite measurements processed by CAMS project. Recalling the essential features of section 5.3, these albedo measures are provided every minute for the two SurfPro extraction points (cell A and cell B) by a linear interpolation from a 0.05° grid.

7.4.1 Comparison between measures and SurfPro model

As introduced previously, SurfPro parameterization for ground albedo provides a time series with seasonal time steps which takes into account the properties of the land use, in this case the common annual cycle of agricultural fields. This pattern shows a minimum value of albedo in correspondence with the period when plowing and seeding is performed and the ground is darker, maximum value is related to the period for which there is the crop over the field, and finally the albedo in autumn and winter is parameterized as for an uncultivated field (i.e. on the ground little weeds appear and the prevalent color is lighter than for a worked field).

This type of parameterization, certainly, is not suitable to describe the daily variability of the albedo, which is governed by the solar zenith angle; therefore a method to compare measured and parameterized time series avoiding inhomogeneities must be found starting from the remote sensing measures. The most judicious way to make it possible is to calculate the daily averages of measured albedo; resultant time series is shown in figure 7.16, where the relevant standard deviation during the summer is related to the higher variability of albedo related to the greater range of zenith angles during a day. Moreover, the obtained time series reveals a remarkable dependence of albedo to the agricultural cycle: the growth of the plant from April to the middle of July (detected by measured leaf area index) corresponds to the increase of albedo because the leaves increase in number; afterward the crop starts the seasoning and the leaves change in color, became dry and smaller, this process matches with the decreasing of albedo until the harvest, when has place a steeper decrease due to mechanical processing on field (i.e. plowing during the winter).

As in the case of leaf area index, the autumnal decrease of albedo due to harvest is the result of the contributes of different crop fields close to the selected extraction point, and therefore one cannot expect to detect the exact date when harvest took

[1]Solar zenith angle is the angle between the zenith and the center of the Sun's disc. It is the complementary of the solar elevation angle and during the day reaches the minimum at the noon. While, in the Northern hemisphere over the year its pattern shows the maximum at the winter solstice and minimum at the summer solstice.

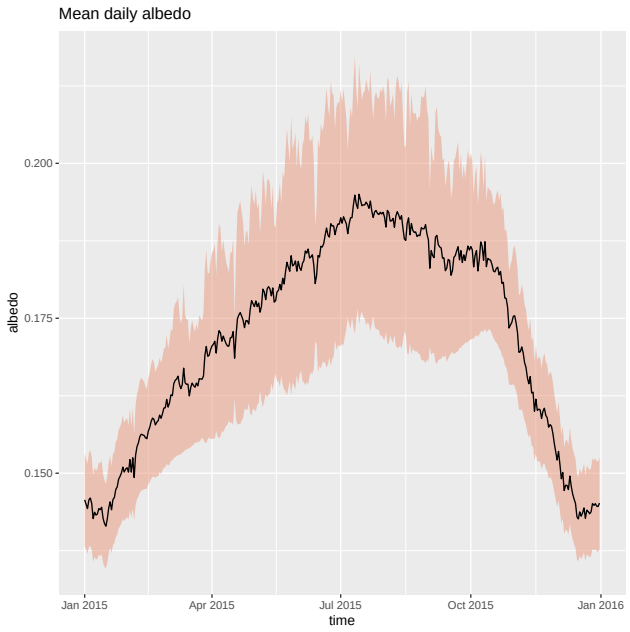

Figure 7.16: Time series of average daily albedo provided by CAMS project. Shaded region defines the standard deviation associated to daily averages.

place in the selected agricultural maize field. Another aspect to consider is the fact that cut plants are usually left on the ground after the harvest and therefore the largest variability of the albedo occurs when the cut plants are collected from the ground and the field becomes darker.

Time series of albedo measured by remote sensing and parameterized by SurfPro are reported in figures 7.17. Considering the extraction cell A, that refers to a cell which prevalent land use is *Arable land, non-irrigated and permanently irrigated* land use, one can note that SurfPro approximates with some accuracy the maximum (in summer) and minimum values of albedo, even if the minimum is shifted from the actual position; on the contrary, the seasonal time step of parameterization makes impossible for SurfPro to describe in a suitable way the intermediate seasons and the period in which the plants grow[2].

Instead, the purpose of parameterization related to cell B (prevalent land use defined as *Heterogeneous agricultural area*) is to provide reasonable values of albedo during the entire year because of the variety of sub-cells included; from this point of view, SurfPro has achieved its purpose because statically parameterization provides for the entire year values not far from the measured value even without follow any pattern.

7.4.2 Comparison between measures and WRF model

WRF implementation of albedo contains the dependence on the solar zenith angle, this must be considered for the comparison with surface albedo from remote sensing

[2]Hypothesis that information about mid-seasons was lost passing from an old SurfPro version to a more recent one has risen, but it must still be demonstrated.

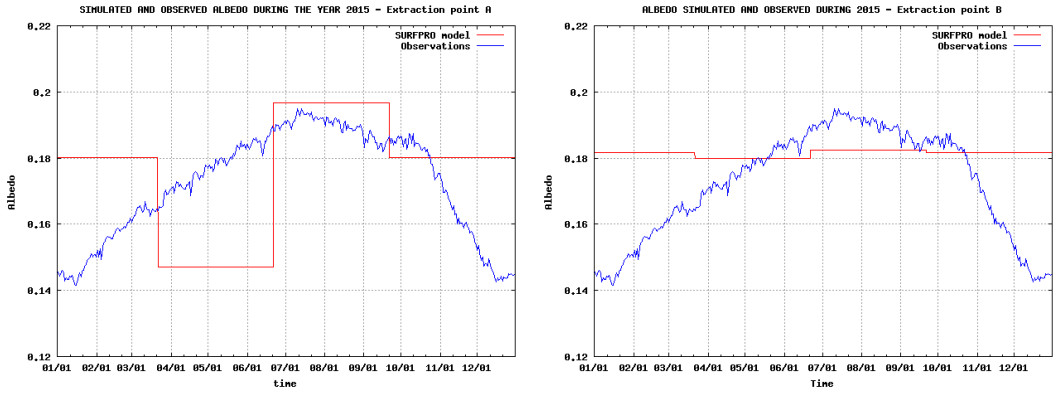

Figure 7.17: Ground albedo defined by CAMS project and parameterized by SurfPro for the year 2015. Two extraction points are selected for model and remote sensing data.

measures. On the contrary, the comparison between the two models is preventively rejected because different quantities would be compared.

As previously said, dependence from zenith angle enters only in the computation of albedo through the black-sky albedo, i.e. the albedo determined for direct solar beam, whilst the white-sky albedo is taken to be isotropic. As an example, the relation between black-sky albedo (direct light) and white-sky albedo (diffuse light) from Coakley (2002) is reported

$$a_{bs}(\theta) = a_{ws}\frac{1+d}{1+2d\cos\theta}, \tag{7.5}$$

where d is a parameter dependent on land use and θ is the zenith angle. Unfortunately, WRF model supplies as output only the final albedo, result of the summation of black-sky albedo and white-sky albedo within the visible and infrared spectral domain (equation 5.10). Therefore, one cannot apply the exact correction to the albedo output of 2015 WRF simulations.

To work around the problem a rough correction is applied using the cosine of the zenith angle and selecting the only measurements at the noon. A remark is made on the fact that this is an attempt performed at the end of the computational process to make comparable two time series (remote sensing measures and output of WRF model). Afterwards, the comparison is made effective selecting the noon measures from the remote sensing data frame. Result of comparison process is shown in figure 7.18.

The graph reports the final time series of albedo used for the validation of WRF modeling through satellite measurements. In the process that made the time series comparable, the different definition of remote sensing time series (i.e. choosing the only measures at noon) has brought to a jagged time series during the period of plant cover and to a smooth line when plants are absent. On the other hand, the WRF albedo time series has undergone a correction too high in January and December, when the solar zenith angle is higher. Despite such difficulties in the analysis, some conclusions can be formulated: the concavity of the annual pattern is rspected; the maximumis well reproduced, even if shifted in time; the winter minimum is underestimated.

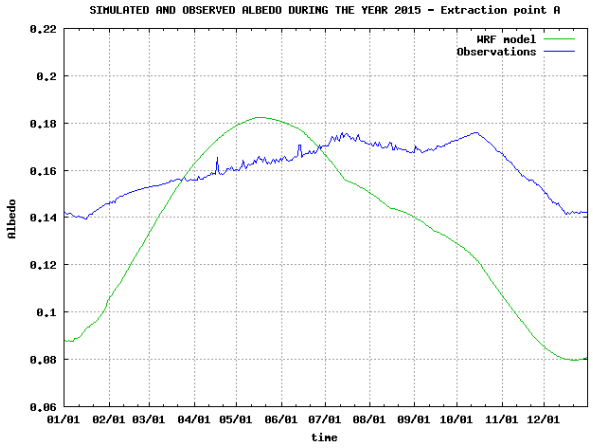

Figure 7.18: Ground albedo defined by CAMS project and modeled by WRF for the year 2015. Only the extraction point A is considered because there are not evident differences between the two cells of extraction, WRF model defines the same land use for the more adjacent computational cells.

7.5 Soil parameter

Soil parameter is a variable defined expressly by SurfPro processor to evaluate the ratio of surface energy balance that goes into the ground and it is defined as $H_c = G_0/R_n$, where G_0 is the ground flux at the surface and R_n is the net radiation at the surface, which expression can be find in equation 1.21. The behavior of net radiation during the day can be easily pictured as a bell curve with the peak at the noon, while the typical diurnal evolution of ground flux at the surface requires a special description.

During daytime the sun heats the Earth's surface, and a portion of heat is conducted downward into the ground from the warm surface; whilst, during nighttime the Earth's surface cools by releasing longwave radiation to space, therefore the ground heat flux is conducted from the warm ground up to the cooler surface. Considering the entire year, a reasonable observation is that the seasonal modulation permits the overall balancing of the ground heat flux at the surface, if that does not happen there was a sink of energy in the deepest layers of the ground.

SurfPro defines the new variable to close the surface energy budget at each computational time step, in order to compute the effective amount of net radiation which is able to start the turbulent heat fluxes. SurfPro parameterization follows Holtslag and Van Ulden (1983) and previous works (e.g. De Bruin and Holtslag, 1982) that provide an estimation of soil parameter during the daytime for a grass covered surface in the Netherlands equal to 0.1. Considering SurfPro runs of year 2015, soil parameter is initialized with a value that remains constant throughout the year; for the extraction cell A this ratio is equal to 0.165, while for cell B it is 0.153. This means that SurfPro does not consider the possibility that during the day or the year some modulation of this ground property can occur.

7.5.1 Soil parameter from measures

Beano station provides separately the half-hour measurements of the quantities involved in the definition of SurfPro soil parameter: the net radiation is measured by a radiometer, while the ground heat flux is measured by a plate placed at 5 cm below the surface. Before starting the analysis, that will be performed studying separately the two quantities, the availability of measures is considered in order to know the limits of data set[3]: for the net radiation critical months are March, April and October, while for ground flux they are July, August and October. In these months the available measures are about the 70% of the amount of possible measures, except for May in which this percentage goes down to 53%. Furthermore, considering the entire year the hourly availability of ground heat flux is lowest between 8.00 to 12.00 local time reaching a minimum of about 84% of the amount of possible measures; while net radiation availability does not have remarkable peaks and it is rather about 90%. Note that these percentage are rather high compared to availability of eddy covariance measures.

The analysis starts considering singularly the median daily fluxes of net radiation and ground heat flux during the year 2015, that are reported on figure 7.19. The net radiation according to the hours and to the months has got the expected pattern: peaks during the central hours of the day and negative values during the nighttime (longwave radiation), with a interquartile range dependent on the hours and the seasons (usually months with variable atmospheric conditions are related to large interquartile distance during the day). On the other hand, the median of the soil heat flux is rather constant during the day, even during the daytime there are some fluctuations resulting in a larger interquartile range.

However, the main feature of figure 7.19 is that all the monthly medians of soil heat flux are positive during both daytime and nighttime, that means a ground flux from the warm Earth's surface to the lower soil layers (compatible only with daytime behavior of solar radiation). Then, the measurements depict a situation in which continuously heat flux (which magnitude changes during the months) is flowing from the warm Earth's surface to the cooler deeper layers. This means that there should be a sink of heat in the deepest soil layer which maintains them cooler than the Earth's surface.

This hypothesis is not realistic and therefore one can easily evince that measurements are affected by an instrumental error that produces a constantly positive contribute to the evaluation of ground heat flux. Therefore, Beano station measurements of ground heat flux must be necessarily rejected, making impossible the evaluation of soil parameter from measures, and consequently the evaluation of SurfPro statically parameter with measurements.

7.5.2 Soil parameter from WRF model

As said previously, soil parameter is an intrinsic parameter defined within SurfPro model for respond to computational needs and to satisfy the energy closure step by step. WRF model is based on a different algorithm for surface exchanges (Noah land

[3] Availability of measurement must be considered because solar radiation and ground heat flux are measured by different instruments than eddy covariance measures, for which the study of availability was performed in section 6.2.

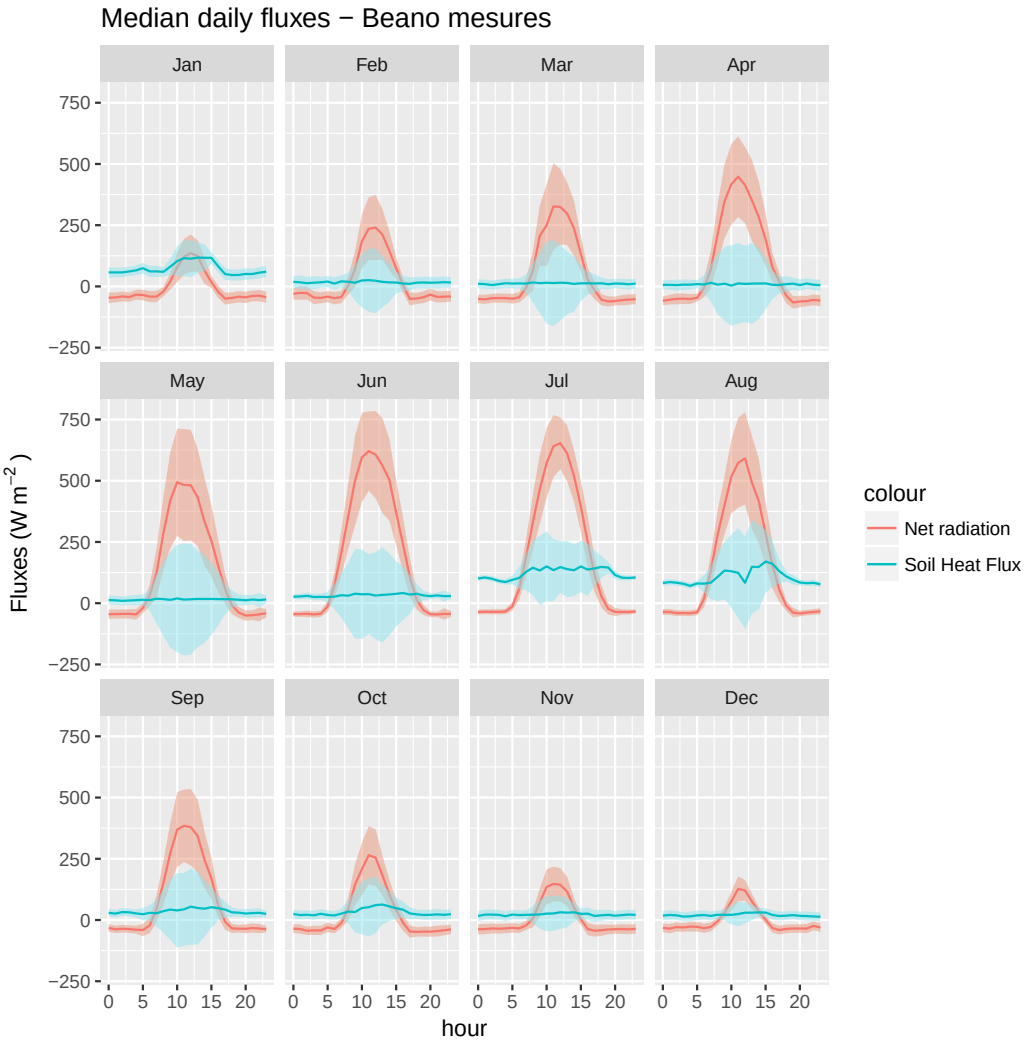

Figure 7.19: Median daily fluxes of net radiation and ground heat flux measured by Beano station during the year 2015. Shaded regions are delimited by 25th and 75th percentiles.

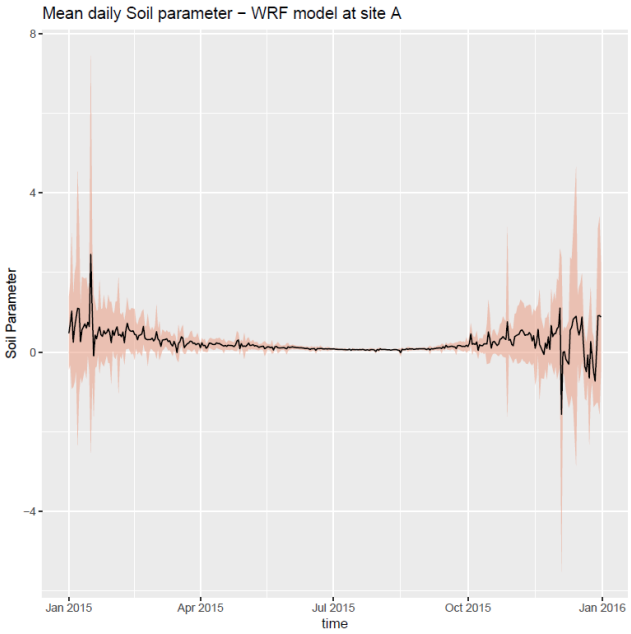

Figure 7.20: Time series of soil parameter calculated by WRF outputs of the year 2015 at the extraction cell A.

surface scheme) and does not need to calculate the soil parameter. Therefore, the Soil parameter from WRF model is calculated starting from the outputs of ground heat flux, latent heat flux and sensible heat flux, plus a field defined by the model as "Noah residuals" which stores the residuals of the surface energy budget and that does not have any physical reasons (in other words, the flux needed to close the surface energy balance).

However, this field is almost always filled by flux values with magnitude of the order of $10^{-1}\ Wm^{-2}$, with rare exceptions where they assume values between 1 and 2 Wm^{-2}. Therefore the field containing residuals can be neglected compared to typical values of average daily heat fluxes (from 10^1 to 10^2), and soil parameter can be calculated using the usual expression is $H_c = G/(G + H + LE)$.

To obtain a time series useful to evaluate the SurfPro parameterization, the analysis of WRF outputs follows what done for the Bowen ratio, that means an individually evaluation of daily average fluxes followed by the evaluation parameter (which turns out to be a daily average). Moreover, as for Bowen ratio, the daily average fluxes are calculated taking into account the central hours of the day, from 9 to 16 local time, to avoid strong fluctuations related to the denominator next to zero. Finally, daily values with high associated error are rejected from the time series (standard deviation greater than 5).

Result of analysis is reported in figure 7.20 for the grid cell A (cell B is not reported because similar result is obtained), where the mean daily soil parameter is reported with the associated standard deviation. One can note a time series similar to what found for Bowen ratio: during the central period of the year (i.e. spring and summer) soil parameter is rather constant, while a period of high variability is detected from October to April. The high variability is likely due to the inclusion

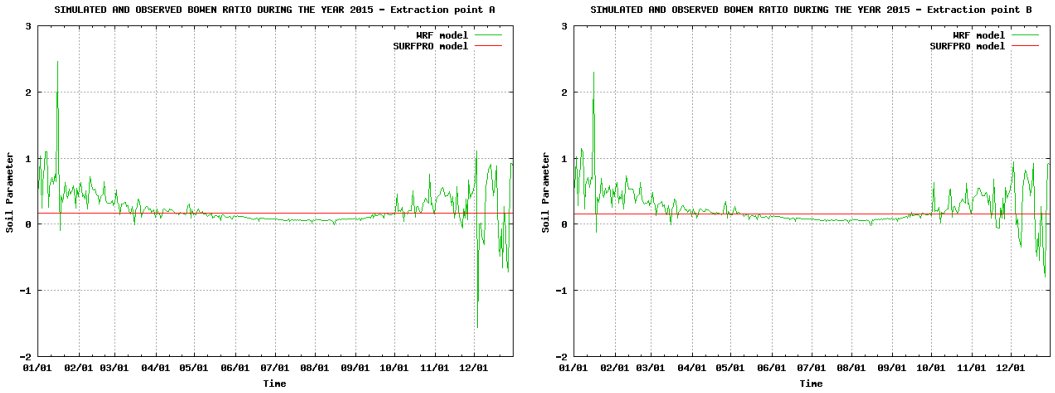

Figure 7.21: Soil parameter parameterized by SurfPro and modeled by WRF for the year 2015. Two extraction points are selected, cell A and cell B.

within data of some measures taken during the sunset.

Furthermore, the comparison of the obtained time series with the single parameter of SurfPro parameterization is reported in figure 7.21 for cell A and cell B. Considering both cases, SurfPro overestimates the amount of heat which goes into the ground from May to October, while for the other months SurfPro provides an underestimations of that, even if for December it seems that SurfPro centers the middle point of oscillations.

7.5.3 Annual budget of ground heat flux

The ground heat flux annual budget is evaluated for the two models and for the observations made by Beano eddy covariance tower. During an entire year the closure of the balance is reasonable, in other words the surface soil layer (infinitely thin) has not sufficient thermal capacity to accumulate energy and heat. Obviously, in the real word some bias from the perfect zero of annual budget is expected. In table 7.4, which shows the annual average of soil heat flux during the year 2015 (all the hours of the day), and the annual summation of the same quantity compared with annual incoming solar radiation, several aspects can be highlighted.

Firstly, SurfPro does not close the balance, the annual heat into the ground is only one dimensional order smaller than supplied annual incoming radiation (10^5 versus 10^6 kJm^{-2}), this can be read as an average annual flux of 12.6 Wm^{-2} which remains in the thinner first layer of the ground. Anyway, the purpose of this model is to provide to air quality models reasonable boundary layers quantities without considering the particularity of soil physics.

Instead, WRF includes the closure of the balance. In fact, the annual heat into the ground is three-dimensional order less than energy supplied by incoming radiation during the entire year (10^3 versus 10^6 kJm^{-2}). A confirm is found considering the annual average flux stored into the ground, that correspond to 0.1 Wm^{-2}, with a high standard deviation due to seasonal and diurnal patterns.

In addition, the problems regarding the in-situ observations finds a confirmation: the annual amount of heat into the ground is 1.1 10^6 kJm^{-2} and we are far from the closure of the balance, as confirmed by the annual amount of incoming radiation ob-

	Annual average flux into the ground (Wm^{-2})	Annual heat into the ground (kJm^{-2})	Annual incoming solar radiation (kJm^{-2})
SurfPro	13 ± 31	$3.97\ 10^5$	$5.45\ 10^6$
WRF	0 ± 44	$2.93\ 10^3$	$5.32\ 10^6$
Measures	54 ± 50	$1.1\ 10^6$	$4.42\ 10^6$

Table 7.4: Annual average flux into the ground, total amount of heat into the ground and incoming radiation simulated at the extraction point A by SurfPro and WRF and measured by Beano station; same results are obtained for grid cell B. The comparison is performed using the only pairwise measurements, therefore there is an amount of 9.88% of possible measurements which do not enter in the annual budget. As an example, typical values for incoming solar radiation at the noon in the Beano site is 300 Wm^{-2} during the winter and 900 Wm^{-2} during the summer; while typical values of the daily amount of solar radiation is 5 10^3 kJm^{-2} during winter and 25 10^3 kJm^{-2} during summer.

served ($4.42\ 10^6$ kJm^{-2}). These results are defected to valid observations clustered in July, August and October that makes both the variables (i.e. total amount of solar incoming radiation and heat into the ground) underestimated by about 10%; this estimation is based on the total number and on the season of occurrence of non available measures. Therefore, because the closure of the budget is far from being observed, a further evidence of the uselessness of the Beano tower ground measurements is found. Probably they have suffered some instrumental problems; even the already observed positivity of ground fluxes is certainly due to the same measurement error.

Finally, observations can be made about the annual incoming radiation, the difference between the two models is due to the different definitions of cloud cover: SurfPro implies the definition of fractional cloud cover (0 corresponds to clear sky conditions and 1 corresponds to total cloudiness), while WRF contains a sub-division of the clouds according to the height of clouds. To give an idea, the difference between the annual incoming radiation of SurfPro and WRF is roughly equal to more than five sunny days of July, each one supplying 25 $10^3 kJm^{-2}$ to the Earth's surface.

Chapter 8

Skill scores and their analysis

Skill scores are generally defined as measures of the accuracy of forecasts or numerical simulations, in comparison with the actual measurements. A set of skill scores is defined in this chapter to give a statistical evaluation of SurfPro parameterizations referred to time series built starting from eddy covariance experiment or remote sensing measures. Moreover, SurfPro skill scores are evaluated as well in reference to WRF outputs, in order to verify if SurfPro statically parameterization establishes an actual improvement of the air quality computational chain; or, on the contrary, if it is better to use directly the WRF outputs, neglecting SurfPro parameterizations.

Calculating skill scores, particular attention must be payed on measured time series used for the comparison, because they can be affected by lack of measurements or by high uncertainty associated, as seen in chapter 7. To take into account these features, statistical indicators are calculated considering pairwise comparison between time series, and weighing them for the inverse of standard deviations of measured time series. Moreover, skill scores are calculated considering the extraction cell A, that is the SurfPro grid point closest to Beano station, which defines the computational cell that incorporates it.

8.1 Definition of skill scores

This section provides the definition of the skill scores used for comparison, they are the weighted fractional bias, the weighted correlation and the variance ratio; in addition to these statistical indicators the Taylor Diagrams are reported for every paramater, they graphically summarize the centered RMSE, the correlation coefficient and the variance ratio (not weighted).

Weighted fractional bias Firstly, an evaluation of the general agreement between parameters and observations is performed by the weighted fractional bias, that is the ratio between the standard deviation-weighted bias and the standard deviation-weighted sum. Defining x_i^m the vector containing time series from models (both parameterized and calculated), x_i^o the time series vector of measures and σ_i

the propagated standard deviation; equation for weighted fractional bias results

$$WFB = \frac{weighted\ bias}{weighted\ sum} = \frac{\frac{\sum_i (x_i^m - x_i^o)\frac{1}{\sigma_i}}{\sum_i \frac{1}{\sigma_i}}}{\frac{\sum_i (x_i^m + x_i^o)\frac{1}{\sigma_i}}{2\sum_i \frac{1}{\sigma_i}}}, \tag{8.1}$$

where $\sigma_i^2 = \sum_{k=m,o} \left(\frac{\partial(x_i^m \pm x_i^o)}{\partial x_k}\right)^2 \sigma_k^2$. The definition of weighted bias implies that positive values indicate that on average the model overestimates observed quantities within the time domain considered, while negative values indicate that model underestimates the actual quantities. Moreover, null value of weighted bias describes the situation in which on average there is accordance between model and measures. Finally, the normalization used to resize the weighted bias (i.e. weighted sum) is defined so that a model estimation equal to the double of actual measurement leads a WFB of about 0.67, on the contrary a modeling equal to the half leads the value -0.67; while a WFB equal to 1 means that the model overestimates the actual time series to the triple.

Weighted correlation Correlation between time series is evaluated by the Pearson correlation coefficient, already met in section 4.2 talking about measure representativeness of Beano station. However, in this case coefficient is calculated weighing the correlation with the inverse of standard deviation, computed by means of variance propagation law. Maintaining previously defined notation, expression for Pearson correlation coefficient results (Pozzi et al., 2012),

$$r = \frac{cov(x_i^m, x_i^o; \frac{1}{\sigma_i})}{\sqrt{cov(x_i^m, x_i^m; \frac{1}{\sigma_i})\ cov(x_i^o, x_i^o; \frac{1}{\sigma_i})}}, \tag{8.2}$$

where

$$cov(x_i^m, x_i^o; \frac{1}{\sigma_i}) = \frac{\sum_i \frac{1}{\sigma_i}\left(x_i^m - \frac{\sum_i \frac{1}{\sigma_i} x_i^m}{\sum_i \frac{1}{\sigma_i}}\right)\left(x_i^o - \frac{\sum_i \frac{1}{\sigma_i} x_i^o}{\sum_i \frac{1}{\sigma_i}}\right)}{\sum_i \frac{1}{\sigma_i}}. \tag{8.3}$$

As for unweighted correlation, even in this situation the coefficient is between -1 and 1, with the lower limit of interval that indicates negative linear correlation and the upper limit that indicates positive linear correlation, whilst null value of coefficient means no correlation between time series. Together with the Pearson correlation coefficients, p-values are calculated to provide the statistical significance of correlation analysis, they will be reported using the widely used statistical notation, that is explained by table 8.1.

Variance ratio and probability density function To evaluate the ability of parameterizations to detect the rare events the probability density function is the best visual tool, because rare events constitutes the tails of distributions. However, one of the quantitative definitions of this ability is provided by the variance ratio, defined as the ratio between the variances of modeled and observed time series,

$$VR = \frac{\sigma_m^2}{\sigma_o^2}. \tag{8.4}$$

p-value	notation
0 - 0.001	***
0.001 - 0.01	**
0.01 - 0.05	*
0.05 - 0.1	+
0.1 - 1.0	No symbol

Table 8.1: General notation for significance of statistical tests starting from p-values.

Moreover, if the variance ratio results close enough to 1, a further evaluation is performed. The non-parametric test of Siegel-Tukey (Siegel and Tuckey, 1960.) is applied to verify if the null hypothesis that the two compared data set have the same dispersion can or cannot be rejected; this test could say if one of the two data set have more widely dispersed values than the other. The test is based on the definition of a cumulative array composed sorting the values of both the data sets, afterwards a rank is provided to array elements taking into account the global sorting order, and finally the sum of the ranks within each initially data set series is calculated. If the null hypothesis cannot be rejected, it is expected that the sum of the ranks will be roughly the same for the data sets; in this situation the p-value (calculated by Wilcoxon distribution) is high, while low values of p-values indicate high-probability that the dispersion of the two data set are not equal.

Summarizing, the utility of Siegel-Tukey test in the context of skill scores evaluation is to provide a further evidence that distributions are comparable when the variance ratio results close to 1. In other cases, i.e. when variance ratio is far from 1, test of Siegel-Tukey almost always tell us to reject the null hypothesis that time series have the same dispersion (p-value less than 10^{-3}).

Taylor diagram Finally, for each of SurfPro statically parameter the summary of skill scores is provided by means of Taylor diagram. This kind of diagram provides a graphical description of the accuracy of models compared to observations through the correlation, the centered root-mean-square (RMS) difference and the amplitude of variations represented by standard deviation (Taylor, 2001).

Before explaining the characteristics of this representation, a remark is made on the fact that Taylor diagram works only with the set of the three just cited statistical indicators; this means that the skill scores calculated taking into account standard deviations of observed measures (e.g. weighted fractional bias) cannot be included in Taylor diagram. Therefore, Taylor diagrams are plotted excluding measures with highest standard deviation; the filter is applied defining the probability density function of all the standard deviations and excluding the measures with an associated standard deviation greater than the 90^{th} percentile.

Now, a brief explanation of how to read Taylor diagrams is provided starting from picture 8.1, that shows the statistical comparison between eight models (red points labeled by letters) and observations (purple point). From an overall reading, the distance between the point describing a model and the point of observations (which lies always in the x-axis) determines the accuracy of the model: the smaller is this distance, and the model better describes the observations. Entering in the details, correlation is reported as the angle from the vertical axis, where the zero

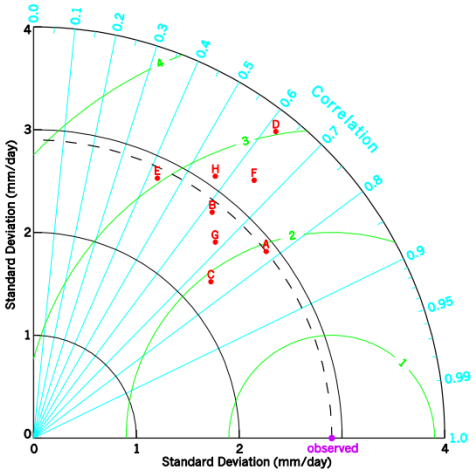

Figure 8.1: Example of Taylor diagram within which the comparison between observations and eight models (described by letters) are reported.

correlation is depicted: clockwise angles define positive correlation (first quarter), while negative angles define negative correlation (second quarter, non reported in this figure). Proceeding with the second statistical indicator, the RMS difference between model and observed patterns is described by the concentric circles centered on point of observations (green lines in figure); once again, the model simulates the observed pattern better when the model point is closer to the observed one. Finally, the standard deviation of the modeled pattern is proportional to the radial distance of the model point from the origin; usually standard deviation is normalized dividing for the measured standard deviation.

8.2 Bowen ratio

Skill scores of Bowen ratio are reported in table 8.2, which shows three columns: the first and the second are related to the comparison between models and measures, while the third one reports the comparison between models; note that the indices reported in the last column should not be considered as "skill scores". Instead, figure 8.2 shows the smoothed probability density functions[1] of the three time series using different colors (red for SurfPro parmeterization, green for WRF model and blue for observed values of Bowen ratio), and the Taylor diagram plotted applying a filter on standard deviations, as explained in previous section. Before analyzing the statistical ability of models related to Bowen ratio, a recall must be done about the fact that skill scores are evaluated considering only pairwise data: in the case of Bowen ratio this means that evaluation is performed starting from the middle of April to the end of the year.

Firstly, SurfPro parameterization of Bowen ratio is compared to measurements (i.e. first column of table); from the weighted fractional bias one can note immediately that SurfPro overestimates the parameter of about two times the actual value,

[1]Probability density functions is drawn by the *ggplot2* package of R software using a Gaussian kernel. Probability density functions are preferred to discrete distributions to make more readable the overlapped graph. For references see http://ggplot2.tidyverse.org/.

	SurfPro vs Measures	WRF vs Measures	SurfPro vs WRF
WFB	0.73	0.20	0.52
r	-0.01	0.54***	-0.35***
VR	0.03	0.11	0.25

Table 8.2: Skill scores for Bowen ratio are reported: weighted fractional bias (WFB), weighted correlation (r) and variance ratio (VR); weighted correlation reports the statistical notation for test significance. Skill scores are calculated to compare models and observations, but also to compare the two models (last column).

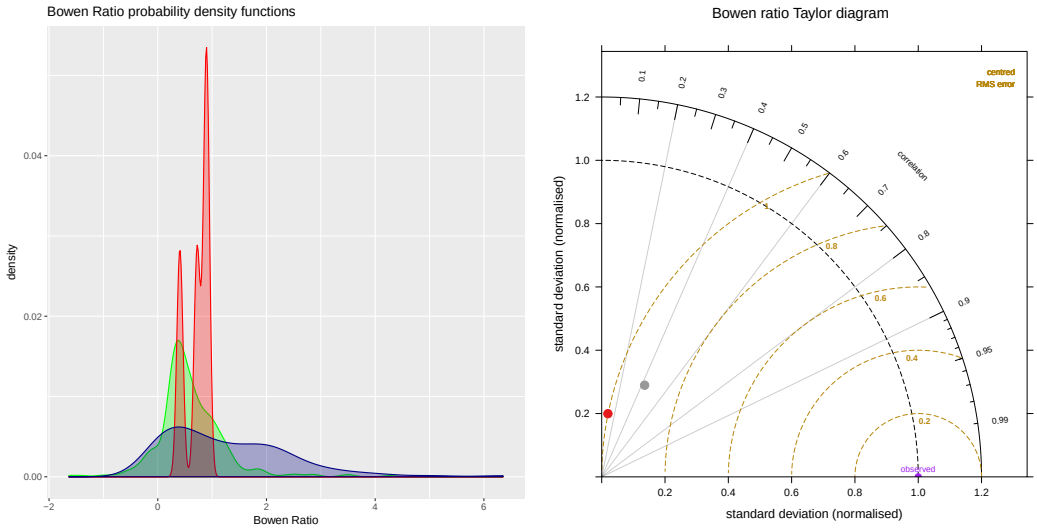

Figure 8.2: On the left-hand side figure reports Bowen ratio probability density functions for measures (blue), SurfPro parameterization (red) and WRF simulations (green). On the right-hand side, Taylor diagram summarizes the skill scores of SurfPro parameterization by means of the red point and of WRF model by the grey point.

it is caused essentially by the summer months, for which the standard deviation associated to measurement is lower. Moreover, no correlation between time series is shown by the weighted Pearson correlation coefficient, even if a low significance of test is detected. In addition, the last skill score (i.e. variance ratio) tells that the distribution of Bowen ratio SurfPro parameterization is definitely more tight compared to measured distribution, as can be observed in the plot on the left-hand side of figure 8.2. This means that SurfPro is not able to describe the actual rare events situated at the extremes of the observed probability distribution. In addition, one can note that, despite the measured distribution being towards high values of Bowen ratio, the weighted fractional bias still results positive; this is a consequence of the low standard deviation during summer, when SurfPro overestimates the actual values. Moreover, the peak of SurfPro distribution can be easily found where the median of the measured distribution has place; this is a positive mark of SurfPro parameterization.

Secondly, comparing Bowen ratio calculated from WRF outputs with measures, one can immediately note that weighted fractional bias is decreased to a value that means that model overestimates the observed values by about one quarter; even in this case, summer months are the period of year which mostly affect in the computa-

tion of this skill score, then a better agreement in these months leads to the decrease of weighted fractional bias. Furthermore, weighted Pearson correlation coefficient shows a relevant positive correlation between model and measures which takes on importance thanks to the high statistical significance. Moreover, the variance ratio is still a lower value, that corresponds to the little skill of WRF model to detect rare events (and in particular the highest Bowen ratio); however at the same time the obtained value is an improvement of one order of magnitude compared to what get from SurfPro comparison.

Finally, last column of table 8.2 reports the statistical scores related to the comparison between the two models; they essentially confirms what said about the models under another light. In particular, a remark must be made on the variance ratio (0.25), which is close enough to the unit but at the same time is not so close to say that times series have got the same ability to detect rare events (i.e. the dispersion of the two time series are comparable). To analyze that, p-value of Siegel-Tukey test is considered: it results equal to 0.30, which means that the null hypothesis that SurfPro and WRF time series have the same dispersion cannot be rejected. Therefore, Siegel-Tuckey test provides a further confirm that the dispersion of the two distributions are actually comparable.

Physical interpretation The overestimation of Bowen ratio is strictly related to an increasing of turbulent sensible heat flux, this means that SurfPro addresses a greater amount of the energy budget to the convectively driven turbulence, compared to what happens in the reality; consequently, a lower amount of water vapor molecules passes from the Earth's surface to the atmosphere. As previously reported, this happens especially during the period in which the plants are on the field (i.e. late spring and summer), that means that SurfPro is not able to reproduce with accuracy processes of evapotransipiration, that during the summer is more efficient and is underestimated by the model. On the other hand, to defend SurfPro parameterization one can say that watering having place in this period contributes to decrease the measured Bowen ratio (i.e. the latent heat at the denominator increases), however this field treatment had influenced a low number of measures, moreover some land use descriptions (such as the land use of the prevalent sub-cell for grid cell A) define the possibility to take into account this agricultural technique.

Finally, as shown by the variance ratio, SurfPro parameterization is not able to detect the high variability of Bowen ratio that occurs during the months in which plants are not present or well-developed. This is an intrinsic problem of seasonal parameterization, that can be a rough estimate of the actual values; in fact, variance ratio enhances considering the Bowen ratio calculated from the WRF outputs of simulations.

8.3 Roughness length

Second parameter analyzed is the roughness length, for which statistical indicators and graphical representations are reported respectively in table 8.3 and figure 8.3, in the same way as for Bowen ratio. In this case the range for observed values comprehends the period in which the roughness length is affected by the agricultural

	SurfPro vs Measures	WRF vs Measures	SurfPro vs WRF
WFB	0.09	-0.34	0.12
r	-0.31***	-0.25***	0.88***
VR	1.24	0.07	7.00

Table 8.3: Skill scores for roughness length are reported: weighted fractional bias (WFB), weighted correlation (r) and variance ratio (VR); weighted correlation reports the statistical notation for test significance. Skill scores are calculated to compare models and observations, but also to compare the two models (last column).

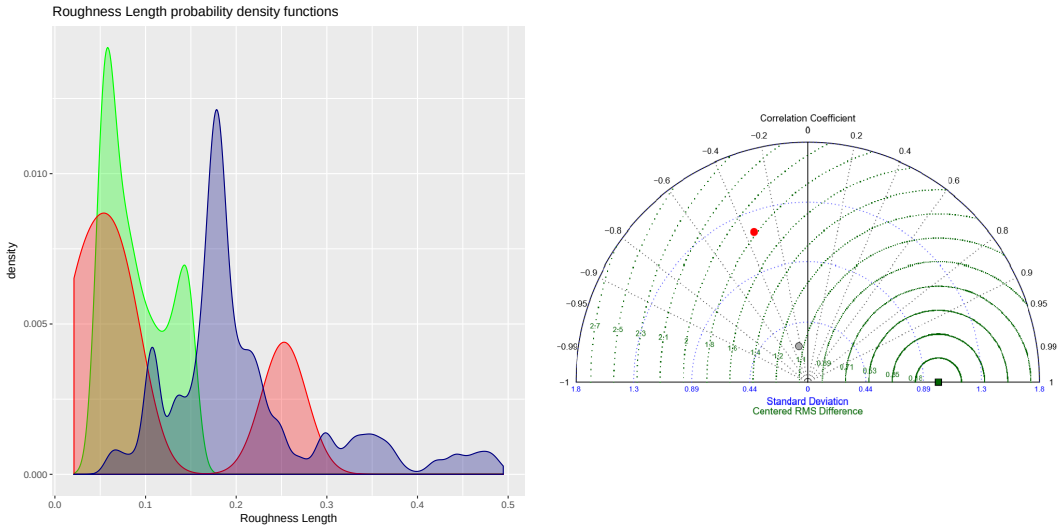

Figure 8.3: On the left-hand side figure reports roughness length probability density functions for measures (blue), SurfPro parameterization (red) and WRF simulations (green). On the right-hand side, Taylor diagram summarizes the skill scores of SurfPro parameterization by means of the red point and of WRF model by the grey point.

cycle (i.e. when plants are on the field, from April to September).

Firstly, the comparison between roughness length parameterized by SurfPro model and measured by eddy covariance tower is considered. From the weighted fractional bias one can observe that SurfPro gives on average a good estimation of the roughness length during the agricultural period, even if with a little overestimation. This is the result of a relevant underestimation associated to low weight during the period in which the plants are increasing, and a moderate overestimation associated to high weight when the plants are well-developed. This pattern is also the reason why negative correlation is detected, i.e. weighted Pearson correlation coefficient equals to -0.31. Finally, variance ratio shows some compatibility between the spread of the probability density functions with a slightly overestimation of variance from SurfPro. To understand why this result is obtained one must consider the distributions in figure 8.3: on the one hand, SurfPro density function is a bi-modal distribution which results from the summer peak in parameterization of roughness length; on the other hand, the distribution of observations contains some high unusual values (comparable with roughness length of dense forests) which stretch the distribution towards high values. Therefore, the two contributes lead toward the same direction and variance ratio shows compatibility between the two distribu-

tions, even their shapes are different. To prove this the non-parametric Siegel-Tukey test allows to reject the null hypothesis that the two distributions have the same dispersion (p-value equals to $2.7\ 10^{-3}$).

Considering the second column of table 8.3, the weighted fractional bias shows on average an underestimation of roughness length by WRF model compared to the observed values; this is a general behavior detected within the entire domain, i.e. when there are maize plants over the field, and is well represented by the figure reporting the probability density functions. Instead, the weighted Pearson correlation coefficient remains stable passing at WRF model; but now the reason of this result is different than before. In fact, in this case the anti-correlation is mainly due to the opposite concavity of WRF model (downwards) compared to the upward concavity traced by the observed time series from June to September, even if a low accuracy is associated to June's measurements. Last skill score is the variance ratio, that shows the inability of WRF model to detect rare events, however this value of skill score could be incremented towards 1 because high values of observed roughness length should be excluded from the computation, as shown by figure 8.3.

Finally, last column of table compares the roughness length modeled by SurfPro and WRF, main results concern the good overall accordance between the models shown by the weighted fractional bias and the high weighted Pearson correlation coefficient; while the variance ratio is mainly affected by the SurfPro discrete distribution.

Physical interpretation By a physical point of view, the overestimation of roughness length by the SurfPro parameterization means that it is overestimated the height where the logarithmic profile of the wind becomes zero. This leads consequences in the simulation of turbulence driven by wind shear, to assess that one must consider the friction velocity, expressed as $u_* = k\frac{\overline{U}}{\ln(z/z0)}$ by the similarity theory (section 1.4.3). Therefore, at the quote $z > z_0$ and with the same horizontal mean wind speed, SurfPro will simulate higher values of u_* and the more turbulence generated by wind shear at the surface.

On the other hand, WRF provides lower values of roughness length than actual values; therefore the usage of WRF roughness length will lead to a smaller amount of turbulence generated by wind shear. Moreover, this consideration is more valid than for SurfPro model because the WRF underestimation of roughness length is widely observed in the entire range of observations.

Finally, a remark is made on the fact that anything can be said about the months in which the plants are not present over the field.

8.4 Leaf area index

Skill scores related to SurfPro and WRF parameterization are summarized in table 8.4; unlike the previous case, time series of leaf area index is available for the entire year from satellite measures, regardless of presence or absence of plant cover.

Following the analysis scheme of previous parameters, comparison between SurfPro statically parameterization and measured values of leaf area index are considered. From the weighted fractional bias one can observe that over the entire year

	SurfPro vs Measures	WRF vs Measures	SurfPro vs WRF
WFB	0.99	1.18	-0.14
r	0.83***	0.93***	0.94***
VR	7.60	4.10	1.86

Table 8.4: Skill scores for LAI are reported: weighted fractional bias (WFB), weighted correlation (r) and variance ratio (VR); weighted correlation reports the statistical notation for test significance. Skill scores are calculated to compare models and observations, but also to compare the two models (last column).

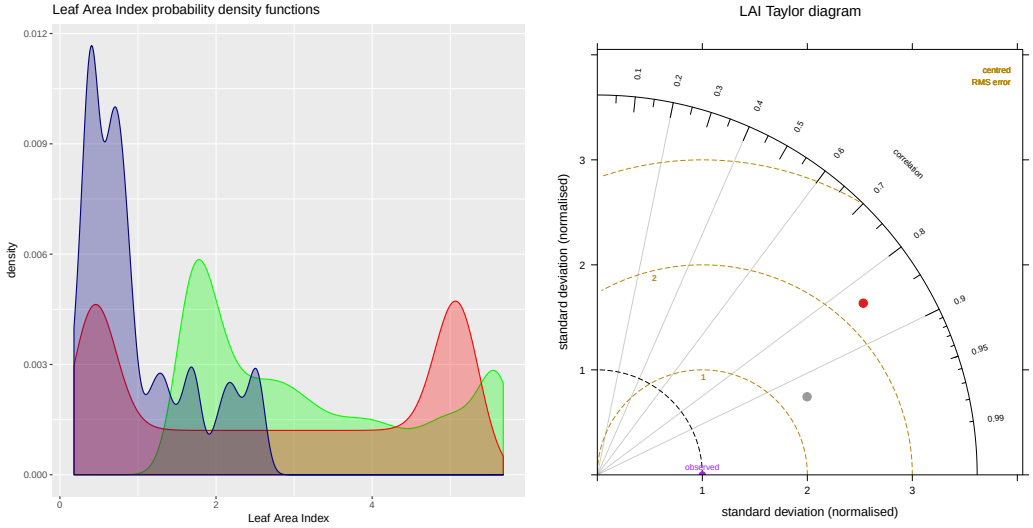

Figure 8.4: On the left-hand side figure reports LAI probability density functions for measures (blue), SurfPro parameterization (red) and WRF simulations (green). On the right-hand side, Taylor diagram summarizes the skill scores of SurfPro parameterization by means of the red point and of WRF model by the grey point.

SurfPro provides on average an overestimation of leaf area index, caused essentially by the summer period, when the parameterization of summer maize culture is highly over evaluated. The SurfPro accurate parameterization of leaf area index when the maize is not present on the field, as seen in section 7.3, is not able to reduce the weighted fractional bias, which shows an overall overestimation equal to about the triple of measured time series. Beyond the detected overestimation, weighted Pearson correlation coefficient shows high agreement (with high significance level) between the time series of parameterized and measured leaf area index; this is mainly due to the easily description of annual agricultural cycle. Moreover, one can evince that some inaccuracy in the times of seeding and harvest does not leads to a drastic worsening of the correlation. Now, the variance ratio is considered together with the probability density functions represented in figure 8.4, in fact the high variance ratio is caused by the large overestimation of leaf area index during summer, which as consequence causes a stretch in SurfPro distribution towards high values.

Proceeding with the second column of table 8.4, related to the comparison between WRF parameterization of leaf area index and remote sensing measures, the overestimation of leaf area index (made by Noah land surface model) is still observed, and is even increased passing from SurfPro to WRF model. This is a consequence

of the fact that WRF parameterization overestimates the actual leaf area index also during the period without crop, i.e. the WRF overestimation of leaf area index is constant during the entire year. However, the weighted Pearson correlation coefficient is increased compared to what observed for SurfPro parameterization, due to the better description of agricultural events by the Noah land use scheme. For instance, the parameterization models in a different way the growth and the harvest of crop, and provides a suitable evaluation of the days of maximum leaf area index. At the end, the variance ratio equals to 4.10 (and then in a way comparable to one) forces us to apply the Siegel-Tukey test to understand the meaning of this result. P-value of the test is equal to 0.64, therefore it says that the null hypothesis that the two distributions have the same dispersion cannot be rejected, even if figure 8.4 shows a principle of bi-modal distribution with a peak at high values.

Finally, last column of table compares the leaf area index parameterized by SurfPro and by WRF, main result concerns the highly compatibility of the two time series variances (variance ratio equals to 1.86), which is a confirm of the high dispersion of both the models with reference to the observed values.

Physical interpretation Focusing on the summer overestimation of leaf area index by the two models, one can find two possible explanations: on the one hand the parameterizations are based on assumptions that are not valid for agricultural methods implemented in Friulan region; on the other hand the SurfPro and WRF computational cells included some sub-cells described by *wood* land use, which affects the parameter calculation. Having performed an accurate analysis devoted to make the measures and models spatially comparable (i.e. averaging the remote sensing measures which enter in the SurfPro computational cell), the first hypothesis is preferable even in the light of fact that leaf area index is a quantity extremely difficult to evaluate in an agricultural context: it can change according to a wide range of variables, for instance plant density, biological treatments and crop health.

By a physical point of view, the overestimation of leaf area index when the crop is on the field means the increase of the efficiency of water exchange between Earth's surface and atmosphere; in fact, a greater leaf surface enhances the number of water molecules that plants can make available for the atmosphere by means of transpiration process. As a consequence, the turbulent latent heat flux enhance at the expence of the other terms of surface energy budget, among which the sensible heat flux; therefore one can evince that a secondly consequence of the overestimation of leaf area index consists in the underestimation of the thermal driven turbulence.

This behavior can be observed only during the summer period (when the net radiation is the largest), because when the field is uncultivated SurfPro provides an accurate parameterization of leaf area index, even if the times and the features of the agricultural events are not well-defined (i.e. SurfPro parameterizes at the same way the growth and the harvest of the crop).

Instead, WRF parameterization of leaf area index is overestimated also during the winter, and therefore an amount of thermal driven turbulence cannot be generated by this model. The reason of a leaf area index so great during the winter is probably related to the fact that WRF computational cell has detected some sub-cells describing a *wood* land use, as previously said; however, the main feature of WRF parameterization of leaf area index is the good approximation of agricultural

	SurfPro vs Measures	WRF vs Measures
WFB	0.09	-0.10
r	-0.01	0.64***
VR	1.24	9.59

Table 8.5: Skill scores for albedo are reported: weighted fractional bias (WFB), weighted correlation (r) and variance ratio (VR); weighted correlation reports the statistical notation for test significance. Skill scores are calculated to compare models and observations, note that two measured time series are defined as a function of model.

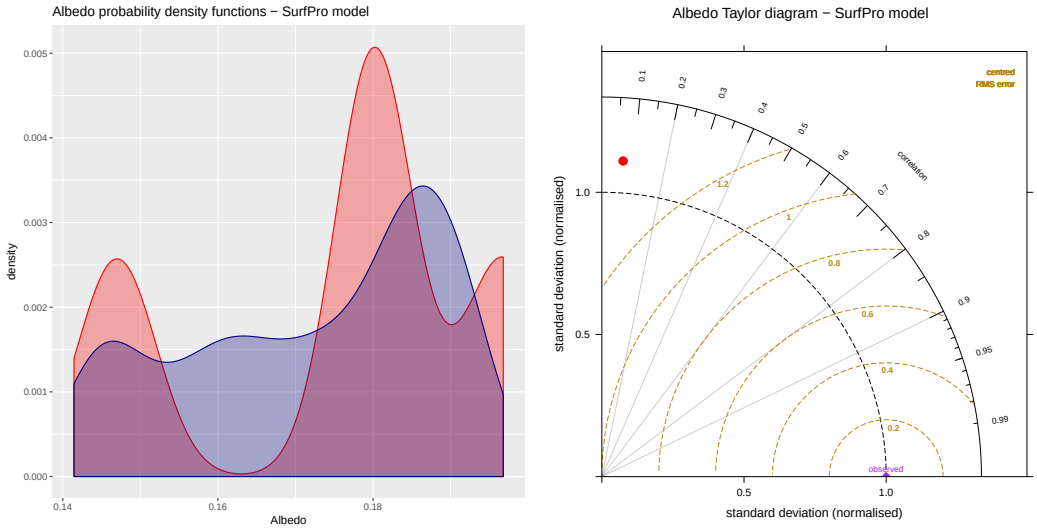

Figure 8.5: On the left-hand side figure reports albedo probability density functions for measures (blue) and SurfPro parameterization (red). On the right-hand side, Taylor diagram summarizes the skill scores of SurfPro parameterization by means of the red point.

cycle, that is probably reached thanks to the implementation of remote sensing data in the Noah land surface scheme.

8.5 Ground albedo

Now, skill scores related to ground albedo are considered remembering that SurfPro and WRF models are compared with different time series obtained from the same remote sensing data frame (section 7.4). Therefore, within table 8.6 only the column reporting the results of statistical comparison between models and measures are reported.

Table is analyzed starting from the evaluation of SurfPro parameterization of ground albedo. Firstly, one can observe that on average the SurfPro values of albedo do not get away so much from the actual values, in fact the reported weighted fractional bias is equal to 0.09, that means a slightly overestimation. However, this acceptable statistical indicator is the result of two distinct periods of year when the model parameterization clearly overestimates and underestimates the ground albedo, respectively during the months of autumn and winter and during the spring; while during the summer a good parameterization of albedo is provided (figure 7.17). The

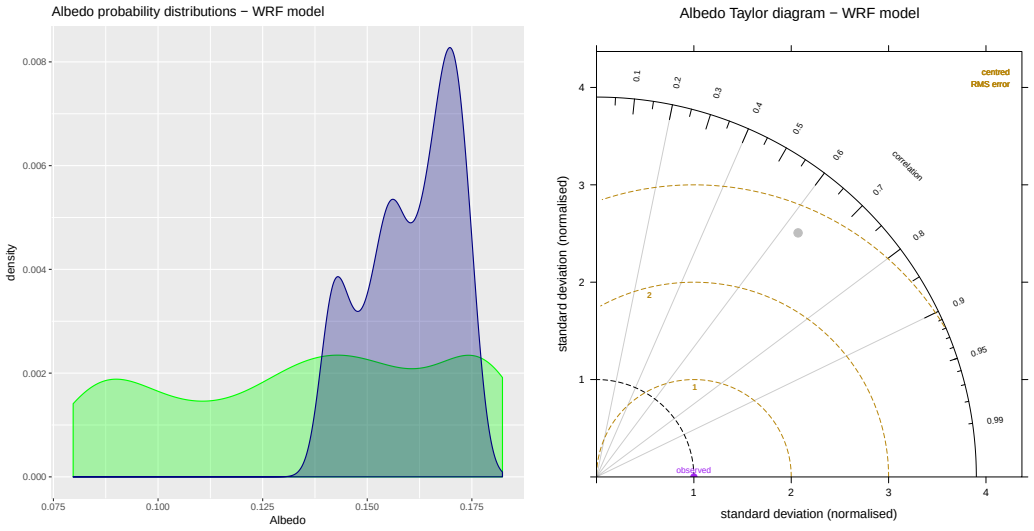

Figure 8.6: On the left-hand side figure reports albedo probability density functions for measures (blue) and WRF simulations (green). On the right-hand side, Taylor diagram summarizes the skill scores of WRF model by the grey point.

just explained pattern is the reason for which the weighted Pearson correlation coefficient results close to zero, even with a low statistical significance probably related to the high daily variability of albedo compared to the seasonal parameterization of SurfPro; in fact, low significance was obtained also for the Bowen ratio, where the same characteristics of measures was observed. Afterwards, the ability of SurfPro parameterization to detect rare events is considered taking into account the variance ratio, that results equal to 1.27; then, as previously, a further investigation is implemented by applying the Siegel-Tukey test. P-value of the test is equal to 0.02 and therefore it says that the null hypothesis that the two distributions have the same dispersion can be rejected; in fact, figure 8.5 shows that SurfPro probability density function is a bi-modal distribution and the concept of dispersion is almost equivalent to the concept of distance between the peaks. In this case, variance ratio says that the tails of measures distribution can be detected by parameterization, but this does not happen for the central values of distribution.

On the other hand, skill scores related to the comparison between WRF parameterization of albedo and measures is considered. As said in subsection 7.4.2, to make WRF output comparable with remote sensing measures an approximate correction is applied. For this reason the analysis of skill scores is limited to say that, despite everything, the two data set are well-correlated with a slightly underestimation over the entire year and that the applied correction enlarges the probability density function producing low values of albedo (figure 8.6).

Physical interpretation Due to uncertainties that affect WRF comparison, SurfPro parameterization of albedo is considered. As said before, the parameterized ground albedo is affected by a spring period in which an underestimation of actual values is detected, and a period comprehending fall and winter when the ground albedo is overestimated. In the first case, a less reflective surface is simulated; as a

	SurfPro vs WRF
WFB	0.48
r	0.02 +
VR	0.00

Table 8.6: Skill scores for soil parameter are reported: weighted fractional bias (WFB), weighted correlation (r) and variance ratio (VR); weighted correlation reports the statistical notation for test significance. Skill scores are calculated to compare models.

consequence, the surface energy budget has available a greater amount of solar radiation that must be divided among turbulent heat fluxes and soil heat flux. In the second case (i.e. overestimation of albedo), a more reflective surface is simulated and a greater amount of solar radiation returns to space without entering in the surface budget. Summarizing, one can say that SurfPro tends to overestimate the energy available for the coupled system Earth's surface-atmosphere during the summer, while during fall and winter SurfPro tends to provide less energy than actual energy. Instead, considering the distribution function, one notes that an intermediate range of albedo (centered on the value 0.162) is completely excluded by SurfPro parameterization, this is a remarkable limit due to seasonal statically parameterization intrinsic in SurfPro.

8.6 Soil parameter

Finally, soil parameter is the last statically parameter initialized by SurfPro. The statistical study of this quantity is limited by two factors: the first one is related to the lack of reliable measurements (as shown by subsection 7.5.1) and the second one to the rough parameterization provided by SurfPro, in fact it remains constant during the whole year. On the one hand, first element permits the only comparison between the models without any actual reference. Considering the purpose of this thesis and the fact that WRF model provides a more accurate soil modeling (using Noah land scheme), the WRF model time series is considered in place of on field measurements. On the other hand, consequence of the second factor is that some skill scores lose their power in evaluating the SurfPro parameterization, such as variance ratio and correlation, as shown in table 8.6.

The unique skill score that permits to make some considerations is the weighted fractional bias, which shows that SurfPro overestimates the soil parameter of less than double compared to WRF values. The overestimation is condensed from April to October, when the low standard deviation of WRF soil parameter permits to overtake the general underestimation during the other months, for which high standard deviation is detected.

Physical interpretation Having performed a comparison only between models, physical evaluation cannot be evinced; however, one can say that SurfPro parameterization compared to WRF model directs on average a larger amount of heat toward the soil. Therefore, a smaller amount of net radiation is devoted to the definition of turbulent fluxes.

Chapter 9

Consequences on simulated turbulence

This chapter provides a summary of the influence of parameterizations on the simulation of turbulence distinguishing between the periods of the year when the plant cover is on the field and when it is absent. Moreover, some examples of how the statically parameters enter in the simulations are reported by means of the scaling parameters such as friction velocity and stability parameter.

Previous sections showed that the statically parameters defined by SurfPro tables are able to affect the simulation of turbulence within the Atmospheric Boundary Layer. In particular, roughness length has an influence on the wind shear generated turbulence; while the other parameters are mainly related to the surface energy balance, and therefore to the energy available for the development of convective turbulence.

Starting from mechanical turbulence, during the first stages of plant growth SurfPro parameterization provides an initial underestimation of actual roughness length, while a subsequent overestimation is depicted after the rapid development of maize plant. Therefore, in the first part of agricultural cycle a lower amount of wind shear driven turbulence is simulated due to the lowering of zero-displacement height, see section 8.3; whilst, in the second stage of life cycle an opposite effect on mechanical turbulence is outlined (i.e. underestimation of roughness length leads to overestimation of mechanical turbulence).

Afterward, the thermal driven turbulence simulated by SurfPro during the agricultural period is considered. In this case, the contributes of the rest of parameters must be taken into account, that are the Bowen ratio, the leaf area index and the albedo. Firstly, the SurfPro parameterization of Bowen ratio tends to increase the energy addressed to the turbulent sensible heat flux; on the contrary, the overestimation of leaf area index when the crop is well-developed leads to the fact that a greater amount of net radiation is detected by the leaves and used in the process of plant evapotranspiration, this at the expense of thermal turbulence formation. Finally, the convective turbulence is affected also by the amount of solar radiation which enters in the surface energy budget (i.e. the part of solar radiation that reaches the Earth's surface and is not reflected toward the space); SurfPro parameterization provides acceptable values of albedo when the plants have already reached the max-

imum growth, while during the growing period it tends to overestimate the amount of radiation which enters in the balance contributing to the development of thermal turbulence.

On the other hand, when the site of interest is not involved by agricultural cycle, only the influence of leaf area index and albedo on turbulence can be evaluated. Doing that, one must consider that the various crops, included in the area corresponding to the SurfPro cell, may have different timing in the transition between cultivated and uncultivated field. Firstly, for uncultivated field SurfPro parameterization of leaf area index is a good estimation even if the timing of harvest do not match with what actually had got place. Secondly, the measured ground albedo with uncultivated field is highly overestimated by SurfPro parameterization; this leads the model to get les radiation than in the reality. Therefore, one can evince that SurfPro model devotes too little energy to surface energy budget and consequently to eddy heat fluxes, underestimating the convectively driven turbulence. Instead, nothing can be said about turbulence generated by wind shear when the field is uncultivated.

Having resumed how SurfPro statically parameters affect the evaluation of turbulence in the different periods of the year, now the focus is on the outputs of this model (e.g. turbulent scaling parameters), and in particular on the influence of initialization parameters on them. Therefore, friction velocity and stability parameter simulated by the model during the year 2015 are shown in comparison with the measurements collected by Beano eddy covariance tower and, when available, with the simulations of WRF model for the same year. Before analyzing the results, a remark must be made on the fact that a clear and evident relation between turbulent scaling parameters and initialization parameters is difficult to be found, in particular when complex quantities are considered.

9.1 Friction velocity

Friction velocity is the scaling parameter which characterizes the shear at the lower boundary of the Atmospheric Boundary Layer (i.e. the Earth's surface). SurfPro calculates the friction velocity by applying the Monin-Obukhov similarity theory for stable and unstable conditions of the Atmospheric Boundary Layer; as reported in section 2.2.3, the quantities involved in this computation are the roughness length, the horizontal wind speed and, for unstable conditions, the air temperature and the turbulent sensible heat flux, which enters in the equations through the Monin-Obukhov length (stability parameter). Therefore, one can note that both the statically parameters (i.e. roughness length, Bowen ratio and albedo) and the meteorological fields supplied by meteorological processor (WRF model) are taken into account in the computation of friction velocity.

Figure 9.1 shows the comparison between friction velocity measured by Beano eddy covariance tower and simulated by SurfPro model during the year 2015. The evaluation is performed considering only the computational time steps for which measurements are available; in order to make comparable the data frames. As made previously, analysis of plot is performed taking into account separately the agricultural period and the period in which plants are not over the field.

Firstly, the months with bare soil are considered (i.e. the period between October

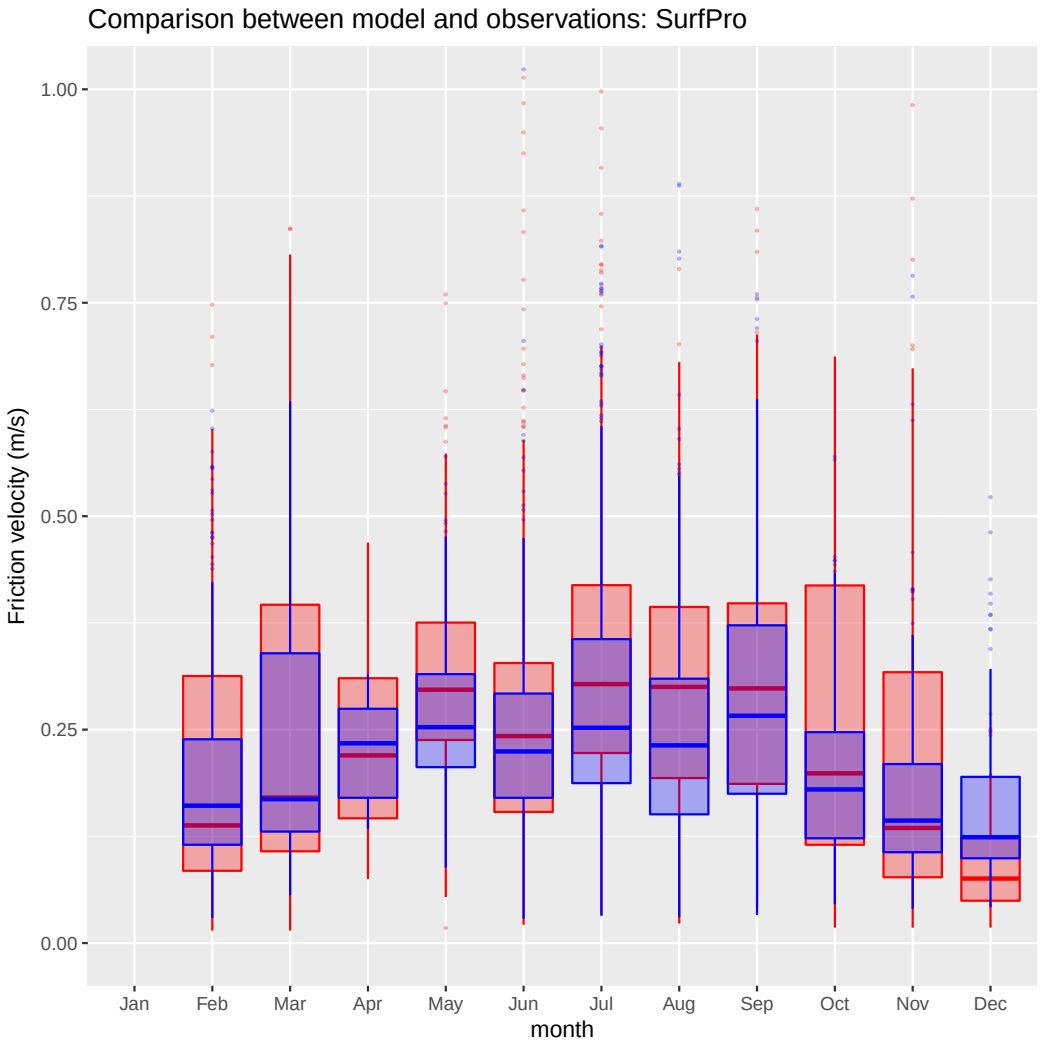

Figure 9.1: Comparison between monthly friction velocity simulated by SurfPro model (red) and measured by Beano eddy covariance tower (blue) for the year 2015. Boxplots represent medians as lines within the boxes, the boundary of boxes correspond to 25th and 75th percentiles and bars delimit the 5th and 95th percentile; finally, the points outside are the outliers of the distribution.

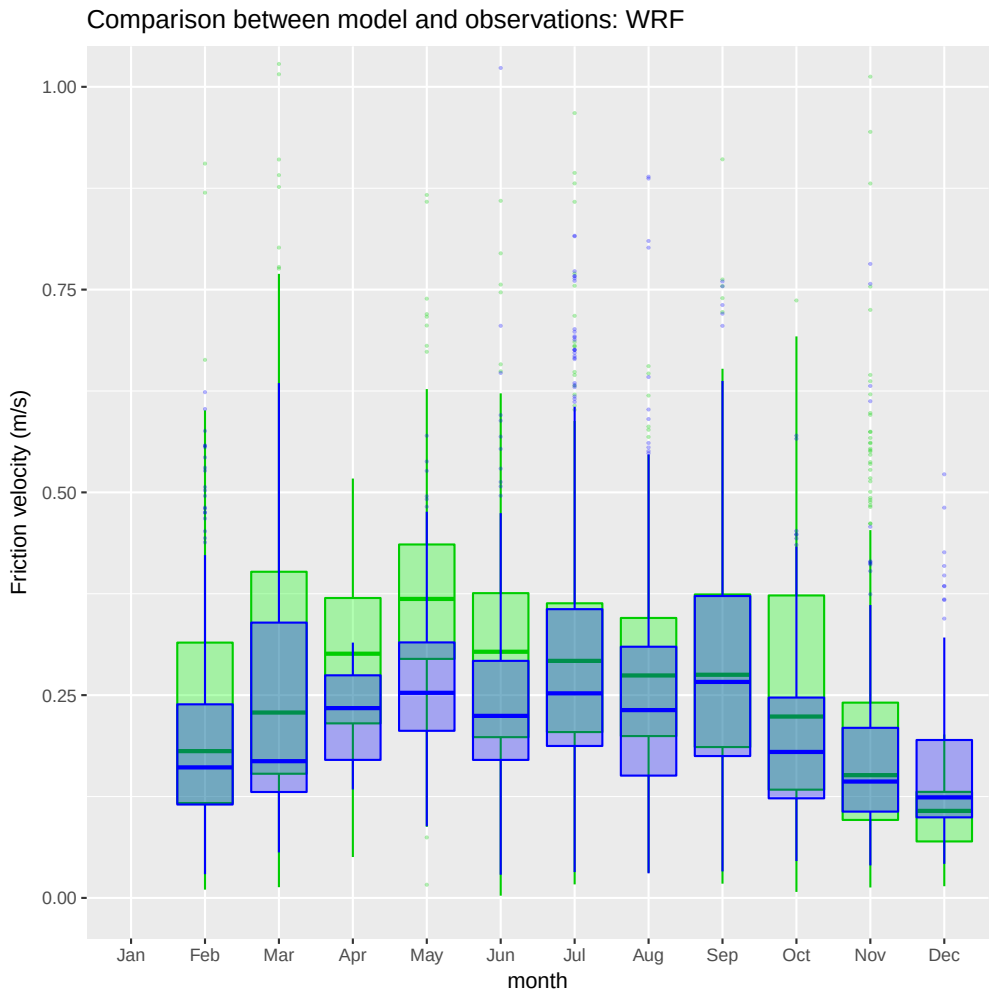

Figure 9.2: Comparison between monthly friction velocity simulated by WRF model (green) and measured by Beano eddy covariance tower (blue) for the year 2015. Boxplots represent medians as lines within the boxes, the boundary of boxes correspond to 25th and 75th percentiles and bars delimit the 5th and 95th percentile; finally, the points outside are the outliers of the distribution.

and April) paying attention on the monthly median, represented by the line within the boxes of graphs. One can note that SurfPro generally slightly underestimates the monthly median values (except in October), but often largely overestimates the monthly 75th percentiles (except in December); October is the only month when the median value is overestimated, probably because nearby agricultural fields with moved forward harvest times enter into the SurfPro computational cell.

When the plant is on the field SurfPro simulations tend to overestimate the mechanical turbulence providing larger values of friction velocity than in the reality. This behavior is consistent with the analysis of roughness length SurfPro parameterization. However, SurfPro performance related to monthly dispersion of friction velocity is generally acceptable even if shifted from the measured values; in particular, one can note that 3rd percentiles are often moved upwards.

Moreover, if WRF simulation of friction velocity is compared to measurements

(figure 9.2), two observations can easily be made: the first one is that monthly medians of friction velocity simulated by WRF are almost always greater than actual medians (with an exception in December), while the second one is that the bias between simulated and measured monthly medians is generally greater than what found in the comparison between SurfPro model and observations. In particular, the period between March and May is critical for WRF simulation of turbulence because both the problems are detected. Therefore, from what seen one could conclude that mechanical turbulence is on average better computed by SurfPro processor than WRF meteorological model. However, goodness of friction velocity simulations are also affected by discrepancies in the simulation of the wind velocity; in particular, within the Friulan plain WRF overestimates the wind speed by on average 1 m/s leading to a greater amount of turbulence generated by wind shear in both SurfPro and WRF computations.

9.2 Stability parameter

The second output of SurfPro model evaluated in the thesis is the stability parameter, previously introduced in section 2.2.3. Within SurfPro architecture, the main task of this parameter is to determine wether the Atmospheric Boundary Layer is in stable, unstable or neutral conditions in order to decide what are the similarity theory's expressions to use in the computation of turbulence.

To compare SurfPro simulations and eddy covariance measurements, the first action is the definition of thresholds which delineate the different boundary layer regimes. Unstable conditions are defined for negative values of stability parameter limited from the above by the value -0.05; on the contrary, boundary layer stability is found for positive values of stability parameter and is limited from the below by the value 0.05. Finally, neutral boundary layer is defined between the values -0.05 and 0.05.

Moreover, the comparison between SurfPro and measurements has been performed dividing the analysis for months and taking into account the thee-hourly occurrence rates of the boundary layer regimes, as shown in figure 9.3. The rates of occurrence are described by circles with variable diameters (the greater are the rates, the largest are the diameters), while the colors discriminate simulations and measurements. However, before evaluating the physical aspects one has to be aware that only pairwise data enter in the evaluation of occurrence rates; this means that simulated stability parameters are excluded if the corresponding measured values are unavailable. Therefore, it could be possible that, if the measures are not enough uniformly distributed during the hours of the months, the expected pattern with instability of boundary layer during the daytime and stability in nighttime could not be observed. On the contrary, when the expected daily pattern of stability parameter is observed, it is very likely that a large and well-distributed amount of measures is available, and then deductions evinced by the graph result more effective. February belongs to the first set, in fact, the figure does not show boundary layer stability during the nighttime (for the measurements), therefore it is safe to exclude the month from the analysis.

From an overview of figure 9.3, one can evince that SurfPro generally simulates much more cases in which the Atmospheric Boundary Layer is neutral (i.e. presence

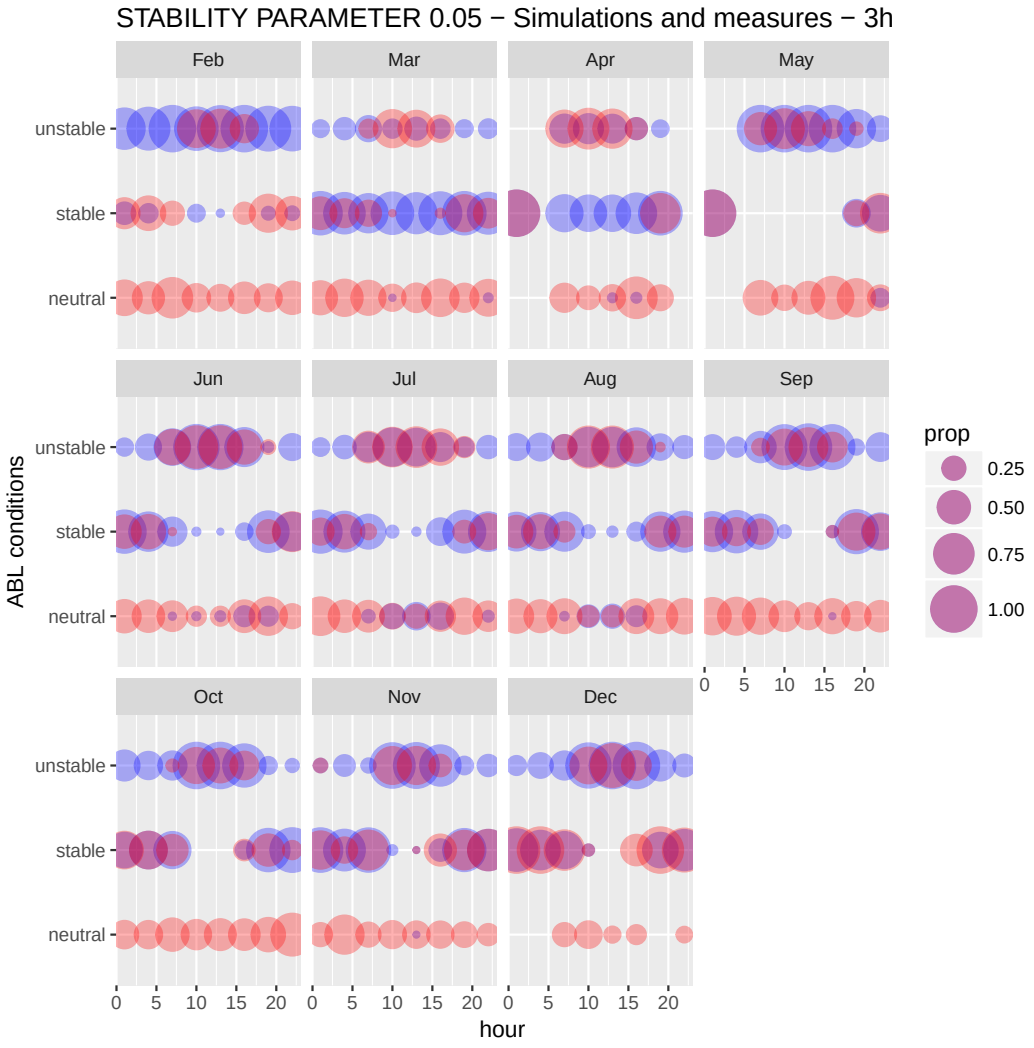

Figure 9.3: Comparison between boundary layer regimes simulated by SurfPro model (red) and measured by Beano eddy covariance tower (blue) for the year 2015. The rate is expressed by the size of circles as a percentage of the total amount of occurrences in each three hours period.

of moderate winds and breezes) than what was actually observed for the year 2015; the same behavior is observed if the thresholds were shifted to the values of plus and minus 0.10 (not reported within the thesis). In fact, when SurfPro simulates neutral conditions of boundary layer, the measurements of stability parameter fall into the stability or instability group enhancing their occurrence rates, and then the size of circles. While, good evaluations of neutral conditions occurrence rates are provided only in July and August during the central hours of the day.

Considering the stable conditions of boundary layer, SurfPro generally provides a good estimation of their rate of occurrence during nighttime, when stable conditions usually take place. On the other hand, during the daytime stable conditions of boundary layer can sometimes occur, but generally SurfPro tends to simulate them as neutral conditions (i.e. April). Instead, SurfPro simulates the unstable conditions with good accuracy when the convective movements are well-defined (i.e. central hours of the day with large radius size). This happens for every month of the year, even if during summer months the occurrence rates of simulated and measured instability match each other with better accuracy. Instead, SurfPro is not able to reproduce the instability in the nighttime, that can be due to residual thermal winds during sunset or to synoptic scale weather fronts which affect the lower layers of the atmosphere.

Now, it is important to pay attention on the transition hours between daytime and nighttime (and viceversa), that means between instability predominance and stability predominance; because these moments are the most inclined to be affected by errors in the simulations. To do that, figure 9.4 reports the same results as before for three months (March, August and December), but considering the monthly hourly occurrences of each stability class. Firstly, March reveals a particular pattern of the measured stability class occurrence, in which the occurrence of stable boundary layer in daytime is larger than unstable class. This pattern is the result of large cloudiness at synoptic scale, which had not permitted a large development of thermal in the daytime. Partial confirm is brought by the fact that March was the second rainy month of 2015, in which synoptic perturbations are likely to occur. Therefore, one can assume that synoptic perturbations in March had inhibited the solar radiation at the Earth's surface, and consequently they did not allow the mixing in the boundary layer. Moreover, it is likely that the availability of measurements matches with the passing of synoptic fronts.

Instead, considering August and December, the expected behavior of the occurrence rate of boundary layer stability classes is observed, i.e. unstable conditions during daytime and stable during nighttime; in fact, one can easily observe that the amount of hours in which each condition is prevalent changes according to the period of the year. Apart from that, the main figures related to these months are that SurfPro in August tends to anticipate the mixing within the boundary layer by about an hour, while in December it tends to anticipate by two hours the stabilization of the lower layers of the atmosphere, this can lead to consequences in the estimation of air quality during the winter evenings. However, before drawing hasty conclusions we have to remark that comparisons are made only when measurements are available and then they represents a sub set of the possible cases, which correspond to the widely subset available from the measurements of the year 2015.

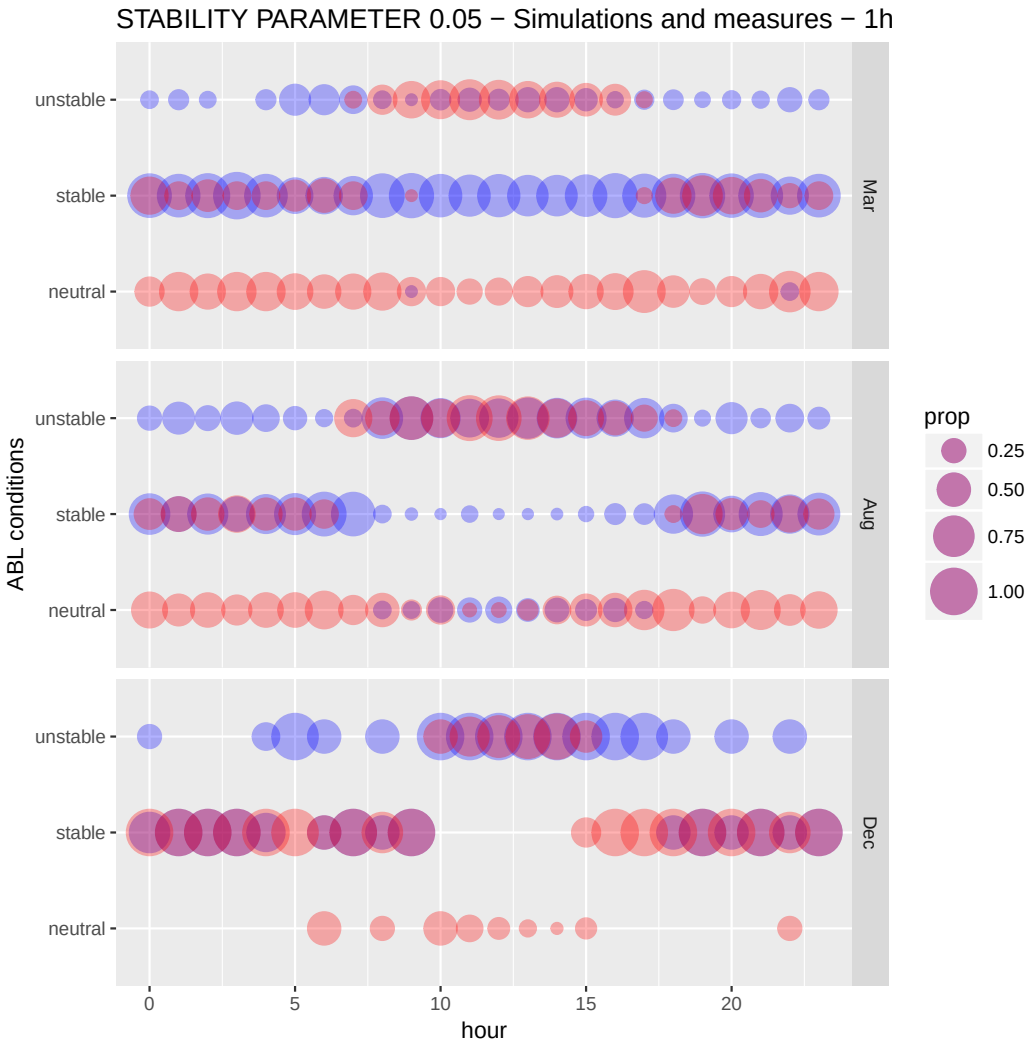

Figure 9.4: Comparison between boundary layer regimes simulated by SurfPro model (red) and measured by Beano eddy covariance tower (blue) for the year 2015. The rate is expressed by the size of circles as a percentage of the total amount of occurrences in each hour.

Chapter 10

Conclusions

This work delineates the improvements of SurfPro statically parameterizations, by means of their statistical performance, which is directly related to structure of parameterization and accuracy of values, in the context of the global framework of CRMA air quality computational chain.

SurfPro initialization parameters are based on a seasonal modulation which can be more or less suitable according to the specific quantities. For instance, from the analysis related to Beano measurements site, a seasonal parameterization of leaf area index can be accepted after the revisiting of the values, as well as for albedo. In fact, these quantities vary in a smooth way during the year following a well-defined pattern, therefore a seasonal parameterization could be able to describe them. However, as just mentioned, if one decide to maintain these parameterizations, the redefinition of constants for this site (and generally for Friulan plain) is necessary. In fact, SurfPro parameterization of ground albedo does not follow the pattern of actual albedo detected by remote sensing data, while the parameterization of leaf area index largely overestimates the actual values. In particular, considering the leaf area index, the CRMA air quality computational chain could be improved if the SurfPro processor would have been implemented with WRF leaf area index (provided by Noah land surface scheme) scaled by a factor near to 1/3, improving the modeling of the agricultural cycle.

On the contrary, Bowen ratio and roughness length would require a more dense sampling, such as a monthly parameterization; benefits of this new concept involve the two parameters in different ways. Firstly, monthly SurfPro parameterization of Bowen ratio would be able to describe better the broad minimum of the pattern, which is detected between spring and summer. Moreover, a greater improvement would be observed if the climatic flag for wetness would be applied, in fact for each month the modeler could define the most suitable index according to the climate characteristics of the area. Therefore, the monthly parameterization together with the activation of climate index lead to improvements in the SurfPro Bowen ratio, however the large variability of this quantity when the crop is not well-developed still remains unpredictable by a statically parameterization such as defined by SurfPro. Considering the CRMA air quality chain, a way to bypass this feature is to initialize SurfPro processor with the Bowen ratio daily computed by mans of Limited Area Meteorological Model WRF. In fact, the obtained time series improves all the skill scores calculated from SurfPro statically parameterization. Secondly, SurfPro

roughness length will take advantage from monthly parameterization particularly during the period of rapidly development of the crop, which covers a range of about 40 days for maize plants. Therefore, detecting the month in which the rapidly increase happens (i.e. June for maize crops in Friulan plain) allows to reduce the errors made by the seasonal parameterization. Benefits of monthly parameterization can not be evaluated when the crop is not on the field; however, one can easily deduce that any relevant changes take place considering the roughness length.

To summarize all these aspects, the structure of SurfPro seasonal parameterization generally provides a rough representation of the reality, while the time series defined by WRF initially parameterization (from the Noah land scheme) or using WRF outputs are more accurate. However, not all the SurfPro statically parameters can be substituted by the corresponding WRF quantities getting an improvement of the results, as shown by the skill scores; this happens only for the parameterization of Bowen ratio, while for the leaf area index a further scaling is required.

Therefore, a significant improvement of SurfPro processor (and of CRMA air quality chain) can be obtained rewriting the tables of statically parameters on monthly basis, but maintaining the land use subdivision. The values contained in new tables must be more suitable for national and regional features (e.g. soil texture, plant species and agricultural practices such as watering), possibly taking into account statistical analysis of on field measurements and remote sensing data. To this end, some long-term datasets provided by eddy covariance experimets are already available for different land cover types, through the European Fluxes Database Cluster. In addition, satellite remote sensing datasets are usually made available by the international projects like Copernicus; therefore, results of this study recommend, where possible, their implementation within tables of parameters. Anyhow, the direct use of remote sensing data, without passing trough statistical data tables, could be a solution only for the analysis products of CRMA (i.e. simulations of previous years) because acquisition and elaboration of remote sensing data usually require months, therefore products can not be available for the forecasts.

In addition, together with the definition of values more suitable for the region, the periodical revisions of tables have to be defined to take into account the changes in agricultural practices and related to the land use.

Last part of conclusions reports the general conclusions and further developments, providing also a summary of the critical issues faced. In addition, the benefits of this study on the air quality forecast with numerical models in Friuli Venezia Giulia region are explained.

The entire work of evaluation and validation of SurfPro parameters has been made possible thanks to the measurements of these quantities, therefore it has been strictly dependent to the availability of them. In particular, the 2015 micrometorological data are collected with non uniform frequency, and clustered during the agricultural period; this has led to incompleteness in the analysis of some parameters, i.e. Bowen ratio and roughness length, which can not be evaluated for the entire year. Other disadvantages of this work are that some SurfPro parameters have not been compared with actual measurements (soil parameter) or with suitable WRF time series (albedo).

Despite this problems, the main worth of work (beside the evaluation of SurfPro parameters) must be sought in the analysis procedure adopted for each parameter,

by means of daily means, moving medians, definition of central hours, which can be exported in other situations and other evaluations. Moreover, the definition of a set of statistical skill scores suitable for the comparison between models and measurements in the context of air quality modeling is another evident result of the work. Moreover, these aspects take greater importance considering that a significant number of Italian regional agencies for the environmental protection (ARPAs) use the SurfPro processor in the computational flow, as well as ENEA, the Italian national agency for new technologies, energy and sustainable economic development.

Finally, this thesis allows for different further developments, mainly devoted to enlarge the statistical analysis of SurfPro parameterization. The set of computational codes developed are ready to the extension, the scripts for the extraction of fields, the analysis tools and the statistical skill scores. To enlarge the statistical analysis two directions can be followed: the first one consists in repeating the analysis in the same site for the years previous to 2015, while the other is the implementation of field measurements in different rural places of Friulan plain. Between the two routes, the first one is the more practicable because eddy covariance measurements were already collected and because CRMA is achieving a database of previous year simulations which can be used for the evaluation of SurfPro statically parameters.

Moreover, another contribution of this thesis in the context of CRMA air quality computational chain is that the work acts as a base to investigate the relations between the SurfPro inaccuracies in the Friulan plain and the forecast errors committed by the models which uses this processor as input.

Appendices

Appendix A

Virtual Potential Temperature

Virtual potential temperature is an atmospheric quantity that includes both the concept of temperature at reference pressure and the regard for the presence of water vapor into an air parcel. The derivation is presented starting from the ideal gas law for moist air

$$p = \rho R_w T, \tag{A.1}$$

where R_w is the gas constant of moist air. It can be wrote as $R_d(1 + 0.61q) = \frac{R}{M_d}(1+0.61q)$, with R_d the gas constant for dry air ($287\ Jkg^{-1}K^{-1}$) and M_d the mean molecular weight of dry air. Using the definition of virtual temperature (indicating the temperature dry air must have to equal the density of moist air at the same pressure) another version of gas law can be written

$$T_V = T(1 + 0.61q) \tag{A.2}$$

$$p = \rho R_d T_V, \tag{A.3}$$

where q is the specific humidity, i.e. ratio between water vapor density and total moist air density. A remark is made on the fact $T_V > T$, in fact water vapor is less dense that dry air that must be heated for obtain the same density.

Now, potential temperature θ is defined as the temperature that would result if a parcel of air were bought adiabatically to a reference pressure p_r. Using Poisson expression for the adiabatic process, $pV^\gamma = const$ with $\gamma = \frac{c_P}{c_V}$, and making some calculations potential temperature results

$$\theta = T\left(\frac{p}{p_R}\right)^{-\frac{R_d}{c_p}}. \tag{A.4}$$

The definition can be extended for moist air parcels to write the virtual potential temperature

$$\theta_V = T_V\left(\frac{p}{p_R}\right)^{-\frac{R_d}{c_p}} = \theta(1 + 0.61q). \tag{A.5}$$

Appendix B

Re-definition of SurfPro parameters

One of the SurfPro modules is devoted to the computation of incoming solar radiation. To reach the purpose, the developers apply a simple parameterization from Holtslang and Van Ulden (1983)

$$K = K_0(1 + b_1 N^{b_2}) = (a_1 \sin\varphi + a_2)(1 + b_1 N^{b_2}), \tag{B.1}$$

where K_0 is the incoming solar radiation in clear sky condition, depending on solar elevation angle φ and turbidity coefficients a_1 and a_2 determined by water vapor and aerosols in the air; instead, the other factor introduces the cloud cover N linked to empirical coefficients b_1 and b_2, which may depend on the climate of the specific site (i.e. cloud layering, cloud thickness). Moreover, the previous equation can be used only for $\varphi > 10$, for smaller solar elevation angle a different parameterization must be defined to avoid negative values of K_0.

In this appendix the parameters of SurfPro are compared with that estimated using the radiometer of Beano station. Solar incoming radiation data are measured every half hour for the year 2015, while the solar elevation angle is calculated applying (Sellers, 1965)

$$\sin\phi = \sin\delta \sin\psi + \cos\delta \cos\psi \cos h, \tag{B.2}$$

where δ is the solar declination, ψ the latitude and h the hour angle that can be calculated starting from the annual day number, the solar longitude and the longitude of the site.

Clear sky conditions Parameters a_1 and a_2 describing the air turbidity must be evaluated in clear sky conditions, therefore the measurements of solar incoming radiation detected in these conditions have to be selected. However, Beano dataset does not provide information about the cloud cover and therefore a filter based on cross-check between Beano dataset and SurfPro output is applied. This means that measures of solar radiation is used in the analysis only if the SurfPro model has simulated a total cloud cover equal to zero at the same time and place. Obviously, it would be better applying a filter based on total cloud cover observations, however these information are available only every three hours during daytime from a nearby

airport and then it has been preferred to include some inaccurate measures in order to compute the analysis with a larger dataset.

Therefore, the least square method is applied to estimate a_1 and a_2 from the equation

$$K_0 = a_1 \sin\varphi + a_2, \tag{B.3}$$

having measured K_0 and knowing $\sin\varphi$. Table B.1 shows the results of linear regression and the parameters set up by SurfPro model. Both the estimates of a_1 and a_2 differs from the SurfPro parameters more than the standard deviation associated to them (physical considerations are further provide considering also the cloud cover conditions). Good quality of the fit is shown by significance level and by the R-squared.

Parameter	SurfPro	Beano site
a_1	990	1052 ± 19 ***
a_2	-30	-59 ± 11 ***
	R^2	0.78

Table B.1: Parameters a_1 and a_2 result from linear regression of equation B.3 compared to the values of SurfPro model. Significance level is provided in statistical notation: three stars mean p-value less than 10^{-3}.

Clound sky conditions In order to estimate b_1 and b_2 parameters, a measure of total cloud cover close to the site of measurements is required. This data are acquired from the METAR (METeorological Air Report) database, that supplied, among others meteorological variable of aeronautical interest, the total cloud cover in the nearby Rivolto airport. Measures of total cloud cover are provided every 3 hours during the daytime, starting from 7:00 to 19:00 local time; these measures are difficult to implement in the practice and visual observation is still widely used for cloud cover determination. The operator provides reports of total cloud cover using a scale from 0 to 8, the extremes correspond to absence of clouds and complete sky cover. Conversion from oktas (eighths) to fractional scale is reported in table B.2, in accordance with USA National Climatic Data Center (2016). When conversion table proposes a range of decimal values, randoms number within these intervals are chosen.

Oktas	00	01	02	03	04	05	06	07	08	09	99
Decimals	0.0	0.01-0.1	0.2-0.3	0.4	0.5	0.6	0.7-0.8	0.9-0.99	1.0	NE	NA

Table B.2: Conversion table of total cloud cover, from oktas to fractional scale. NE means that cloud cover is not evaluable (i.e. usually in presence of fog) and NA means data not available. From *National Climatic Data Center, 2016, Federal Climate Complex Data Documentation For Integrated Surface Data.*

Finally, a remark is made on the distance between the measurements of incoming solar radiation and the observations of total cloud cover: it is about 3.6 km, shorter than the representativeness radius of Beano incoming solar radiation measurements; therefore, the compatibility of the two measures is proved.

The estimation of parameters b_1 and b_2 related to cloud cover conditions is performed using a database composed by 753 couples of incoming solar radiation and total cloud cover observations, for which the total cloud cover is different to zero. The Pearson correlation coefficient (computed by Pearson test) between the two set of values is equal to -0.60, an acceptable anti-correlation value considering that total cloud cover does not consider differently the cloud levels (i.e. low, medium, high), and that only the cloud cover condition is considered, in fact the absence of clear sky conditions has lowering the absolute value of correlation coefficient.

A non linear regression in applied using R tools starting from the equation

$$K = K_0(1 + b_1 N^{b_2}), \tag{B.4}$$

where K_0 is obtained introducing the coefficients for clear sky conditions previously estimated. Results of the fit are reported in table B.3 together with the significance level and residual standard error. As previously good quality estimates are obtain but in this case the one of the parameters (b_1) is quite similar to the value implemented by SurfPro, even if outside the associated standard deviation range.

Parameter	SurfPro	Beano site
b_1	-0.75	-0.72 $\pm$ 0.01 ***
b_2	3.4	4.2 $\pm$ 0.2 ***
	RSE	0.19

Table B.3: Parameters b_1 and b_2 result from linear regression of equation B.4 compared to the values of SurfPro model. Significance level is provided in statistical notation: three stars mean p-value less than 10^{-3}.

Physical interpretation of results Considering the tables of parameters, a summary of the properties of Beano atmosphere that affect incoming solar radiation at the Earth's surface can be proposed, taking into account the differences with respect those found in Cabauw site, for which the SurfPro parameters are valid.

In clear sky conditions the parameters a_1 and a_2 are respectively greater than and less than the SurfPro parameters. Because of this disagreement, one cannot evince anything about the amount of aerosols or water vapor in the air, or about their optical properties. However, the fact that the computed parameter a_1, linked to the solar elevation angle and then to site latitude, is greater than SurfPro parameter would say that likely a less value of latitude is connected to a greater annual average of incoming solar radiation in clear sky conditions.

Whilst, the calculated parameters related to cloud cover conditions result linked to SurfPro parameters in different ways. Parameter b_1 is rather comparable with tabulated parameter, even if it falls outside the standard error range, and anything can be deducted. Instead, estimated b_2 is remarkable greater than SurfPro value. Remembering that it is found at the exponential of a number between 0 and 1, one can deduce that the clouds that form in the region of Beano site have got larger ability to hold solar radiation than the clouds that form in the Netherlands. This feature is related to the color of the clouds (i.e. opaqueness) and to the thickness of them, that decrease the solar incoming radiation reach the surface in cloud cover

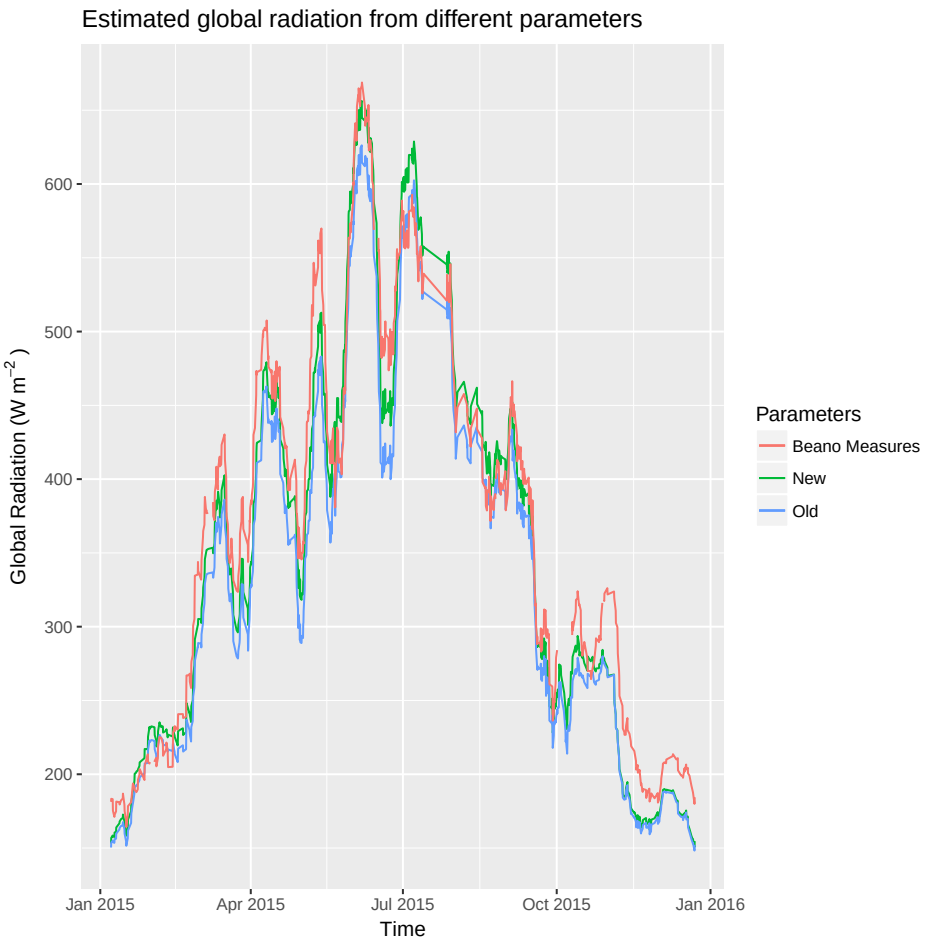

Figure B.1: Time series of incoming solar radiation for the year 2015 calculated from SurfPro parameterization using two sets of parameters (new and old) and measured in Beano site of measures.

conditions. For instance, the high occurrence of convective precipitations in Friuli Venezia Giulia region helps to explain what was found.

Re-computation of solar incoming radiation Having calculated the suitable parameters for the Beano site of measurements, now these parameters are used to compute the incoming solar radiation using the SurfPro parameterization for solar elevation angle greater than 10° (equation B.1). The purpose is to compare the time series of incoming solar radiation computed using new parameters to what computed using old parameters, and to site measurements in the year 2015.

Computed time series are obtained starting from the three hours measures of total cloud cover provided by METAR, for these hours the solar elevation angle is calculated and data with $\varphi > 10°$ is selected. After the incoming solar radiation computation, moving average is performed using 40 measures to avoid that lack of METAR cloud cover observations create inhomogeneities in the data frame. At the end, when METAR data are not available for a long time, as well the correspondent on site measurements of solar radiation are excluded by the comparison (this is done

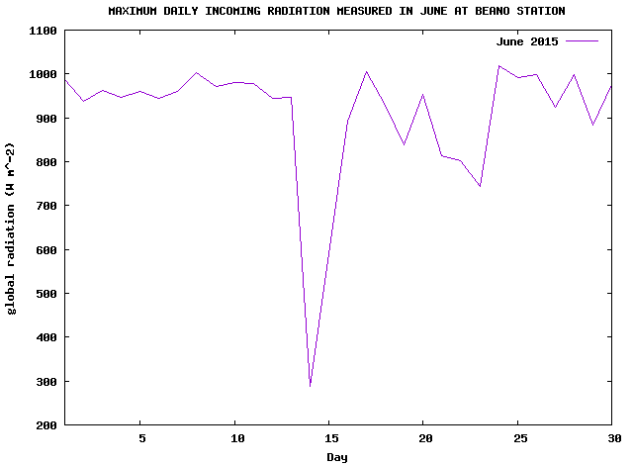

Figure B.2: Time series of maximum incoming solar radiation measured during June 2015 by Beano radiometer. An evident dip is detected on 14^{th} June.

to make data comparable). The three time series are shown in figure B.1.

One can note that the pattern of measured incoming solar radiation is well represented by the two computed time series, even if almost always they underestimate it. The benefit of using the new set of parameters is showed especially during spring and summer, when time series of new parameters is constantly closed to measured one; starting from august this benefit seem to decrease. From this figure a sinking in both measured and detected radiation can be noted in the middle of June. It is caused by a single very cloudy day of June in which the radiation collapse, as shown by the maximum measured radiation in figure B.2; the use of moving average spreads its contribute to nearby measures.

Anyway, noted a general underestimation of incoming solar radiation by the two models, now the attention is payed on the comparison between the two computations (i.e. using old and new set of parameters). To do that, the relative bias is defined as

$$RB = \frac{K_0^{new} - K_0^{old}}{K_0^{old}} \tag{B.5}$$

and its discrete probability function is provided in figure B.3 together with the main quantiles of distribution. One can note that distribution is centered on the value of 0.055; therefore considering the whole year, SurfPro parameters underestimate the incoming solar radiation of about 5% with respect the improved set of parameters. However, underestimation has place mainly during the central months of the year (as shown in figure B.1), when the underestimation can be quantified between 10% and 15 %, that correspond to the extreme values of the distribution histogram. During the summer, a deficit like this (that must be summed to the underestimation of the new set of parameters) can rather affect the total amount of energy available to the thermals growths and finally results in ABL thick and mixing height.

Remembering that b_1 and b_2 SurfPro parameters contribute to overestimate the incoming solar radiation (because of they refer to clouds that form in Cabauw site), a positive median of relative bias means that necessarily the contribute of remaining SurfPro parameter a_1 and a_2 must be addressed to underestimate the incoming

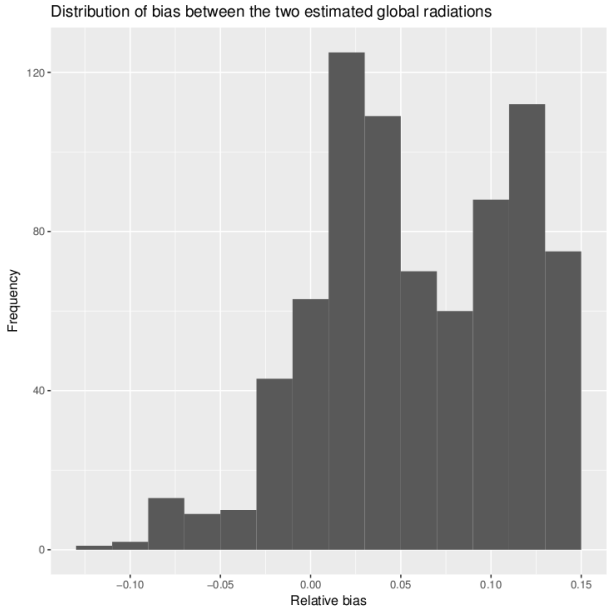

Quantiles of distribution	
0.05	-0.026
0.25	0.019
0.50	0.055
0.75	0.108
0.95	0.135

Figure B.3: Relative bias of incoming solar radiation computed using new and old set of parameters: histogram of probability distribution and related quantiles.

radiation. In particular, a_1 play an important role in this because it is less than just computed parameters; therefore a better estimate of this parameter could bring to the improvement of incoming solar radiation (due to its weight in the computation).

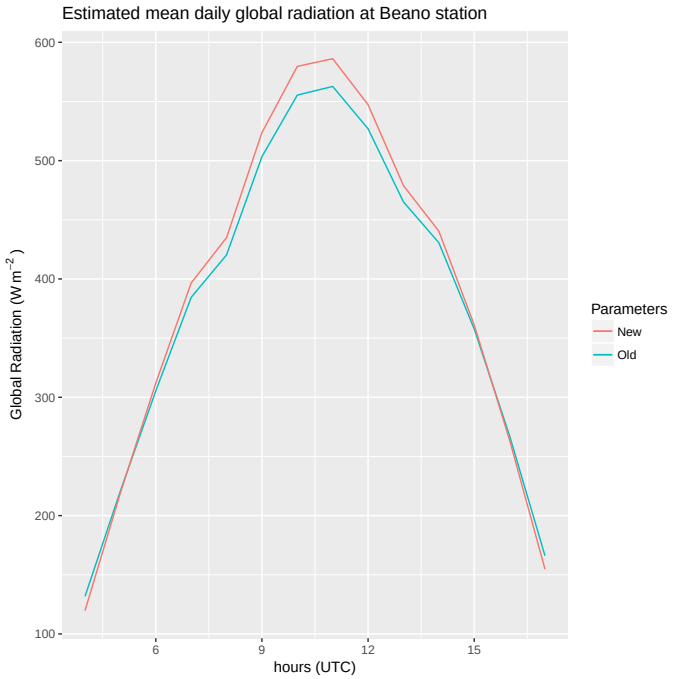

Figure B.4: Mean daily incoming solar radiation estimated using the two sets of parameters. Standard deviation is not reported because the seasonal variability makes it very large and it does not help the comprehension of graph.

Finally, the average annual day is considered for the two computations and reported in figure B.4, note that perform this operation means consider an annual average cloud cover. One finds the confirmation of what said previously: the discrepancy between the two estimations is much noticeable during the central hours of the day, when the parameter a_1 counts more (see equation B.1). While during sunrise and sunset the parameter loses importance and SurfPro parameter a_2 provides an overestimate of solar radiation; this can be due to the lower amount of aerosols and water vapor in the Cabauw site and/or to the different optical properties of aerosols.

Conclusions Calculating the incoming solar radiation in a site of Friulan plain using the SurfPro standard parameters, instead of the more suitable parameters computed by regression method, one can meet an annual median error of about 5% that can rise to 10%-15% during the hottest months, when important energies are involved in the surface balancing.

The estimated coefficients of the parameterization reported in equation B.1 weight in different ways in the final calculation of incoming solar radiation. In fact, it was evinced that parameter a_1 is able to equalize and overtake the inaccuracy of other parameters and therefore an accurate estimate of it is necessary to improve the yield of SurfPro processor, especially during summer. The importance of a_1 comes from the link to the solar elevation angle, that is the most important feature that enters in the parameterization (others are aerosols, water vapor, cloud thickness and cloud color).

Appendix C

Albedo on-ground measurements

Beano station is implemented with two radiometers positioned in order to detect incoming and outcoming visible light. Radiometer oriented upwards is able to detect direct and diffused (by particles in atmosphere) solar radiation, while the radiometer oriented downwards should measure the solar radiation reflected by the Earth's surface. Knowing incoming and outcoming shortwave radiation, one can simply determine albedo calculating the ratio between the two quantities; corrections related to topography, which are necessary to give a correct estimate of reflected solar radiation, are not required for this site of measurements.

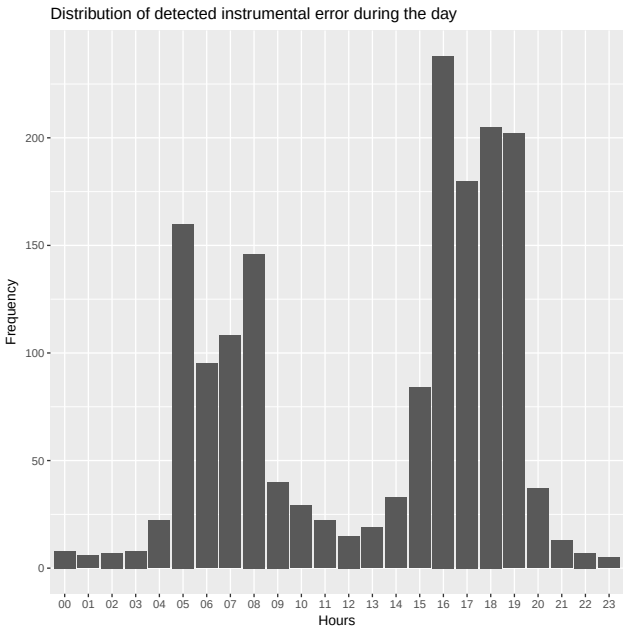

Figure C.1: Daily discrete probability distribution of the measurements for which reflected solar radiation overtakes the incoming solar radiation (i.e. instrumental error). Measures are made in Beano station during 2015 and hours reported refer to local time.

However, from a first analysis of data one can find that half-hour measures of reflected solar radiation often exceed the correspondent incoming solar radiation, that is impossible considering the definition of reflected radiation. In particular, the observed overtake affects the hours of sunrise and sunset, as shown by figure

C.1 which plots the discrete distribution of the measurements for which reflected radiation overtake incoming solar radiation.

This suggests the possibility for an instrumental error, in particular it is likely that this error consists in a tilt of the downward radiometer towards North-West or South-West, because the peak at the sunset is highest. Therefore, during sunrise and sunset the radiometer had measured also a portion of radiation directly coming from the sun. Moreover, if this kind of error took place all the measurements are affected too, even if the reflected solar radiation does not exceed the incoming component, and its magnitude depends on the solar elevation angle.

An attempt to correct the error was made subtracting from all the measurements of reflected radiation the annual mean value of instrumental error (i.e. the difference between reflected and incoming solar radiation when the first one exceeds the second one), however this correction can not be perform without rising further uncertainties related to the dependence of the instrumental error to solar elevation angle and to cloud cover, the last dependence is derived by the observation that during the daytime (i.e. after the sunrise and before the sunset) the instrumental error can be detected mainly in the case of cloud cover, i.e. associated to the lowering of direct solar radiation without the lowering of reflected solar radiation. For these reasons it was decided to discard the on-ground measurements of albedo and to explore the world of remote sensing measures.

Appendix D

WRF accuracy in modeling precipitations

The WRF ability to reproduce rainy precipitations is investigated by means of comparison with Beano raingauge measurements. Firstly, plots of cumulative precipitations over the hours of the day and over the months are reported to provide to reader an information about the distribution of the 2015 rainy events: therefore, the figure D.1 shows all the water collected by the pluviometer placed near Beano tower, removing the contribution of the irrigation. Dew and frost are still comprehended in the comparison, however these phenomena do not affect the whole assessment because their magnitude is comparable with the sensitivity of the measure instrument, i.e. 0.2 mm.

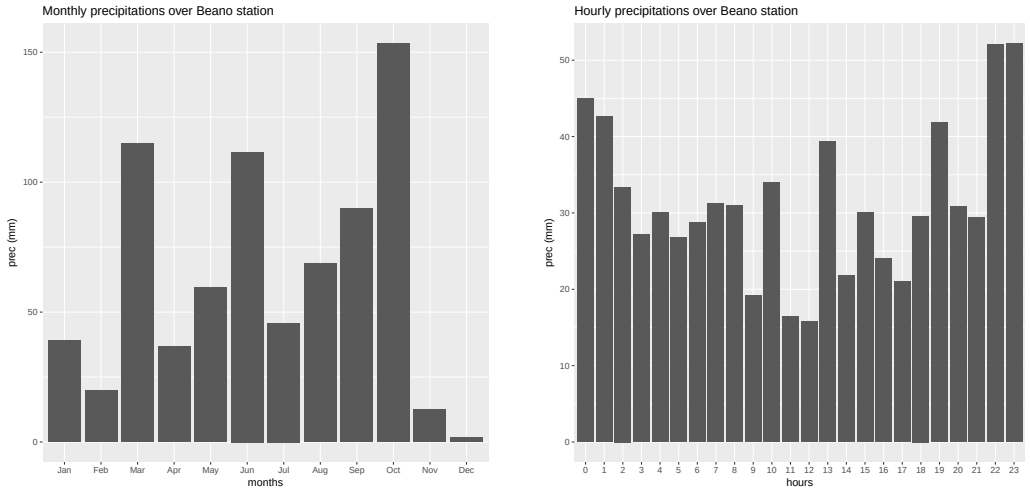

Figure D.1: Cumulative precipitations measured by Beano pluviometer over the months (on the left-hand side) and over the whole hours of the year (on the right-hand side).

The assessment of the WRF performance in the simulations of rainy events is performed comparing the empirical distribution functions of WRF model and Beano measurements, both of them are plotted considering the total amount of precipitations over a day. This approach permits to evaluate the global characteristics of WRF algorithm for precipitations during an entire year, therefore its purpose is

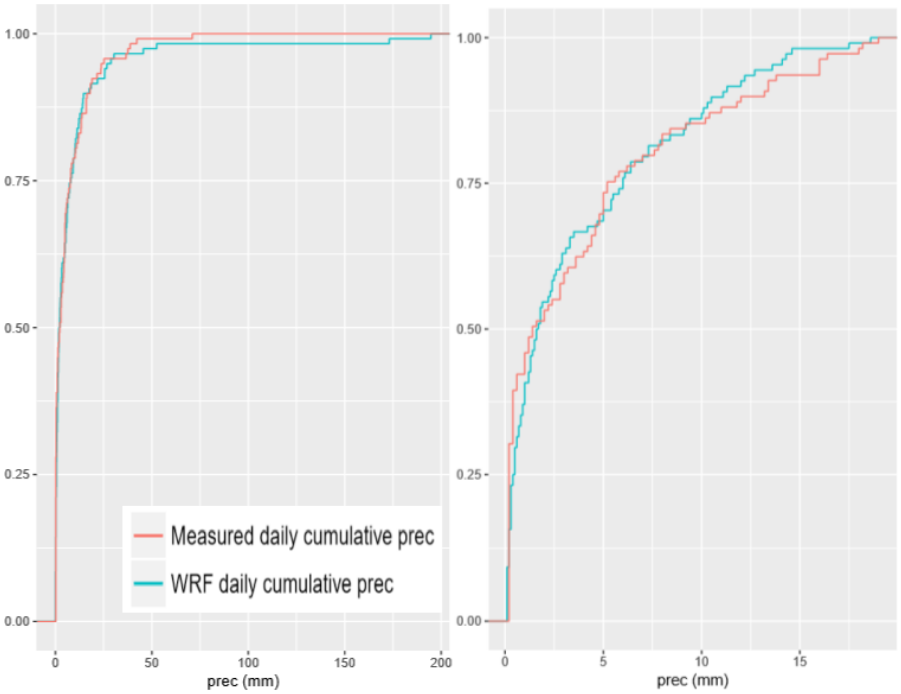

Figure D.2: Empirical distribution function of the amount of daily precipitations measured by Beano station and modeled by WRF. On the left the entire distribution is plotted, on the right only the days for which less than 20 mm are measured are taken into account.

not to assess the WRF performance related to single rainy events, for instance if the precipitation occurs one hour after the WRF forecast and if the rain quantity matches, this analysis considers this event as an algorithm success. On the contrary, this approach considers an algorithm failure the correct forecast of the occurrence time associated to an incorrect modeling of amount of precipitation.

The empirical distribution functions of daily precipitations are showed in figure D.2, which on the left-hand side reports the entire distribution, and on the right-hand side it displays a subset related to weak events, i.e. daily measurements of less than 20 mm. The shape of the two empirical distributions is the same and a good agreement between measures and model is observed, slightly differences can be found for large precipitation events and in the distribution curve, however they do not affect the goodness description of the reality. To confirm that, two-sample Kolmogorov–Smirnov test is applied for the cumulative daily precipitations, obtaining a p-value equal to 0.94 over the entire year, and equal to 0.44 considering only days in which presipitations are detected. In both cases one can say that the null hypotesis that samples come from the same distribution cannot be rejected.

Entering in details, one can observe that WRF has modeled for the year 2015 two events with a daily amount of precipitation between 175 and 200 mm which have not occurred in the reality, in fact the maximum daily measurement is close to 75 mm. Moreover, from the left figure one can evince that WRF model overestimates the amount of precipitations of strong events, from 25 mm on, with an exception related to days in which 30 mm of precipitations are detected, where the red line goes down to the blue line. Now the focus is on the right-hand side picture, from 2 to 20 mm the

WRF algorithm of precipitations underestimates the occurrence of these amounts of daily precipitations, this behavior is well-defined in the range from 10 to 20 mm and between 2 and 5 mm. Finally, considering values less than 2 mm, WRF overestimates the precipitations.

List of Figures

List of Tables

References

[1] Alberti et al., 2010. *Changes in CO2 emissions after crop conversion from continuous maize to alfalfa.* Agr. Ecosyst. Environ., 136, 139-147.

[2] Arianet, 2011. *SURFPRO3 User's guide (SURFace-atmosphere interface PROcessor, Version 3).* Release 2.2.0. December, 2011.

[3] Blanc et al., 2014. *Twelve monthly maps of ground albedo parameters derived from MODIS data sets.* Proceedings of IGARSS 2014, 13-18 July 2014, Quebec, Canada, 3270-3272.

[4] Burba G., 2013. *Eddy Covariance Method for Scientific, Industrial, Agricultural and Regulatory Applications.* LI-COR Biosciences, Lincoln, Nebraska.

[5] Carson D.J., 1973. *The development of a dry inversion-capped convecticely unstable boundary layer.* Q. J. R. Met. Soc., 99, 450-467.

[6] Cattivello C., 2013. *L'orticoltura regionale al tempo della crisi.* Notiziario ERSA, 1, 16-24.

[7] Cescatti A. et al., 2012. *Intercomparison of MODIS albedo retrievals and in situ measurements across the global FLUXNET network.* Remote Sens. Environ.,121, 323-334.

[8] Cleveland W.S. Grosse E. and Shyu W.M., 1992. *Local regression models.* Statistical model in S, 2, 309-376.

[9] Coakley J.A., 2002. *Reflectance and albedo, surface.* In: Holton JR, Curry JA, Pyle JA (eds) Encyclopedia of the atmospheric sciences. Academic Press, pp 1914–1923.

[10] De Bruin H. and Holtslag A.M., 1982. *A simple parameterization of the surface fluxes of sensible and latent heat during daytime compared with the Penman-Monteith concept.* Bound.-Layer Meteor., 20, 1610-1621.

[11] Fogaken T., 2006. *50 years of the Monin-Obukhov similarity theory.* Bound.-Layer Meteorol., 119, 431-447.

[12] Foken T. and Wichura B., 1996. *Tools for quality assessment of surface-based flux measurements.* Agr. Forest. Meteorol., 78, 83-105.

[13] Garratt J.R., 1992. *The atmopsheric boundry layer.* Cambridge University Press, 316 pp.

[14] Garratt J.R., 1994. *Review: the atmospheric boundary layer.* Earth-Sci. Rev., 37, 89-134.

[15] Garrigues S. et al., 2008. *Validation and intercomparison of global Leaf Area Index products derived from remote sensing data.* J. Geophys. Res., 113, G02028.

[16] Godfrey C.M. and Stensrud D.J. , 2010. *An empirical latent heat flux parameterization for the Noah land surface model.* J. Appl. Meteor. Climatol., 49, 1696–1713.

[17] Holtslag A.A.M. and van Ulden A.P., 1983. *A simple scheme for daytime estimates of the surface fluxes from routine weather data.* J. Clim. Appl. Meteorol., 22, 517-529.

[18] Hoyer-Klick C. et al., 2008. *Management and exploitation of solar resource knowledge.* Proceedings, EUROSUN 2008, 1st International Congress on Heating, Cooling and Buildings, Lisbon, Portugal.

[19] Hu et al., 1997. *Validation of kernel-driven models for global modeling of bidirectional reflectance.* Remote Sens. Environ., 62, 201-214.

[20] Knyazikhin Y. et al., 1999. *MODIS Leaf Area Index (LAI) and Fraction of Photosynthetically Active Radiation Absorbed by Vegetation (FPAR) Product (MOD15).* Algorithm Theoretical Basis Document.

[21] Lefèvre M. et al., 2013 *McClear: a new model estimating downwelling solar radiation at ground level in clear-sky conditions.* Atmos. Meas. Tech., 6, 2403–2418.

[22] Liang S. et al., 1999. *Retrieval of Land Surface Albedo from Satellite Observations: A simulation Study.* J. Appl. Meteorol., 38, 712-725.

[23] Liu J. et al., 2009. *Validation of Moderate Resolution Imaging Spectroradiometer (MODIS) albedo retrieval algorithm: Dependence of albedo on solar zenith angle.* J. Geophys. Res., 114, D01106.

[24] Mauder M. and Foken T., 2004 *Quality control of eddy covariance measurements (C: 0,1,2).* CARBOEUROPE-IP, Task 1.2.2.

[25] National Climatic Data Center, 2016. *Federal Climate Complex Data Documentation For Integrated Surface Data* 14th Weather Squadron Fleet Numerical Meteorology and Oceanography Detachment.

[26] Niu G.-Y., 2011. *The community Noah Land-Surface model (LSM) with multiphysics options.*

[27] Optis M. et al., 2014. *Moving Beyond Monin–Obukhov Similarity Theory in Modelling Wind-Speed Profiles in the Lower Atmospheric Boundary Layer under Stable Stratification.* Bound.-Layer Meteorol., 153, 497.

[28] OSMER - ARPA FVG, 2014. *Il clima del Friuli Venezia Giulia.*

[29] Pozzi et al., 2012. *Exponential smoothing weighted correlations.* Eur. Phys. J. B, 85, 6.

[30] Roujean J.-L. et al., 1992. *A bidirectional reflectance model of the Earth's surface for the correction of remote sensing data.* J. Geophys. Res., 97, 20455-20468.

[31] Schaaf et al., 2002. *First operational BRDF, albedo nadir reflectance products from MODIS.* Remote Sens. Environ., 83, 135–148.

[32] Schuepp P.H. et al., 1990. *Footprint prediction of scalar fluxes from analytical solution of the diffusion equation.* Bound.-Layer Meteorol., 50, 355.

[33] Sellers W.D., 1965. *Physical Climatology.* The University of Chicago Press, 272 pp.

[34] Siegel S. and Tuckey J., 1960. *A Nonparametric Sum of Ranks Procedure for Relative Spread in Unpaired Samples.* J. Am. Stat. Assoc., 55(291), 429-445.

[35] Soil Science Society of America, 2008. *Glossary of Soil Science Terms 2008.* SSSA, Madison, WI, pp. 92.

[36] Stefanutto L., 2003. *Il clima del Friuli-Venezia Giulia.*

[37] Strahler A.H. and Muller J.-P., 1999. *MODIS BRDF/Albedo Product: ALgorithm Theorethical Basis Document Version 5.0.*

[38] Stull R.B., 1988. *An Introduction to Boundary Layer Meteorology.* Dordrecht: Kluwer Academic Publishers, 666 pp.

[39] Taylor K.E., 2001. *Summarizing multiple aspects of model performance in a single diagram.* J. Geophys. Res., 106, 7183-7192.

[40] Venkatram A., 1980. *Estimating the Monin-Obukhov lenght in the stable boundary layer for dispersion calculations.* Bound.-Layer Meteorol., 19, 481-485.

[41] Viterbo P., 2002. *A review of parametrization schemes for land surface processes.* ECMWF, Meteorological Training Course Lecture Series.

[42] Wang J. et al., 2008. *Simulation of diurnal variations of CO2, water and heat fluxes over winter wheat with a model coupled photosynthesis and transpiration.* Agr. Forest. Meteorol., 137, 194-219.

[43] Wang S. et al., 2016. *Validation of Regional-Scale Remote Sensing Products in China: From Site to Network.* Remote Sens., 8, 980.

[44] Wanner et al., 1995. *On the derivation of kernels for kernel-driven models of bidirectional reflectance.* J. Geophys. Res., 100, 21077-21090.

[45] WMO - World Meteorological Organization, 2008. *Guide to Meteorological Instruments and Methods of Observation.* WMO-No.8, Seventh edition.

[46] WMO - World Meteorological Organization, 2015. *Manual on the Global Observing System. Volume I - Global Aspects.* WMO-No.544, Anne V to the WMO Technical Regulations.

[47] Yu et al., 2017. *A Method for Estimating the Aerodynamic Roughness Length with NDVI and BRDF Signatures Using Multi-Temporal Proba-V Data.* Remote Sens., 9, 6.

Sitography

[S1] http://www.arpa.fvg.it/cms/tema/aria/

[S2] http://95.228.102.186/trac/SURFPRO

[S3] http://land.copernicus.eu/pan-european/corine-land-cover

[S4] http://www.wrf-model.org/

[S5] http://www.ral.ucar.edu/research/land/technology/lsm.php

[S6] http://www.europe-fluxdata.eu

[S7] http://www.expeeronline.eu/about-expeer.html

[S8] https://fluxnet.ornl.gov/site/4083

[S9] https://modis.gsfc.nasa.gov/data/dataprod/mod15.php

[S10] https://www.umb.edu/spectralmass/terra_aqua_modis/modis

[S11] http://www.soda-pro.com/web-services/radiation/
cams-radiation-service/info

[S12] https://www.rdocumentation.org/

[S13] https://cran.r-project.org/web/packages/ggplot2/index.html